US Army Corps of Engineers®
Engineer Research and
Development Center

ERDC
INNOVATIVE SOLUTIONS
for a safer, better world

Development of Conceptual Designs for the Prevention of Ice Formation in the Proposed Maple River Aqueduct

Steven F. Daly, Meredith Carr, Kevin Bjella, and Robert Haehnel

September 2014

The U.S. Army Engineer Research and Development Center (ERDC) solves the nation's toughest engineering and environmental challenges. ERDC develops innovative solutions in civil and military engineering, geospatial sciences, water resources, and environmental sciences for the Army, the Department of Defense, civilian agencies, and our nation's public good. Find out more at www.erdc.usace.army.mil.

To search for other technical reports published by ERDC, visit the ERDC online library at http://acwc.sdp.sirsi.net/client/default.

Development of Conceptual Designs for the Prevention of Ice Formation in the Proposed Maple River Aqueduct

Steven F. Daly, Meredith Carr, Kevin Bjella, and Robert Haehnel

Cold Regions Research and Engineering Laboratory (CRREL)
U.S. Army Engineer Research and Development Center
72 Lyme Road
Hanover, NH 03755-1290

Final Report

Abstract

The Fargo-Moorhead Metropolitan Area Flood Risk Management Project is to include an aqueduct to carry the flow of the Maple River over a proposed diversion channel. This study quantified the amount of ice that forms in the aqueduct under different winter operating scenarios. To achieve this, this study developed an aqueduct flow and ice simulation that simulated five different operation scenarios: the proposed aqueduct alone, a case with downstream stage control, and three different cases of applied heating. Each scenario was run with 6 in., 3 in., and no insulation on the outside of the aqueduct. The flow conditions and the ice formation in the aqueduct were simulated every day for the winters of 1995 to 2013, allowing estimates to account for the natural variability of the flow and air temperature. The simulation found that, though ice formation in all scenarios caused the stages to rise, the unheated scenarios saw the largest stage rise; and the impact of the insulation in the unheated scenarios was significant. Applying heat reduced stages compared to the unheated cases, the amount of heat applied determined the decrease in the upstream stages, and insulation had less impact when heat was applied.

Contents

Illustrations

Figures

Tables

Preface

Abbreviations and Acronyms

AFDD	Accumulated Freezing Degree Days
AFISM	Aqueduct Flow and Ice Simulation Model
COV	Coefficient of Variation
DSC	Downstream Control
F-M	Fargo-Moorhead
GHCND	Global Historical Climatology Network
GIS	Geographic Information Systems
HEC-RAS	Hydrologic Engineering Center River Analysis System
IDNR	Illinois Department of Natural Resources
NAVD88	North American Vertical Datum of 1988
NCDC	National Climate Data Center
RM	River Miles
RRN	Red River of the North
TES	Thermal Energy Storage
UMass	University of Massachusetts
USACE	U.S. Army Corps of Engineers
US DOE	U.S. Department of Energy
USGS	United States Geological Survey
WMO	World Meteorological Organization

Unit Conversion Factors

Multiply	By	To Obtain
British thermal units (International Table)	1,055.056	joules
British thermal units per hour	0.2928104	watts
cubic feet	0.02831685	cubic meters
degrees Fahrenheit	(F-32)/1.8	degrees Celsius
feet	0.3048	meters
inches	0.0254	meters
miles (U.S. statute)	1,609.347	meters
pounds (mass)	0.45359237	kilograms
square feet	0.09290304	square meters

Executive Summary

An aqueduct has been proposed to carry a portion of the flow of the Maple River over the proposed diversion channel as part of the Fargo-Moorhead Metropolitan Area Flood Risk Management Project. Aqueducts that operate throughout the winter in cold regions are rare; none are currently operated by the Corps of Engineers.

Winter flows in the Maple River are low. The flows are slowly changing and are often in recession. A review of the meteorological and hydrological conditions indicate that recorded Maple River flows and local air temperatures have increased over the period of record, which extends from about 1948 to the present.

This study quantified the amount of ice that can form under different operating scenarios in the aqueduct during the winter months. We did this by simulating the flow conditions and the ice formation in the aqueduct every day for each operating scenario for the most recent 18 winters for which data is available—the winter of 1995–1996 through the winter of 2012–2013. This allowed us to estimate and compare the ice formation that would result from each operating scenario under the natural variability of the flow and air temperature that occurs at the proposed aqueduct location.

The simulation used an aqueduct flow and ice simulation model developed for this study. The model has five submodules that determine the aqueduct flow conditions and ice conditions. The model operated with a daily time step over each winter starting on 1 October of each year.

We simulated five different scenarios of aqueduct operation:

1. The aqueduct with no applied heating or downstream control (base case)
2. The aqueduct with downstream control and no applied heating (base case with downstream control); we maintained the downstream elevation to keep a depth of about 11.5 ft in the aqueduct throughout the winter
3. The aqueduct with applied heating of 5 Btu/hr ft² in the low-flow channel and no downstream control

4. The aqueduct with applied heating of 30 Btu/hr ft² in the low-flow channel and no downstream control

5. The aqueduct with applied heating of 60 Btu/hr ft² in the low-flow channel and no downstream control

We simulated each of these five basic scenarios for three different cases of insulation applied to the outside of the aqueduct: no insulation, 3 in. of insulation, and 6 in. of insulation. We developed a total of 15 simulations.

Both the base case and the base case with downstream control produced roughly the same ice volume when they were uninsulated. The accumulated freezing degree days (AFDD) recorded over the winter strongly controlled the volume of ice formed.

Ice volume in the basic aqueduct was reduced 25.8% by 3 in. of insulation and 31.8% by 6 in. of insulation. Ice volume in the basic aqueduct with downstream control was reduced 18.3% by 3 in. of insulation and 22.9% by 6 in. of insulation.

Application of heat significantly reduced the volume of ice formed. In the case of the uninsulated aqueduct, 60 Btu/hr ft² produced only 31.6% of the ice volume of the basic aqueduct without heat, 30 Btu/hr ft² produced only 37.0% of the ice volume of the basic aqueduct without heat, and 5 Btu/hr ft² produced only 51.6% of the ice volume of the basic aqueduct without heat.

The ice formed in the heated aqueduct was influenced by the flow rates and to a lesser degree by the AFDD recorded over the winter. The ice volumes in the heated aqueduct displayed much more year to year variability than in the unheated cases.

The use of insulation on the outside of the aqueduct did little to improve the ice reduction performance of the heated aqueduct. Compared to the uninsulated case, the ice volume in the aqueduct heated with 60 Btu/hr ft² in the low-flow channel was reduced 3.5% by 3 in. of insulation and 4.1% by 6 in. of insulation. Compared again to the uninsulated case, the ice volume in the aqueduct heated with 30 Btu/hr ft² in the low-flow channel was reduced 2.8% by 3 in. of insulation and 3.2% by 6 in. of insulation. Finally, when compared to the uninsulated case, the ice volume in the aqueduct

heated with 5 Btu/hr ft² in the low-flow channel was reduced 1.3% by 3 in. of insulation and 2.2% by 6 in. of insulation.

Under all the scenarios, the formation of ice in the aqueduct reduced the conveyance of the aqueduct and caused the upstream stages to rise. The unheated scenarios saw the largest stage rise, and the impact of the insulation in the unheated scenarios was significant. Applying heat to the aqueduct reduced stages compared to the unheated scenarios; but it is interesting to note that when the aqueduct was heated, the impact of the insulation was greatly reduced. In the heated cases, the decrease in the upstream stages was determined almost totally by the amount of heat applied; and the thickness of the insulation had little impact.

1   Introduction

The Fargo-Moorhead (F-M) Metropolitan Area Flood Risk Management Project is to include an aqueduct to carry the flow of the Maple River over a proposed diversion channel (USACE 2011). The diversion channel will allow flood flows of the Red River of the North to bypass around the Fargo, ND, and Moorhead, MN, Metropolitan Area. In cold regions, aqueducts that operate throughout the winter are rare; and none are currently operated by the U.S. Army Corps of Engineers (USACE). In Europe, there are several large navigation aqueducts that operate throughout the winter; however, these aqueducts flow completely full all winter. The Maple River Aqueduct will not flow full during the winter. In fact, winter records for the Maple River show flows as low as 1 cfs and less. As a result of these low wintertime flows, the water depths in the aqueduct will be very shallow. Shallow flows, with large surface area to depth ratios, can cool quickly and form ice. In addition, heat transfer through the bed of the aqueduct to the frigid air below the aqueduct can be a significant heat loss from the flowing water and can also contribute to ice formation.

The purpose of our study is to quantify the amount of ice that can form in the aqueduct during the winter months under different operating scenarios. Quantifying the amount of ice is difficult because of the complex way that the flow in the aqueduct and the ice formation process can interact and influence each other. This complex interaction made it difficult to select test cases to analyze. In addition, a review of the recorded Maple River flows and air temperatures over the period of record showed that both are not stationary with respect to time but slowly increase over decadal time scales. This increase also complicated the selection of test cases. Because of these complications, we decided to simulate the flow conditions and the ice formation in the aqueduct for each day of the most recent 18 winters for each operating scenario. We simulated from the winter of 1995–1996 through the winter of 2012–2013. This allowed us to estimate and compare the ice formation that would result from each operating scenario under the natural variability of the flow and air temperature that occurs at the proposed aqueduct location.

This simulation used an aqueduct flow and ice simulation model developed for this study. Simulating the flows and ice formation in an aqueduct is a complicated task as both the flow and ice formation change from day to day as the meteorology and flow conditions change. Fortunately, flow in the Maple River changes slowly during the winter, especially during cold periods when ice formation occurs. This suggested that we could use the standard step method for varied flow computations to simulate the flows in the aqueduct each day. This is a well-known flow model that is very flexible to apply to the aqueduct where the effective channel geometry changes continuously due to the ice formation. Similarly, we could estimate the ice formation in the aqueduct by using a quasi-steady approach. This type of approach has long been used with great success and accuracy to estimate surface ice growth. It is also applied here to the growth of bed ice, ice that forms on the bed of the aqueduct due to heat conduction through the aqueduct to the air. (In this report, we are referring to ice that forms on the bed of the aqueduct as bed ice as opposed to anchor ice. Anchor ice results from the deposition of frazil ice crystals during periods of supercooled water. The formation of bed ice does not require deposition or supercooling.)

The aqueduct flow and ice simulation model has five submodules. These modules determine the water surface profile through the aqueduct, the water temperature resulting from the interaction of proposed bed heaters and the surface ice conditions, the formation of bed ice by heat conduction through the aqueduct to the outside air, the formation of surface ice through heat transfer from the water surface to the atmosphere, and the interaction of the bed and surface ice. We needed two additional modeling efforts to support and verify the aqueduct flow and ice simulation model. These were a HEC-RAS (Hydrologic Engineering Center River Analysis System) (USACE 2010) and the GeoStudio 2012 finite element thermal conduction model of the aqueduct (Geo-Slope International 2012). We modified the HEC-RAS model of the Maple River developed by the St. Paul district to include the proposed aqueduct and upstream and downstream realigned channel geometries. The simulations performed using this revised HEC-RAS model helped to determine the aqueduct's downstream water surface elevation boundary condition that the aqueduct flow and ice simulation model would used. We also used the HEC-RAS model to verify the open water flow estimation of the aqueduct flow and ice simulation model. We used the GeoStudio 2012 finite element thermal conduction model to develop a 2-D simulation of the thermal conduction through the

aqueduct cross section. The thermal conduction model allowed us to analyze the heat flow through the aqueduct structure under different flow conditions, heating elements applications, and thermal insulation applications. We integrated these results into the aqueduct flow and ice simulation model.

This report begins with a short review of the FM Area Diversion Project and the proposed aqueduct. We then describe the wintertime operation and ice problems of other aqueducts in the U.S. and Europe. These aqueducts range in size and are all navigable. They differ from the proposed Maple River aqueduct in that all are designed to flow full during the winter or to be drained completely. The next section of this report is a review of the meteorological and hydrological conditions that have been recorded in the area of the proposed aqueduct in winter. The recurrence statistics of the monthly air temperatures and the monthly Maple River flows were determined along with their trends with time. The trend analysis indicates that recorded river flows and air temperatures have increased over the period of record, which extends from about 1948 to the present. We then describe the aqueduct flow and ice simulation model development, the HEC-RAS model, and the 2-D Finite Element Heat Conduction model. Following a short description of the operation of the aqueduct in the winter and the conceptual ice control approaches, our report presents the application of the simulation model. This includes discussion of the model boundary conditions and the operation procedure. Lastly, we discuss the results of the Aqueduct Flow and Ice Simulation Model. This report includes three appendixes: plans for the conceptual bed heaters; charts of the wintertime flows and air temperatures; and the extremes in air temperature at Fargo, ND.

2   Background

2.1   Fargo-Moorhead Metropolitan Area Flood Risk Diversion Project

The F-M Metropolitan Area has a relatively high risk of flooding. The flood stage of the Red River of the North (RRN) at Fargo, ND, was exceeded in 48 out of the last 109 years; and the average annual flood damages are greater than $194 million (Diversion Authority 2013). The all-time peak stage occurred on 28 March 2009, causing major flooding in the F-M Area. To mitigate future flooding, USACE developed plans (Figure 1) for a diversion channel to bypass a large portion of RRN flood flows around the F-M Area (USACE 2011). The Project includes a gated structure located on the RRN about 27 river miles (RM) south of Fargo that would divert as much as two-thirds of the 100-year flow into the diversion channel around the F-M Area on the North Dakota side. The channel will cross and intercept flow from several tributaries and re-enter the RRN about 34 RM north of Fargo. The Diversion Authority estimates that building the project will cost about $1.8 billion and will take 10–20 years (Diversion Authority 2013).

The route of the proposed diversion channel crosses the Sheyenne, Maple, Lower Rush, and Rush Rivers. Systems of hydraulic structures are necessary at the points where the diversion channel crosses these rivers. Current plans call for the Sheyenne and Maple Rivers to cross over the diversion channel in aqueducts that are open to the air. The Rush and Lower Rush Rivers will flow into the diversion channel through drop structures. The aqueduct structure systems include spillways upstream of each aqueduct, which limit the amount of water that enters the aqueducts. This system maintains low flows for fish and habitat protection in the aqueduct and downstream reaches of the Sheyenne and Maple Rivers. Flows greater than the required minimums are diverted into the diversion channel to prevent flooding in the downstream reaches of these tributaries.

Figure 1. Fargo-Moorhead Metropolitan Area Flood Risk Management Project.
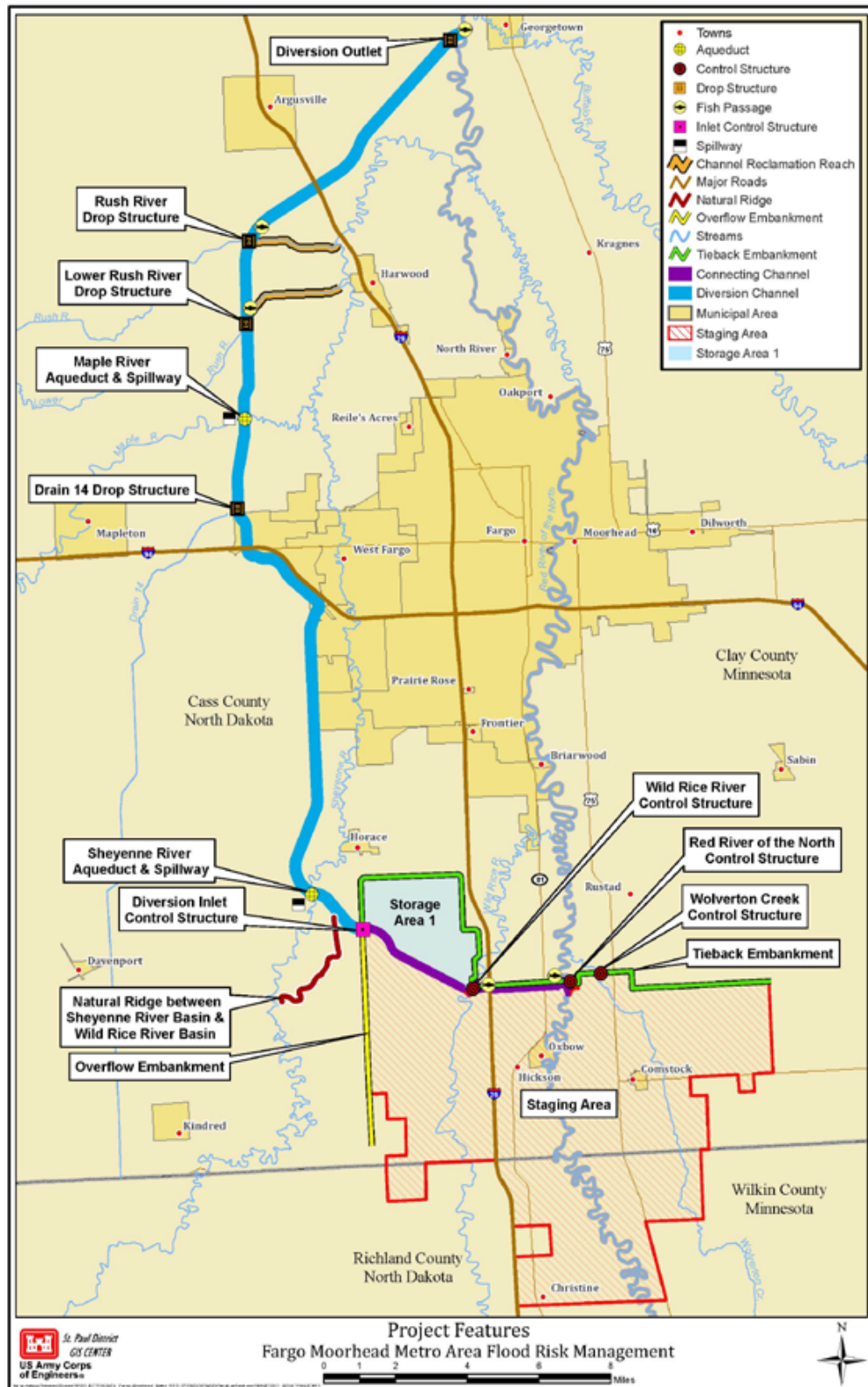
2.2 Maple River Aqueduct

The F-M Metropolitan Area Flood Risk Management Project is to include an aqueduct structure system to carry a portion of the Maple River flow over the proposed diversion channel (USACE 2011). The aqueduct structure system consists of an aqueduct, an upstream realigned channel, a downstream realigned channel, a spillway control weir, and a spillway. The proposed aqueduct crosses the diversion channel a little distance to the south of where the existing Maple River crosses the proposed diversion channel route. The upstream realigned channel would carry flow from the existing Maple River channel to the aqueduct, and the downstream realigned channel would carry flow from the aqueduct back to the existing Maple River channel. A spillway control weir located at the upstream end of the upstream realigned channel would divert high flows from the Maple River down the spillway and into the diversion channel (Figure 2). The spillway design would limit flows in the proposed Maple River Aqueduct to approximately a 2-year return flow or less. As a result, this would control flow in the existing Maple River channel downstream of the diversion channel and protect that reach from flooding.

The proposed Maple River Aqueduct is a reinforced concrete structure consisting of a thick floor slab and two vertical side walls. It spans the diversion channel on piers with 30 ft spacing. The aqueduct is 250 ft long with an internal width of 50 ft. A V-shaped low-flow channel is built into the floor slab at the center of the channel and is 12 ft wide. The floor slab is 4.5 ft thick at its internal outer edges, 4 ft thick at the edges of the low-flow channel, and 2 ft thick at the center of the low-flow channel. Figure 3 shows a typical cross section through the aqueduct from the final feasibility report.

Figure 2. Plan view of the Maple River structures.
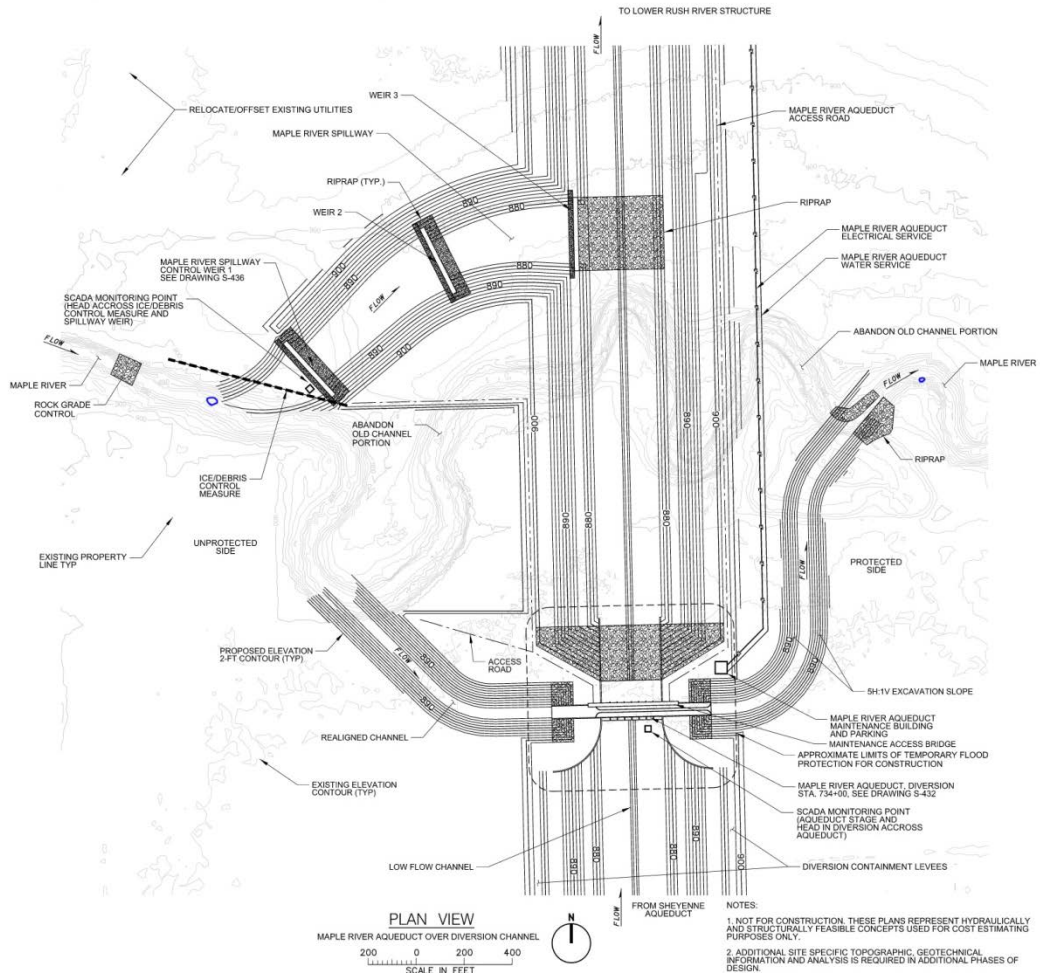
Figure 3. Cross Section of the Proposed Maple River Aqueduct.
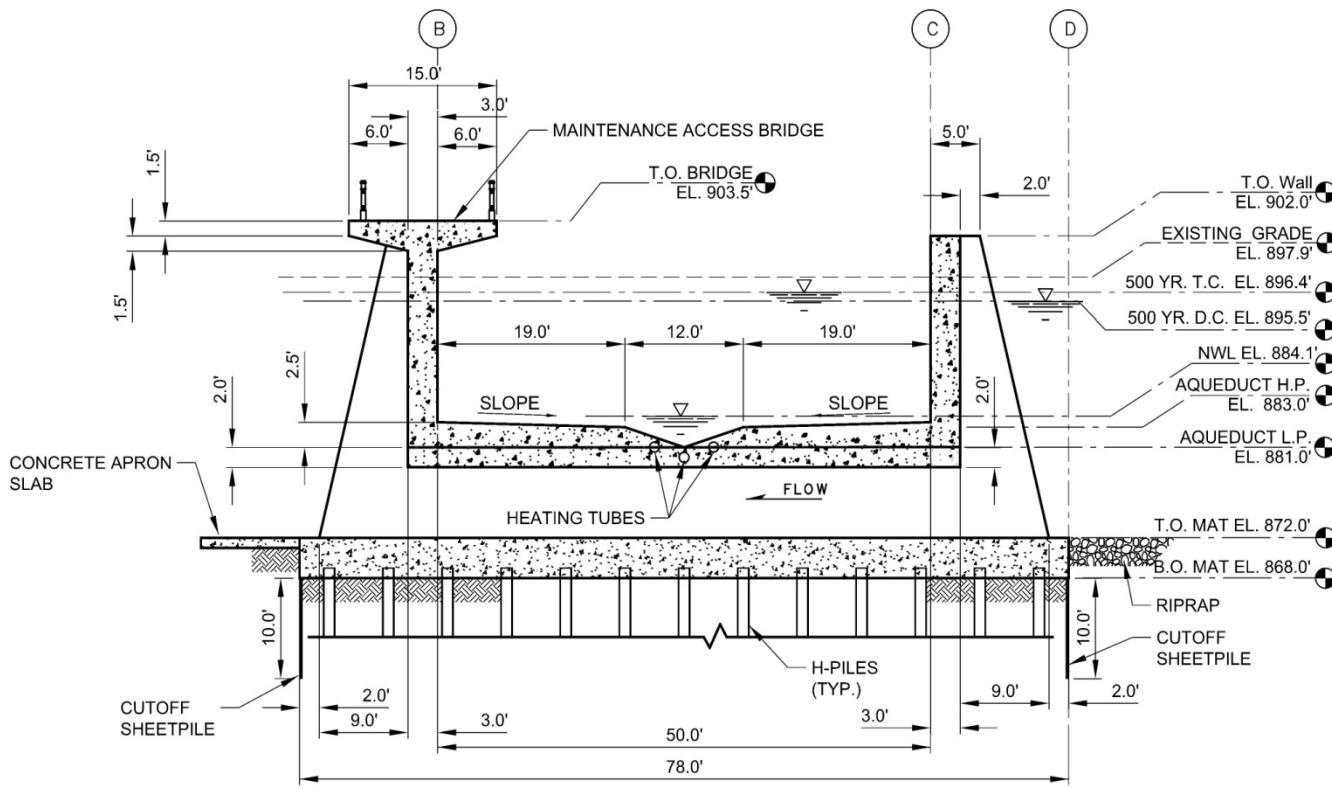
2.3   Aqueducts in cold regions

There are a number of aqueducts in Europe that provide channels for navigation and are in service year-round. All flow completely full throughout the winter season. A few U.S. navigation aqueducts exist. These also flow full in winter or are drained. Below we discuss existing aqueducts that operate in cold regions, and Table 1 summarizes these.

2.3.1   The Lune Aqueduct

The Lune Aqueduct carries the Lancaster Canal and is located in the relatively warm and wet climate near Lancaster, UK (Canal and River Trust 2013a). Cooler winters since 2007 have led to ice formation in the aqueduct in December 2007, February 2009, and January 2010. At these times, the surface ice was 3–4 in. thick and could support occasional foot traffic (T. Churchill, personal communication). Bed ice occurred in 2009 when the canal was dewatered for repairs.

Table 1. Existing cold regions aqueducts.

Aqueduct	Date Built	Trough Material	Width × Depth × Length Height Pier Spacing	AFDD (°F-days) Avg. Max.	Crosses/Canal	Ice Observations/ Design Solutions
Lune Aqueduct, Lancaster, UK	1797	Concrete (originally stone)	20 × 1 × 664 ft 61 ft 70 ft	7 62	Lune River/ Lancaster Canal	Surface floes and ice cover in cold years
Pontcysyllte Aqueduct, Wrexham County Borough, UK	1805	Cast iron	11 × 5.25 × 1000 ft 126 ft 53 ft	27 151	River Dee/ Llangollen Canal	Surface floes in cold years
Briare Canal, Châtillon-sur-Loire, France	1896	Steel	20 × 7 × 2170 ft 85 ft 40 ft	76 254	Loire River/ Loire to Briare Canals	Sluices to allow emptying during severe freezes
Magdeburg Water Bridge, Magdenburg, Germany	2003	Steel and concrete	111 × 14 × 3000 ft 295 ft 347 ft	307 900	Elbe River/ Elbe-Havel Canal to Mittland Canal	Air bubblers prevent ice formation on surface and bed
Hennepin Canal Aqueducts, IL, USA	1907	Reinforced concrete	50 × 6 × up to 350 ft various heights 35 ft	1675 2244	7 creeks and the Green River/ Hennepin Canal	Solid cover, flows full in winter
Maple River Aqueduct, MN, USA	Proposed-	Concrete and rebar	50 × 21 × 250 ft 9 ft 30–35 ft	2293 3592	Red River Diversion Channel/ not navigable	-

Figure 4. Shallow water divers at Lune Aqueduct,
9 January 2010 (Taylor 2010).

2.3.2 The Pontcysyllte Aqueduct

The Pontcysyllte Aqueduct, which crosses the River Dee in the UK, was built for and saw heavy use for coal and limestone transport during the industrial revolution and is currently used only for tourist navigations (Canal and River Trust 2013b). The UK experienced severe winters in 2010 and 2011, and surface ice completely covered the aqueduct in January 2010. Most locals had never seen ice on the aqueduct before. The ice condition at the bed is unknown. Ice floes were also observed in 2011 in early winter (Figure 5) (T. Churchill, personal communication).

Figure 5. Pontcysyllte Aqueduct, 3 December 2010.

2.3.3 Briare Aqueduct

The Briare Aqueduct (*le pont canal de Briare*) (Figure 6) carries the navigable Loire Canal across the Loire River to the Briare Canal in France (Ligerien 2013). The Briare Aqueduct was designed and built with four sluice gates in each end to allow emptying of the aqueduct to protect the structure from expansion in the case of severe freezing. The aqueduct was closed to navigation in February 2012 after 4 in. of surface ice formed.

Figure 6. Briare Aqueduct (Clair 2006).

2.3.4 Magdeburg Water Bridge

The longest aqueduct in Europe is the Magdeburg Water Bridge (Saschen-Anhalt 2013) located in Germany (Figure 7). Though construction began pre-World War I, most construction occurred from 1999–2002, making it one of the newest aqueducts in Europe. The Magdeburg Water Bridge crosses over the Elbe River and connects the Elbe-Havel Canal to the Mittellandkanal, providing access from Berlin's inland harbor to the Rhine River. Intended to flow full throughout the year and to manage large barges, the aqueduct was built with an air bubbler system to prevent freezing at the surface and at the bottom of the aqueduct.

Figure 7. Magdenburg Water Bridge, Germany.

2.3.5 Hennepin Canal aqueducts

The Hennepin navigation canal is located in central Illinois. Completed in 1907, it was intended for navigation; but improvements on the Illinois and Mississippi waterways soon made it obsolete. Therefore, it was used for recreation from the 1930s to 1950s (IDNR 2013). There were originally nine aqueducts along the canal. Historically, the canal flowed full throughout the winter and thick surface ice covers formed. The ice that formed in the canal was removed and sold to support the canal maintenance costs. No wintertime problems due to ice have been reported recently.

Figure 8. Hennepin Canal (Conro 2011).
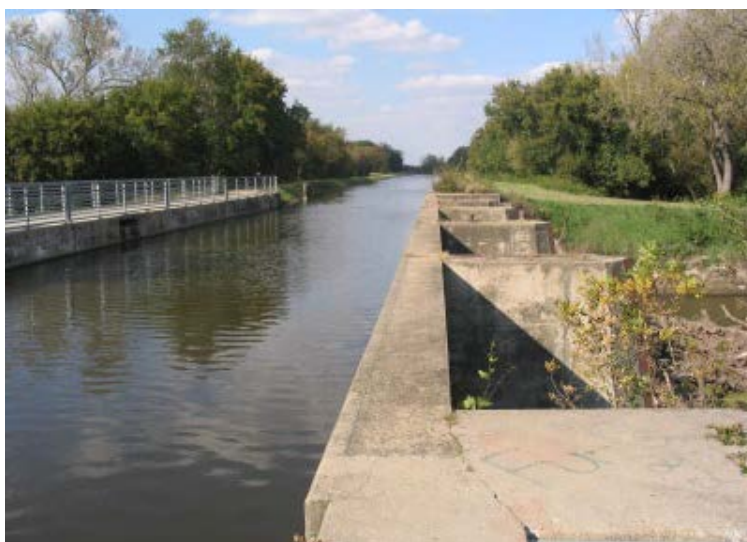
2.3.6 Other U.S. open canal aqueducts

Historically, most other U.S. open water aqueducts in cold regions were drained and closed during the winter months, including aqueducts along the New York Erie Canal, the Indiana Wabash and Erie Canal, and the Illinois and Michigan Canal (Rochester Public Library 2013; Wabash and Erie Canal Park 2009). The ice harvested from these canals in the late 19th to early 20th century was a source of income, but the loss of commerce during the closed winter months and competition from the burgeoning railroad industry, which operated year-round, contributed to the economic failure of many of these canals (Canal Corridor Association 2013).

Figure 9. Erie Canal Aqueduct over the Genesee River in 1908–1910 drained of water for the winter (Sadowski 2012).

From the Albert R. Stone Negative Collection, Rochester Museum & Science Center, Rochester, N.Y.

3 Hydrology and Meteorology

3.1 Data

The Maple River flow data was recorded at two USGS (United States Geological Survey) gages (Gage 05060000 MAPLE RIVER NR MAPLETON, ND, located about 14 RM upstream of the Maple River Aqueduct and Gage 05060100 MAPLE RIVER BL MAPLETON, ND, located about 7 RM upstream). Gage 05060000 recorded from April 1944 to September 1958. Gage 05060100 recorded from October 1958 through September 1975 when it was discontinued. The gage was restarted in March 1995 and has recorded through the present (USGS 2013). As a result, data for the Maple River is available for two periods of time, 1944 through 1975 and 1995 through the present, with a twenty year gap in between. In reviewing the winter flow data, the records for Gage 05060000 and Gage 05060100 were combined. It is immediately obvious that there is a notable difference in the magnitudes of the low winter flows between the two time periods of data (1944–1975 and 1995–2013). For the period 1944–1975, while their records did not overlap, both gages display consistent and lower winter discharges than the Gage 05060100 recorded after 1995. The cause of these changes is not immediately apparent. They may be due to changes in the data collection procedures or other factors, such as modifications to upstream drainage systems, land use changes, sedimentation, and climatic variation (Rahman and Lin 2013).

Temperature and precipitation data was recorded at the Fargo Hector International Airport (GHCND: USW00014914 and WMO: 727530), which is located about 6 miles east-southeast of the Aqueduct. Data is available for January 1948 through May 2013 (NCDC 2013). Average daily temperatures, including calculation of AFDD, were used in the analyses described below unless otherwise indicated.

3.2 Maple River winter flows

Flows in the Maple River typically decline throughout the fall and winter (Figure 10). The winter discharge can show some variation; but often the river is in recession, and the discharge is monotonically decreasing. The

average daily discharge typically drops from 50 cfs at the beginning of December to a minimum of about 10 cfs in late January to mid-February. The historical extreme lows of daily discharges are in early to mid-March when the daily discharge can drop to near zero. On average, the flow typically increases near the beginning to middle of March. In some years, the increase in flow can be rapid. To provide an overview of the flows expected in winter, Figures 11–13 show the annual exceedance probabilities for the flows recorded on the first day of each of the winter months (January through March). Table 2 summarizes the data in these figures. We used the entire period of record to calculate the exceedance probabilities. Because many days during the winter have zero flows, we applied the conditional probability adjustment describe in Appendix 5 of Bulletin 17B (USGS 1982).

Figure 10. Range of daily winter flows in the Maple River for 1995–2012.
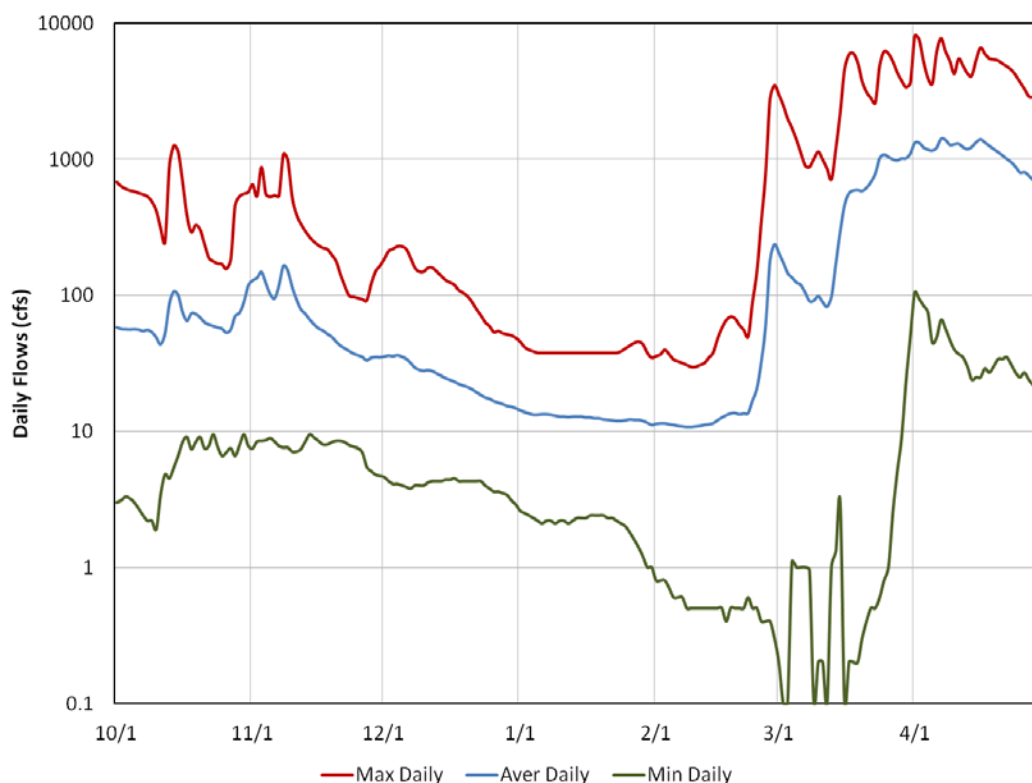
Figure 11. The 1 January flow frequencies at Mapleton.
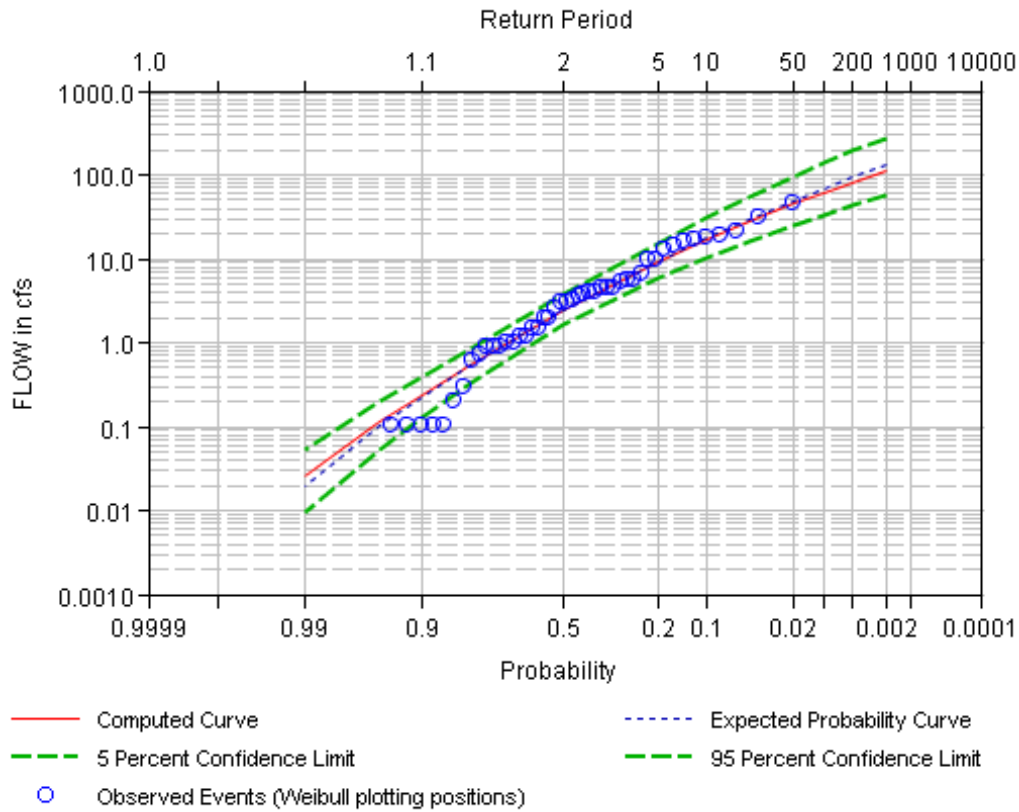
Figure 12. The 1 February flow frequencies at Mapleton. Symbols and lines are the same as for the above figure.
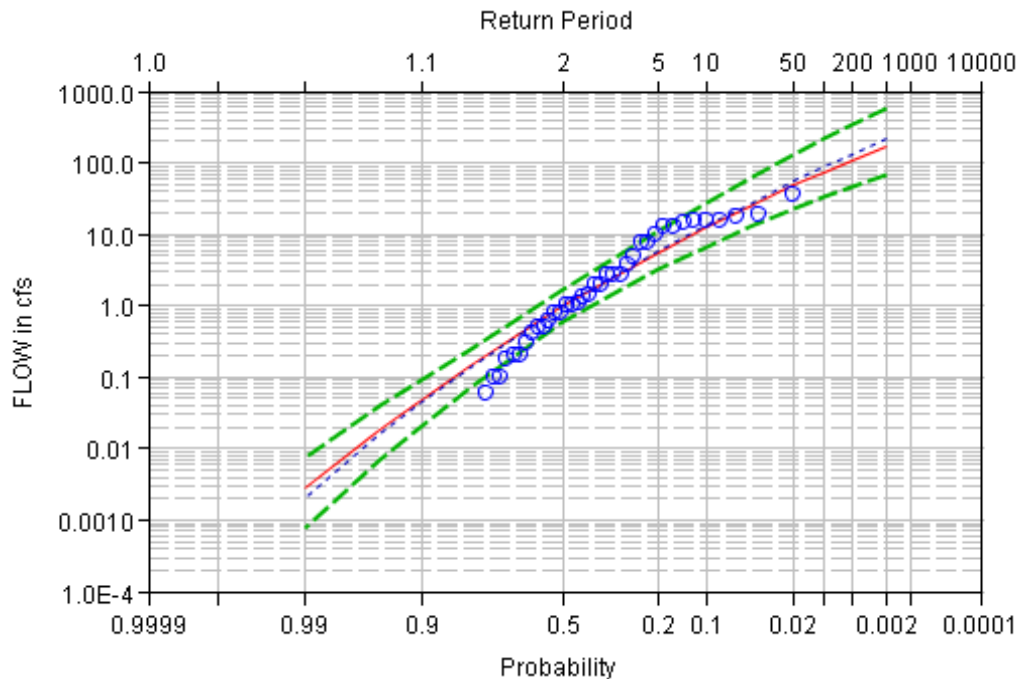
Figure 13. The 1 March flow frequencies at Mapleton. Symbols and lines are the same as for the above figures.
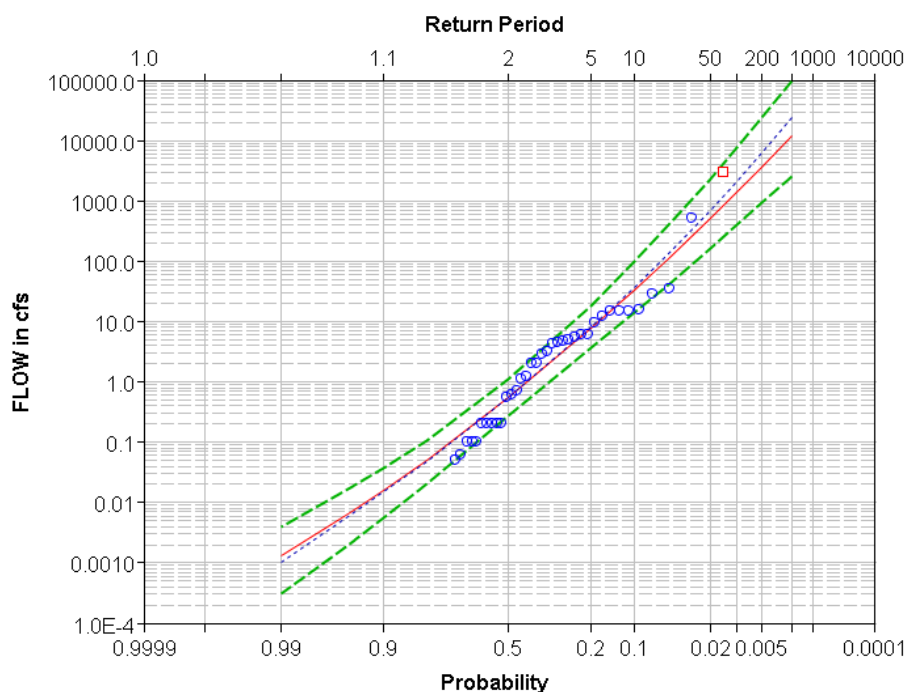
Table 2. Summary of frequency analysis for first-of-month flows (cfs).

	Return Period (years)				
	2	10	20	50	100
1 January	2.4	16.9	27.2	44.8	61.4
1 February	1	12.8	24.4	48.5	74.8
1 March	1.8	60.8	198.0	822.5	2252

3.2.1 Trends in monthly flows

In reviewing the two periods of discharge records (1944–1975 and 1995–2013), it was apparent that there was both a quantitative and a qualitative difference in the discharge regimes between the two periods. As a result, we reviewed the trends with time of the monthly discharge for each winter month. Figure 14 shows monthly average flow through time for both periods of records along with a 5-year moving average. A small increasing trend is apparent in the 1944–1975 data, ranging from 0.02 to 8.0 cfs/year (Table 3).

For the 1995–2013 data, the trend is positive for some months and negative for others. For the entire period of record, the trends are increasing

from 0.25 to 8.0 cfs/year. It is clear from Table 4 that the flow rate jumped between the two data sets, with an increase of the average monthly flow of about 29 cfs for February. The difference in flow is less marked in the higher flow period of March.

Figure 14. Monthly average flow and 5-year running average.
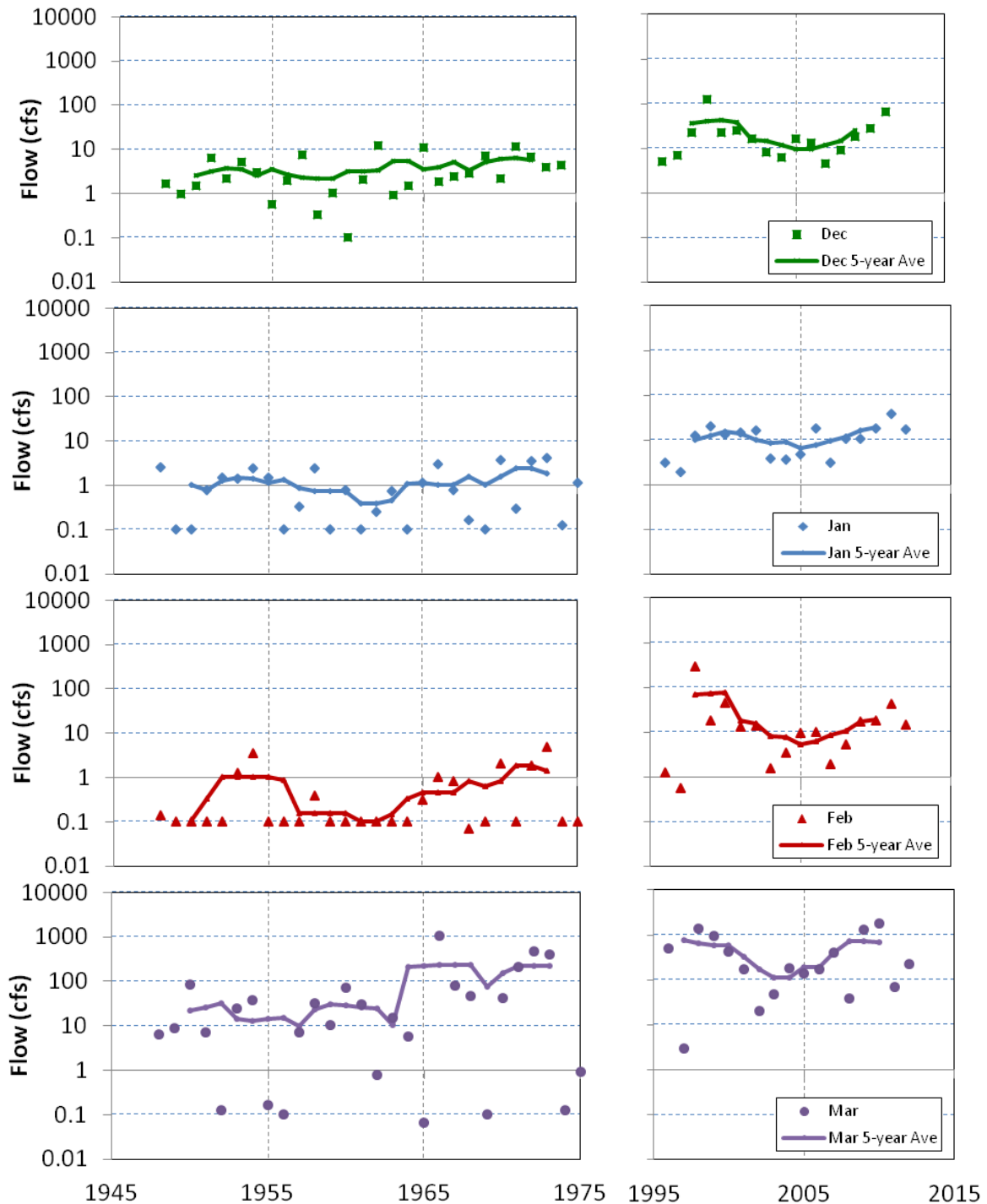
Table 3. Trends in average monthly Maple River flows with time over different periods.

Month	Slope (cfs/year)		
	1944–1975	1995–2013	1944–2013
December	0.1439	−0.1467	0.4517
January	0.0294	0.7922	0.2573
February	0.0354	−3.4784	0.5503
March	8.4120	−4.7380	8.1025

Table 4. Maple River monthly average flows over different time ranges.

Month	Average of Monthly Averages (cfs)		
	1944–1975	1995–2013	1944–2013
December	3.8	24.5	11.8
January	1.2	12.6	5.5
February	0.6	29.7	11.6
March	94.2	486.8	242.6

Over the entire period of record, these results show an overall increase in monthly flow rates with time. Others have noted similar increases in this region (see, for example, Novotny and Stefan 2007).

3.2.2 Winter flow recession

The flow in the Maple River is generally in recession during the winter months when ice is likely to form. During this time, the air temperatures remain below freezing (32°F). There is little to no liquid precipitation or snowmelt available for runoff, and the flow in the river derives from water draining from unfrozen soil and ground-water layers. Figure 15 shows flows in the Maple River during recession periods. We determined the recession periods by reviewing the data records. The recession follows the last peak of 50 cfs or less in the fall and continues until the flow is sustained at a constant value or begins to increase. In Figure 15, the daily flows have been normalized by flow at the start of the recession period. This figure also shows the best-fit exponential curve. We found that the length of time for recession varies between the two periods, with values of near 105 for 1944–1975 and near 45 for 1995–2013 (Figure 16).

Figure 15. Recession behavior of the Maple River (1996–2013).
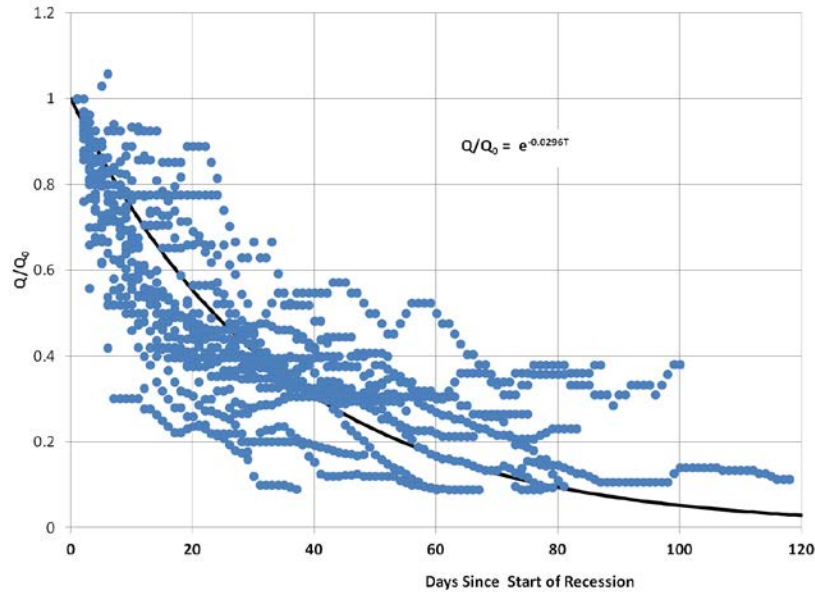
Figure 16. Length of recession flow and days meeting simulation requirements.
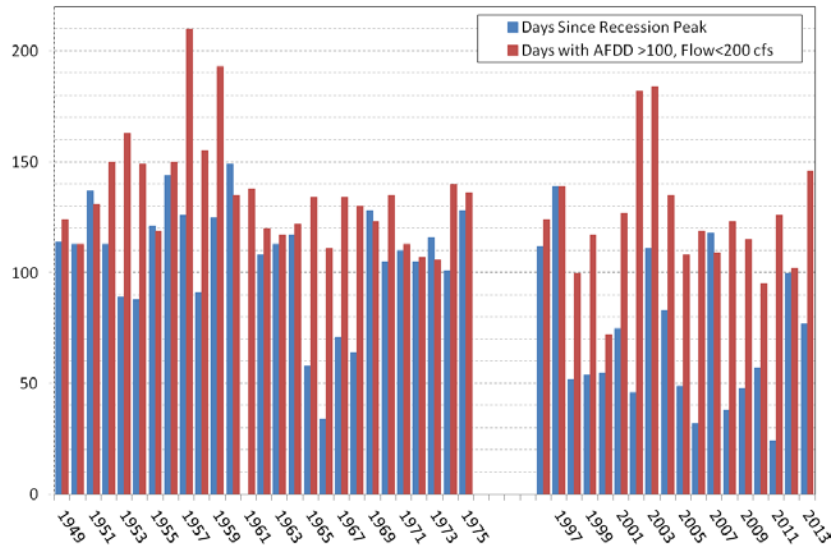
3.3 Winter air temperatures

An analysis of winter temperatures near the Maple River Aqueduct indicates that the lowest temperatures occur in the end of January, with a typical range of 0°F to 20°F and extremes ranging from −35°F to just above 40°F (Figure 17). The average temperature generally remains below freezing from mid-November to mid-March. Daily average highs are typically below freezing from early December to early March.

Figure 17. Temperature statistics (°F) for each day of the winter season based on observations during 1948–2013.
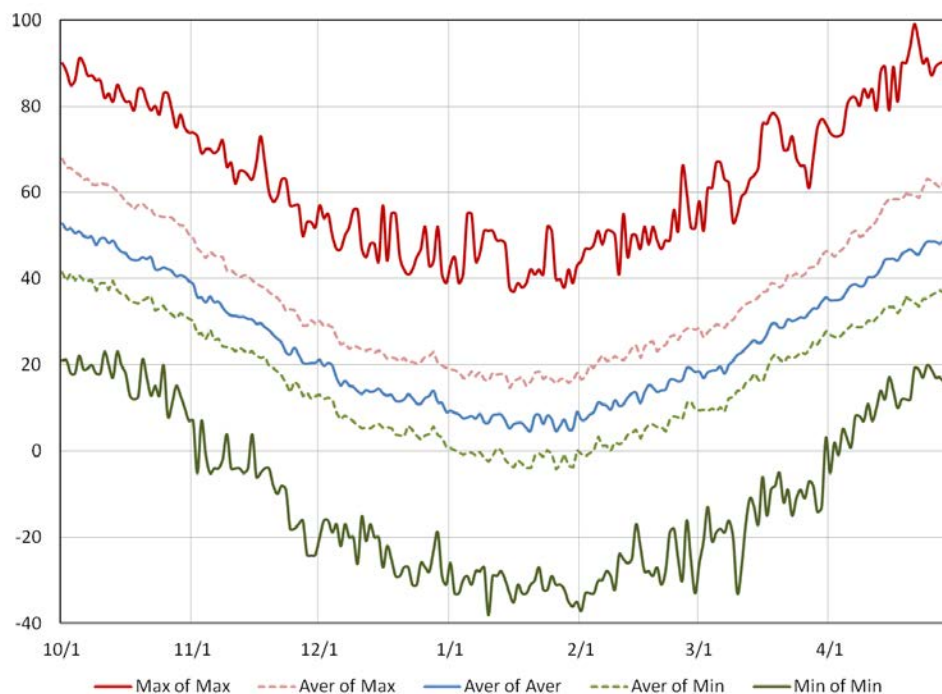
An analysis of the area's long-term temperature trends examined monthly temperature averages for each winter month. The temperature data displays an upward trend in winter temperatures, which appear to be more extreme during the colder months of January and February. The magnitude of linear fits to the 5-year moving average of temperature ranged from 0.397°F to 1.11°F per decade for the 60 years of record (Table 5). No notable trend in the average of maximum AFDD for each of the three periods (1944–1975, 1977–1995 when no flow data was taken, and 1995–2013) was apparent (Table 6).

Table 5. Linear slope of increasing trend in temperature data at Fargo, 1948–2013.

Month	Increase (°F/decade)
November	0.397
December	0.545
January	1.111
February	0.516
March	0.707
April	0.505

Table 6. Maximum AFDD for periods of record.

Year	Maximum AFDD (°F-days)	Year	Maximum AFDD (°F-days)	Year	Maximum AFDD (°F-days)
1944–1976		1977–1995		1996–2013	
1949	2754	1977	2731	1996	3044
1950	3078	1978	3176	1997	3156
1951	3030	1979	3592	1998	1542
1952	2819	1980	2399	1999	1723
1953	1813	1981	1784	2000	1495
1954	2083	1982	2952	2001	2766
1955	2334	1983	1559	2002	1561
1956	3165	1984	2337	2003	2286
1957	2318	1985	2361	2004	2089
1958	1683	1986	2676	2005	1896
1959	2508	1987	1359	2006	1576
1960	2370	1988	2032	2007	1876
1961	2045	1989	2598	2008	2534
1962	2630	1990	1991	2009	2731
1963	2332	1991	2011	2010	2006
1964	2026	1992	1587	2011	2661
1965	3338	1993	2450	2012	1086
1966	2656	1994	2624	2013	2283
1967	2689	1995	1889	2013	2283
1968	2200				
1969	2749				
1970	2587				
1971	2535				
1972	2693				
1973	2105				
1974	2700				
1975	2211				
1976	2094				
Average	2484		2321		2136

Because the most ice is expected to grow during periods of intense cold, we analyzed 1-, 3-, 5-, 10-, and 30-day periods of intense cold (Table 7). Appendix C details in ranked tables the average flow and the AFDD at the start of the intensely cold period for each intense cold period for each winter. About half of the top-ten intense cold periods were recorded between

1975 and 1995 when there was no flow record. The other half of the 10 most intense cold periods occurred in 1996–2013. Figure 18 shows frequency plots of the periods of intense cold determined using Weibull plotting positions and assuming a normal distribution. The results are summarized in Table 8.

Figure 18. Frequency analyses for periods of intense cold.
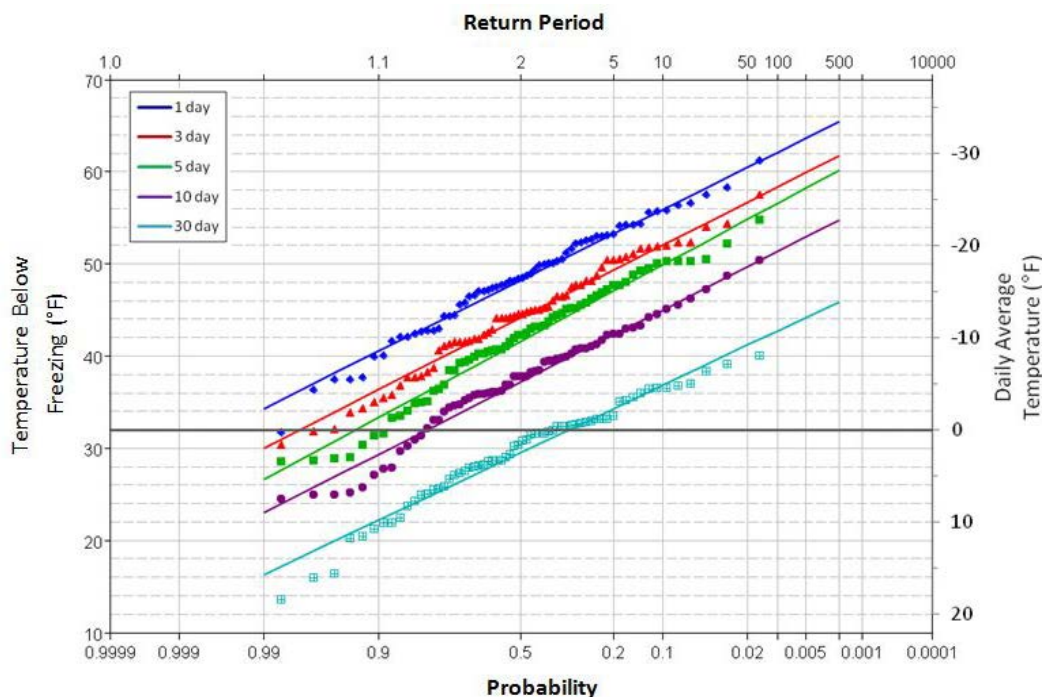
Table 7. Most severe periods of intense cold.

Period Length (Days)	Water Year	Date	Average Temperature (°F)	Average Flow (cfs)	AFDD (°F-days)
1	1996	2/1	−29.5	1.0	1612
3	1996	2/1–2/3	−27.7	1.0	1730
5	1996	1/30–2/3	−24.5	1.2	1730
10	1996	1/25–2/3	−18.8	1.6	1730
30	1982	1/7–2/5	−7.7	-	1617

Table 8. Summary of frequency analysis for intense low temperature (°F) periods.

Period Length (Days)	Return Period (years)				
	2	10	20	50	100
1	−3.93	−8.55	−11.18	−16.21	−30.12
3	0.35	−4.36	−7.05	−12.18	−26.37
5	3.59	−1.38	−4.21	−9.63	−24.6
10	7.39	2.67	−0.02	−5.17	−19.39
30	14.16	9.77	7.27	2.48	−10.75

4   Aqueduct Flow and Ice Simulation Model

4.1   Introduction

To quantify the volume of ice that may form in the aqueduct, it is necessary to determine the flow conditions in the aqueduct throughout the winter. Bed ice and surface ice form only in the areas of the aqueduct covered by flow. As the ice grows, it modifies the channel geometry. This changes the water surface elevation throughout the aqueduct and controls the areas of the aqueduct where ice forms. There is an interaction between the ice growth and flow that impacts both processes. It is difficult to assess the ice formation process without accounting for this interaction. Specifically for this report, we developed a hydraulic model of the aqueduct that estimates bed and surface ice growth and accounts for the interaction between the ice and the flow.

The Aqueduct Flow and Ice Simulation Model (AFISM) contains five modules:

- The Flow Module calculates, based on the discharge and the ice conditions, the water surface elevation throughout the aqueduct.
- The Water Temperature Module estimates, based on the balance between the heat flux supplied by the heaters in the low-flow channel and the heat loss at the surface to the ice cover or to the open air if no ice is present, the water temperature throughout the aqueduct.
- The Surface Ice Module calculates, based on the heat loss from the surface to the atmosphere and any heat gain from the water below, the ice growth at the water surface. There must be sufficient space beneath the ice cover to allow growth to occur.
- The Bed Ice Module estimates the ice growth, caused by heat transfer through the structure of the aqueduct to the frigid air, on submerged portions of the aqueduct bed. There must be sufficient submerged depth above the bed ice to allow growth to occur.
- The Ice Interaction Module keeps track of the surface ice and bed ice at each location. If the surface ice contacts the bed ice, then this module combines both together. The bed ice is increased by the surface ice thickness and the surface ice thickness is set to zero at that time step.

4.2   Flow Module

The winter flow through the aqueduct during periods of sub-freezing air temperatures will be relatively small and steady or declining in magnitude. Rapid changes in flow are not recorded during the winter. Rapid changes in flow are only observed when the air temperatures rise to above freezing and ice formation is no longer possible. Given these flow conditions during the ice formation period, we decided to model the flow in the aqueduct using the standard step method for varied flow computations. This method starts at the downstream end of the aqueduct at each time step and uses the recorded discharge for that time. We use a rating curve developed from the HEC-RAS model to estimate the downstream water-surface elevation. The standard step method estimates the next upstream water-surface elevation, Y_2, based on the following procedure:

1. The channel conveyance, K_1, is determined at the downstream section along with the downstream water velocity, U_1. K_1 is estimated as

$$K_1 = \frac{1.486}{n_{eff\,1}} A_{f1} R_1^{2/3} \tag{1}$$

where

$\quad n_{eff}$ = the effective Manning's n value,
$\quad\;\; A_f$ = the effective flow area,
$\quad\;\; R$ = the hydraulic radius of the flow.

U_1 is estimated as

$$U_1 = \frac{Q_j}{A_{f1}} \tag{2}$$

where Q_j is the flow rate on day j. The presence of ice is accounted for in determining n_{eff}, A_f, and R. Areas blocked by bed ice or surface ice beneath the water-surface elevation are assumed to be unavailable to flow. The underside of the ice is included in the wetted perimeter estimation and the hydraulic radius is modified.

2. The upstream water surface elevation, Y_2, is assumed to be equal to the downstream water surface elevation, Y_1. The channel conveyance and flow velocity are estimated using the same procedures as in equations (1) and (2) above.

3. The friction slope, $\overline{S}_f$, and the head losses, h_e, between section 1 and 2 are estimated as

$$\overline{S}_f = \left(\frac{2Q_j}{K_1 + K_2} \right)^2 \qquad (3)$$

$$h_e = L_{xs}\overline{S}_f + C \left| \frac{\alpha_2 U_2^2}{2g} - \frac{\alpha_1 U_1^2}{2g} \right| \qquad (4)$$

where

L_{xs} = the distance between cross sections,
g = the acceleration of gravity,
α_1 and α_2 = the velocity weighting coefficients,
C = the expansion or contraction coefficient.

4. The water surface elevation at section 2 is then estimated using the energy equation

$$Y_{2\_calc} = Y_1 + \frac{\alpha_1 U_1^2}{2g} + h_e - \frac{\alpha_2 U_2^2}{2g} . \qquad (5)$$

5. If $|Y_2 - Y_{2\_calc}| < 0.01$ ft, then the water level at section 2 is assumed to be known. If not, $Y_2 = Y_2 + 0.70(Y_{2\_calc} - Y_2)$ and the steps 1 through 4 are repeated.

6. If the water levels do not agree the third time, then the secant method, as described in USACE (2010), is used to estimate the upstream water level. The secant method is repeated for a total of ten times if necessary. If the water-surface elevations do not balance at that time, then the water surface elevation is assumed to be the average of the last two estimations.

The above procedure is repeated until the water surface elevation has been estimated for every cross section from the downstream to the upstream end of the aqueduct. This procedure is repeated for each day of the winter season.

4.3   Water Temperature Module

We estimated the water temperature starting with the complete flow equations for one dimensional flow and considered the flow in only the low-flow channel. The water temperature, T_w, for an open channel is estimated as

$$\frac{\partial T_w}{\partial t} + U\frac{\partial T_w}{\partial x} = \frac{\partial}{\partial x}\left(\psi\left(\frac{\partial T_w}{\partial x}\right)\right) + \frac{Bh_{wa}\left(T_a - T_w\right)}{\rho C_p A_f} + \frac{Fw_f}{\rho C_p A_f} \tag{6}$$

where

ψ = the longitudinal dispersion coefficient,
x = distance along the channel,
t = time,
B = the surface top width,
P = water density,
C_p = the water heat capacity,
A_f = the flow area,
F = the flux from heaters through the bed of the low-flow channel into the flow,
w_f = the wetted area of the low-flow channel that is heated,
T_a = the air temperature,
h_{wa} = the water to air heat transfer coefficient.

The water temperature for an ice covered channel is

$$\frac{\partial T_w}{\partial t} + U\frac{\partial T_w}{\partial x} = \frac{\partial}{\partial x}\left(\psi\left(\frac{\partial T_w}{\partial x}\right)\right) + \frac{Bh_{wi}\left(T_m - T_w\right)}{\rho C_p A_f} + \frac{Fw_p}{\rho C_p A_f} \tag{7}$$

where

T_m = the ice/water interface temperature (32°F),

h_{wa} = the water to ice heat transfer coefficient.

Typical assumptions that the flow temperature does not vary with time at any location and that the longitudinal dispersion effect is small compared to convection lead to the following estimates for water temperature (Gosink 1986) in the aqueduct for open channel flow

$$T_z = T_0 + \left(\frac{Fw_p}{h_{wi}B} - T_0 + T_a \right) \left(1 - e^{-\frac{h_{wa}z}{\rho C_p Ud}} \right) \tag{8}$$

and ice covered flow

$$T_z = T_0 + \left(\frac{Fw_p}{h_{wi}B} - T_0 + T_m \right) \left(1 - e^{-\frac{h_{wi}z}{\rho C_p Ud}} \right) \tag{9}$$

where

T_z = the downstream temperature at a distance z,
T_0 = the upstream water temperature,
d = B/A_f.

The water-to-ice heat transfer coefficient is estimated using the standard approach for large channels (Ashton 1986)

$$\mathrm{Nu} = c\, \mathrm{Re}^{0.8}\, \mathrm{Pr}^{0.4} \tag{10}$$

where

Nu = the Nusselt number, the non-dimensional heat transfer coefficient;
Re = the flow Reynolds number;
Pr = the Prandtl number of the water;
c = a non-dimensional constant.

Expanding these terms arrives at the expression for the water to ice heat transfer coefficient,

$$h_{wi} = \frac{ck_w}{R^{0.2}}\left(\frac{U}{v}\right)^{0.8} \mathrm{Pr}^{0.4} ,$$ (11)

where

k_w = the thermal conductivity,
v = the kinematic viscosity of water respectively. (See Table 10 for parameter values used in study.)

4.4 Bed Ice Module

Bed ice can form on the bed of the aqueduct as a result of heat transfer through the structure of the aqueduct to the frigid air. In this report, we are referring to ice that forms on the bed of the aqueduct as bed ice as op-posed to anchor ice. Anchor ice results from the deposition of frazil ice crystals during periods of supercooled water. The formation of bed ice does not require deposition or supercooling. Unlike anchor ice or deposit-ed frazil ice, bed ice can continue to form and thicken beneath a solid ice cover. Bed ice would not form on sections of the aqueduct low-flow chan-nel that are heated sufficiently to keep the surface temperature at 32°F or higher. Bed ice can only form in portions of the bed of the aqueduct that are covered by flow with a water surface elevation greater than the eleva-tion of the upper surface of the bed ice. As the bed ice grows, new bed ice forms at the upper surface of previously formed bed ice as long as that por-tion of the aqueduct bed remains covered by flow and there is room be-tween the bed ice and the surface ice above. The bed ice analysis starts with estimating the steady-state heat transfer rate, $H_{x\,bed}$, through the bed of the aqueduct, through the insulation on the outside of the aqueduct (if present), and through any bed ice that may be present:

$$H_{xbed} = \frac{g_x\left(T_m - T_b\right)}{\left(\dfrac{\eta_{bed}}{k_i} + \dfrac{L_{cx}}{k_c} + \dfrac{L_s}{k_s}\right)}$$ (12)

where

T_b = the outside surface temperature (assumed to be equal to the air temperature),
η_{bed} = the bed ice thickness,

k_i = the ice thermal conductivity,

L_{cx} = the concrete thickness between the outside surface of the aqueduct and the bed of the aqueduct (measured perpendicularly to the outside surface),

k_c = the concrete thermal conductivity,

L_s = the insulation thickness,

k_s = the insulation thermal conductivity,

g_x = a geometric "enhancement" or modification factor to account for the heat transfer impacts of the shape of the aqueduct. It can be greater or less than one.

Note that the concrete thickness, L_{cx}, and the geometric factor, g_x, both vary with the position across the flume (denoted by x); and as a result, the steady-state heat transfer rate, H_{xbed}, varies with position as well. This steady-state approximation is appropriate to this model given the very large latent heat of ice compared to the heat capacity of the ice, concrete, and insulation. This approximation assumes that behind the slowly moving solidification boundary of the ice, the temperature distribution is equivalent to the steady-state distribution that would occur if the boundary were to be fixed in position at that instant (Crank 1984). This approach, referred to as the "quasi-steady," "pseudo steady-state," "linear temperature profile," or "zero heat capacity" model, is widely used in the field of ice engineering and has seen considerable application for estimating ice thickness through thermal growth. The quasi-steady model can include any number of layers, each with its own thermal properties, to represent the thermal influence of the ice cover, the concrete, and the insulation. The ice growth rate is estimated as

$$\frac{\partial \eta_{bed}}{\partial t} = \frac{H_{xbed}}{\rho_i \lambda} = \frac{g_x\left(T_m - T_b\right)}{\rho_i \lambda \left(\dfrac{\eta_{bed}}{k_i} + \dfrac{L_{cx}}{k_c} + \dfrac{L_s}{k_s}\right)} \tag{13}$$

where

ρ_i = ice density,

λ = the latent heat of ice.

An analytical solution of equation (16) can be found as

$$\eta_{bed\ j+1} = \sqrt{\left(\eta_{bed\ j} + \frac{k_i L_c}{k_c} + \frac{k_i L_s}{k_s}\right)^2 + g_x \frac{2k_i}{\rho_i \lambda}\left(FDD_j\right)} - \left(\frac{k_i L_c}{k_c} + \frac{k_i L_s}{k_s}\right) \qquad (14)$$

where

$\eta_{bed\ j}$ = the bed ice thickness on day j,
FDD_j = the freezing degree days recorded on day j.

4.5 Surface Ice Module

Surface ice can form at the water surface when the heat loss from the ice surface to the frigid air is greater than any heat transferred to the underside of the ice by water warmed by the aqueduct heaters. As the surface ice grows, new ice is formed at the bottom of the surface ice. Heat is transferred from the bottom of the surface ice and through the ice cover to the frigid air. Surface ice can only form in portions of the aqueduct that contain water and where there is sufficient room between the bottom of the surface ice and the bed ice.

The surface ice analysis starts by neglecting the heat that may be added from warm water beneath the surface. The impact of this heat will be estimated next. By neglecting the heat flux from the warm water, we find the classic result that the thickness is proportional to the square root of the AFDD. This approach allows the ice growth parameters that are found empirically based on local data to be included in the overall analysis. The surface ice analysis begins by estimating the steady-state heat transfer rate, $H_{surface}$, through the surface ice:

$$H_{surface} = \frac{k_i}{\eta_{surface}}\left(T_m - T_s\right) \qquad (15)$$

where

T_s = the upper surface temperature of the ice cover (assumed to be equal to the air temperature),
$\eta_{surface}$ = the surface ice thickness,
k_i = the ice thermal conductivity.

This steady-state approximation is appropriate for surface ice growth given the very large latent heat of ice compared to the heat capacity of the ice. The surface ice growth rate is found as

$$\frac{\partial \eta_{surface}}{\partial t} = \frac{H_{surface}}{\rho_i \lambda} = \frac{k_i}{\eta \rho_i \lambda}(T_m - T_s).$$ (16)

Equation (16) has the analytical solution

$$\eta_{surface\ j} = \alpha_{ice} \sqrt{AFDD_j}$$ (17)

where $AFDD_j$ is the Accumulated Freezing Degree Days from the onset of ice formation until day j (USACE 2002). The constant α_{ice} has the nominal value ([24] [3600] is the seconds to days conversion)

$$\alpha_{ice} \approx \sqrt{\frac{2k_i(24)(3600)}{\rho_i \lambda}}.$$ (18)

However, α_{ice} is usually determined by empirically using observed ice thicknesses and AFDD's throughout the winter season. Typically, the empirically determined value, $\widehat{\alpha}_{ice}$, is less than the nominal value due to the thermal insulation provided by snow cover on the ice, air bubbles in the ice, and other effects. Equation (16), modified to account for the possibility of a heat flux from beneath, is

$$\frac{\partial \eta_{surface}}{\partial t} = \frac{\widehat{\alpha}_{*ice}^2}{2\eta}(T_m - T_s) - \frac{h_{wi}(z)}{\rho_i \lambda}(T_w - T_m)$$ (19)

where

$$\widehat{\alpha}_{*ice} = \frac{\widehat{\alpha}_{ice}}{\sqrt{(24)(3600)}}.$$ (20)

Unfortunately, equation (19) does not have an analytical solution. It is solved using a fourth-order Runge-Kutta discretization.

4.6   Ice Interaction Module

The ice interaction module keeps track of the surface ice and bed ice at each location. If the surface ice contacts the bed ice, then this module combines both together. The bed ice is then increased by the surface ice thickness and the surface ice thickness is set to zero at that time step. The surface ice is assumed to float at its hydrostatic equilibrium, and the bed ice is assumed to remain fixed to the bed.

4.7   Model operation

AFISM runs as shown in Figure 19. We designed the simulation to run over the entire winter season. Each year was started on 01 October, and the model progressed in daily time steps. The model used the recorded daily air temperature and river discharges. As the season progressed, AFISM calculated the AFDD's based on the recorded air temperature. AFISM did not allow ice formation to occur in the aqueduct until the $AFDD_{min}$ of 100 AFDD's was met. We ended the simulation each winter after the AFDD were greater than 1000 and the flow equaled or exceeded 300 cfs.

Figure 19. The Aqueduct Flow and Ice Simulation Model flow chart.
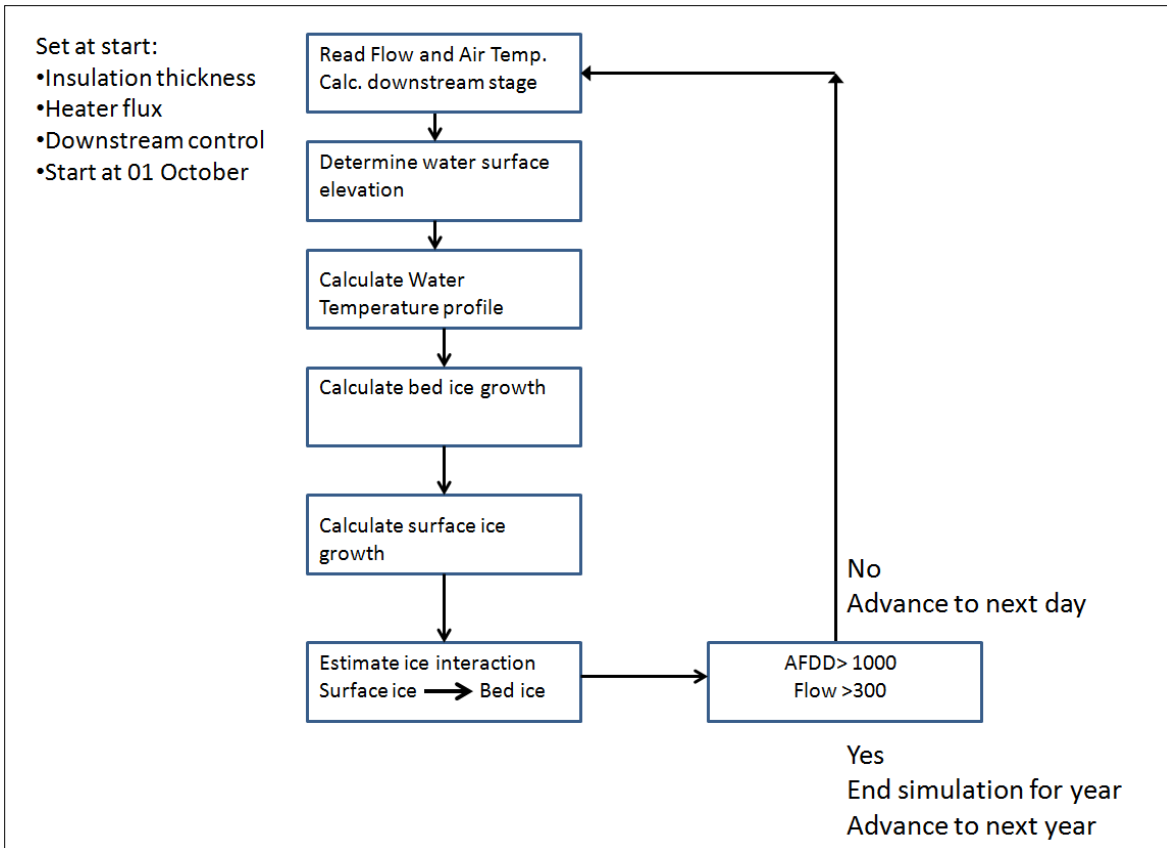
5   HEC-RAS Model

The flows in the aqueduct, the upstream and downstream realigned chan-
nels, and the Maple River were simulated with HEC-RAS (USACE 2011).
The HEC-RAS simulation was used to estimate the water surface profile
through the aqueduct during ice-free periods; to develop open-water and
ice-influenced rating curves at the downstream end of the aqueduct; to es-
timate the impact of ice formation in the aqueduct on water levels up-
stream at the location of the overflow weir spillway; and to verify the water
surface profiles of AFISM.

The reach of the Maple River that we modeled extended from the mouth of
the Maple River on the Sheyenne River to approximately 16,000 feet up-
stream of the aqueduct at the location of USGS Gage 05060100. The exist-
ing channel geometry for this reach of the Maple River had been previous-
ly developed by the St Paul District (A. Buesing, personal communication).
We revised this channel geometry to include all of the portions of aqueduct
structure system (including the aqueduct, upstream realigned channel,
downstream realigned channel, and the spillway control weir) except for
the spillway downstream of the spillway control weir (Figure 20). The
downstream boundary condition for the HEC-RAS model was a rating
curve that was developed for both open water and ice covered conditions
upstream of the mouth of the Maple River at the Sheyenne River. Man-
ning's n value was set to 0.04 through the aqueduct to represent rough-
ness due to fish passage elements and was set to 0.06 downstream of the
aqueduct to represent roughness elements that would likely be added to
smooth out water-surface elevations through the aqueduct. All other Man-
ning's n values were left as in the original model.

In general, given the mild channel slopes, the flow in the Maple River, rea-
ligned channels, and the aqueduct is subcritical. However, HEC-RAS was
run in mixed mode (to simulate both subcritical and supercritical flows)
because of a specific flow situation. At very low flows there is a sharp drop
in the water surface profile along the length of the aqueduct. Low flows
approach critical at the downstream end of the aqueduct. This is partly due
to the raised thalweg elevation of the aqueduct compared to the realigned
channels (Figure 21). In effect, the aqueduct acts like a broad crested weir

with the weir crest equal to the length of the aqueduct. This drop at the downstream end of the aqueduct is also partly due to the flow expansion caused by the downstream transition of the aqueduct. The original aqueduct design called for a very short transition from the aqueduct channel to the realigned channel with a width expansion ratio of 1:1. General hydraulic practice calls for transitions that are at least 1:4 (4 times longer than one half the width of the channel) (Henderson 1966). This gentler transition was used in the HEC-RAS geometry to reduce the steepness of the water elevation jump at the downstream end of the aqueduct. Figure 21 shows an example of the water surface profiles through the aqueduct at very low flows. The sharp drop near the downstream end of the aqueduct is clearly evident. Figure 22 shows the stage discharge curves for the upstream, midpoint, and downstream end of the aqueduct for a range of low discharges (less than 120 cfs). Again, the drop near the downstream end of the aqueduct is clearly evident.

Figure 20. HEC-RAS geometry at the Maple River Aqueduct.
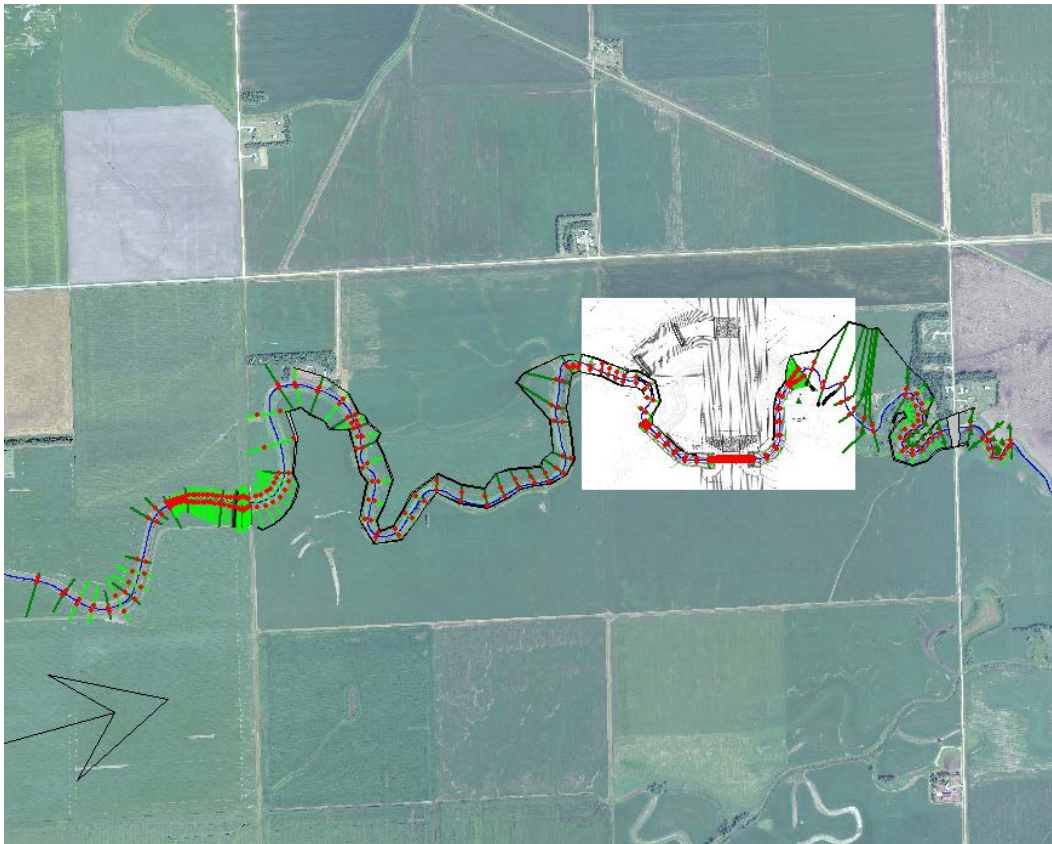
Figure 21. Open water surface profile through the aqueduct at 1, 5, and 10 cfs.
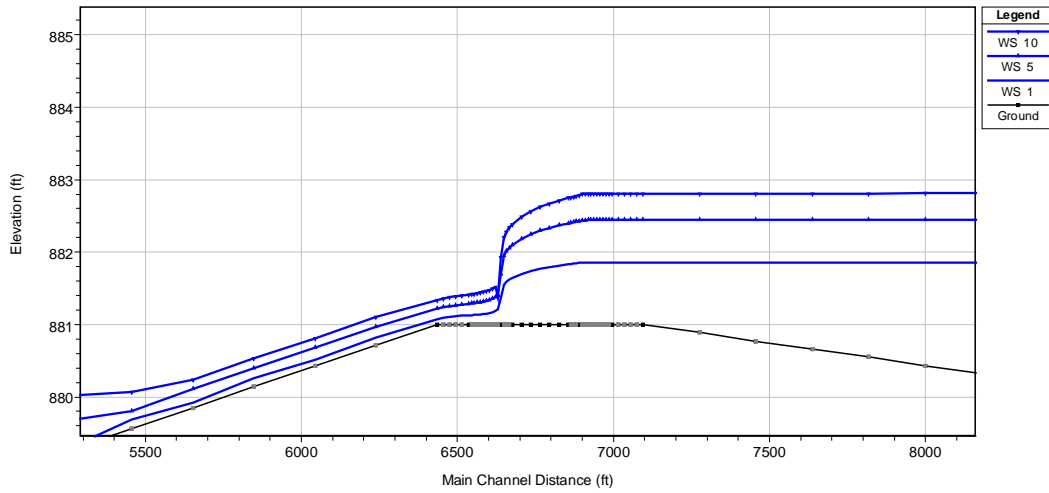
Figure 22. Open water flow depth vs. discharge at three locations along the aqueduct.
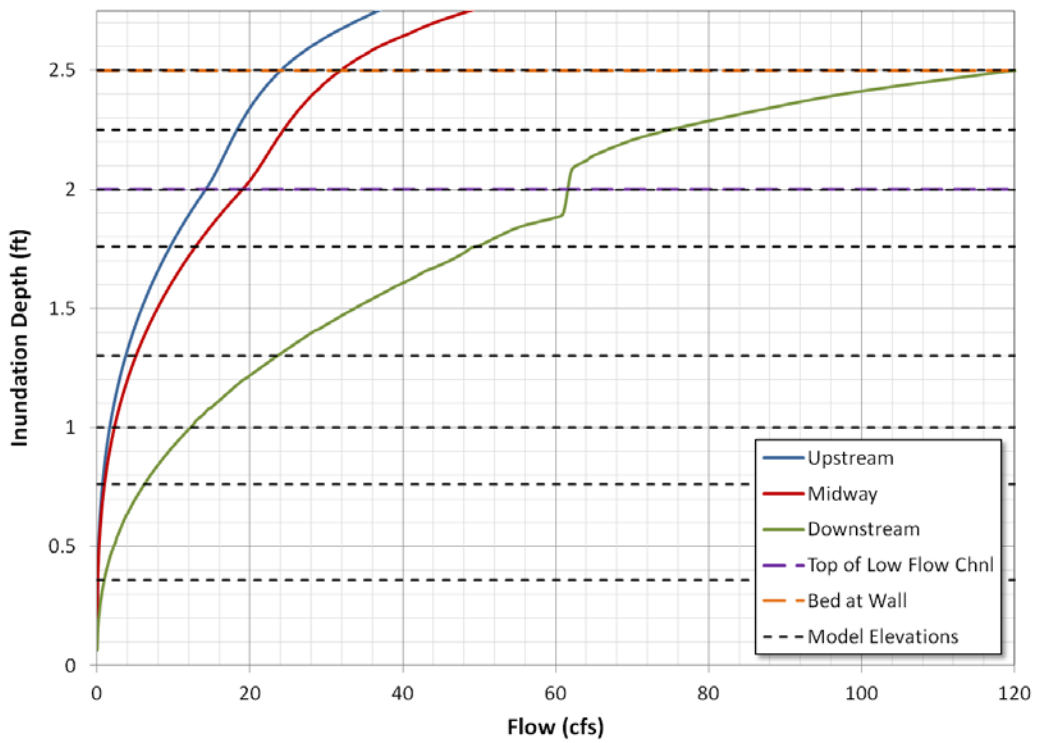
6 2-D Finite Element Thermal Model

We developed a 2-D finite element heat conduction mesh of the aqueduct to use in a commercial 2-D thermal conductivity model (Geo-Slope International 2012). The mesh described a typical cross section of the aqueduct (Figure 23). To analyze the impact of insulation, we modified the mesh to include insulation installed on the outside of the aqueduct (Figure 24). We assumed that the thermal conductivity of the aqueduct was to equal that of concrete. (See Table 10 for parameter values used in the study.) We applied the 2-D finite element heat conduction model in two ways. The first was to support the Bed Ice Module of AFISM by calculating the geometric enhancement factors to account for the impact of the geometry of the aqueduct on the heat conducted through the aqueduct bed. Once determined, we used the geometric enhancement factors in the Bed Ice Module to estimate the bed ice that would form during the simulations. The second application of the 2-D finite element heat conduction model was to investigate the application of heating elements in the bed of the aqueduct to reduce ice formation.

Figure 23. A thermal model of the aqueduct structure. Blue nodes represent inundated area for the specific run while red nodes indicate areas that are exposed to the ambient air temperature.
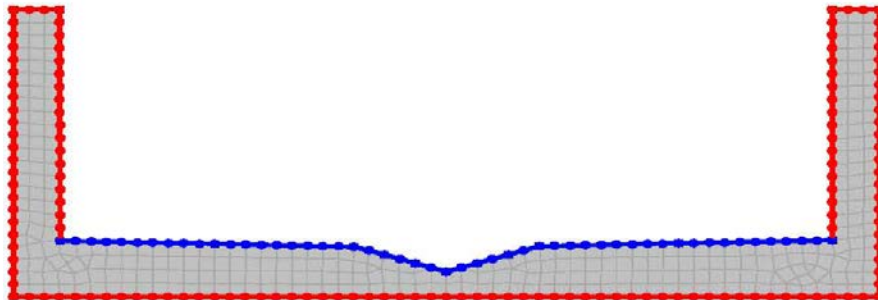
Figure 24. A thermal model of the aqueduct structure with insulation applied. Yellow indicates nodes that have insulation applied. Blue and red nodes are as in Figure 23.
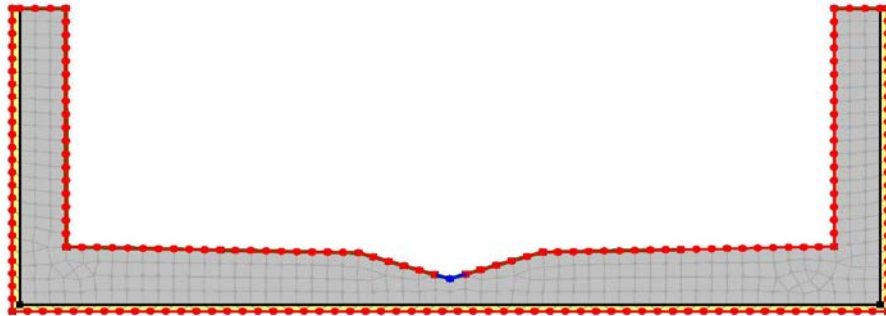
6.1 Heat conduction through the aqueduct

We used the 2-D finite element heat conduction model to estimate the rate of heat conduction from inundated portions of the interior of the aqueduct through the portions of the aqueduct exposed to the cold air. We did this by fixing a thermal boundary condition of 32°F to the inundated portions and setting the rest of the boundary portions of the aqueduct to the assumed air temperatures. To start the simulation, we set the mesh node point temperatures to an arbitrary initial temperature. We then propagated the model through time until a steady-state temperature was achieved throughout the structure. We then compared the heat flux calculated through the bed of the aqueduct, F_x, to a heat conduction formula to estimate the geometric enhancement factor along the bed of the aqueduct, g_x. The variable g_x, used in equation (12) of the Aqueduct Flow and Ice Simulation Model, describes the modification in steady-state heat conduction through the aqueduct that is caused by the shape and form of the aqueduct. We can estimate the steady-state heat conduction without considering the shape and form of the aqueduct as

$$H_{xbed} = \frac{k_c}{L_{cx}}(T_m - T_b) \tag{21}$$

where, as before,

T_b = the outside surface temperature (assumed to be equal to the air temperature),

L_{cx} = the concrete thickness between the outside surface of the aqueduct to the bed of the aqueduct (measured perpendicularly to the outside surface),

k_c = the concrete thermal conductivity.

We then use the steady-state heat conduction estimated by the model, F_x, to estimate g_x as

$$g_x = \frac{F_x}{H_{xbed}} = \frac{F_x}{\dfrac{k_c}{L_{cx}}(T_m - T_b)}.$$ (22)

In the case where insulation (R-Value of 4 per inch of insulation thickness) was applied, the geometric enhancement factor was found as

$$g_x = \frac{F_x}{H_{xbed}} = \frac{F_x}{\dfrac{(T_m - T_b)}{\left(\dfrac{L_{cx}}{k_c} + \dfrac{L_s}{k_s}\right)}}.$$ (23)

where

L_s = the insulation thickness,

k_s = the insulation thermal conductivity.

Figure 25 shows the values of g_x across the bed of the aqueduct for the case of a shallow inundation of the aqueduct. In this case, the depth of the flow is 2.5 ft at the center line of the channel, just deep enough to have flow extend across the entire bed of the aqueduct and to contact the walls. Figure 25 shows that the values of g_x are equal to one across most of the distance. This indicates that the heat transfer is approximately equal to the steady-state value for a concrete slab of the appropriate thickness. There is a slight enhancement in the center of the low-flow channel due to its geometry. There is a substantial enhancement at the outer edges of the channel. This results from the presence of the outside wall of the aqueduct but also from heat transfer through the inside of the vertical walls to the cold air. Figure 26 shows the values of g_x across the bed of the flume for the case of the aqueduct flowing full. It can be seen that the enhancement of g_x at the

outer edges of the channel are reduced. This is because the inner wall of the aqueduct is kept warm by being in contact with the flow.

Figure 25. Heat flux geometric enhancement factor for an aqueduct with a shallow flow.
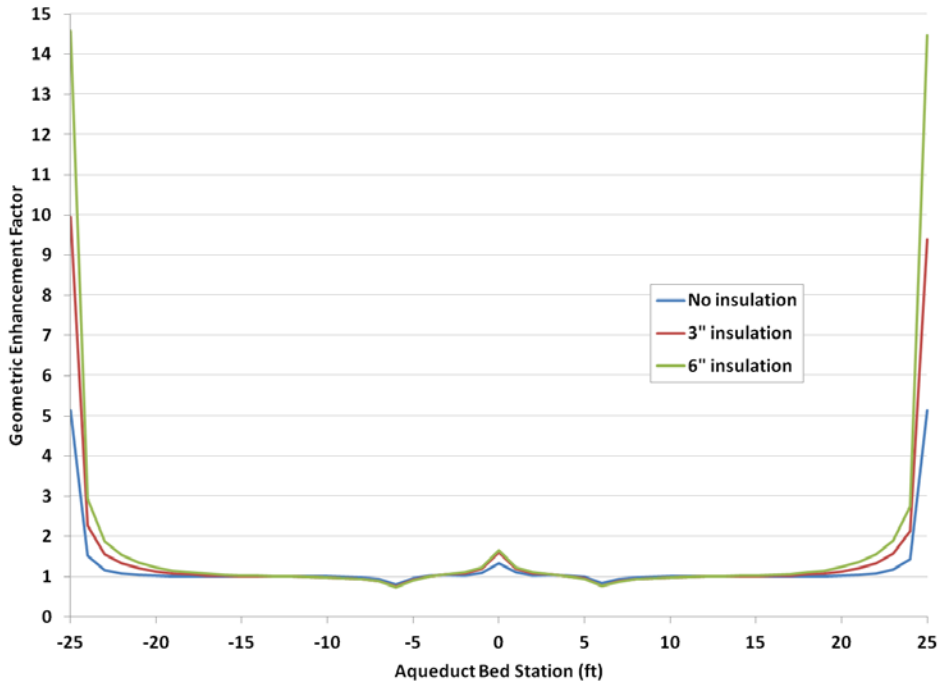
Figure 26. Heat flux geometric enhancement factor for a full aqueduct.
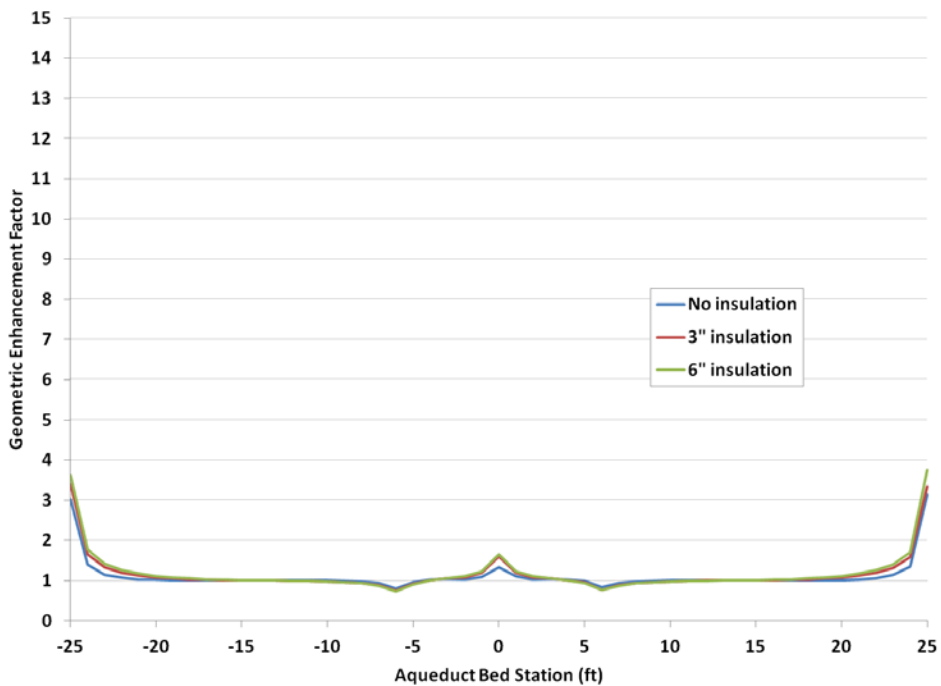
6.2 Heat Application in the bed of the aqueduct

We used the 2-D finite element heat conduction model to estimate the application of heat in the bed of the flume. To model heating elements, we applied a line of unit length with a total flux at specific locations beneath the bed of the low-flow channel. It was necessary to place insulation (R-value of 4 per inch) under the heating elements to make sure that the heat was directed to the surface. We distributed 15 heat cables across the width of the low-flow channel, each rated at 20 W/ft, to provide 60 Btu/ft² hr.

Figure 27. Heating element layout. As in Figures 23 and 24, blue nodes indicate areas inundated by flow, red nodes indicate areas exposed to ambient air temperature, and yellow indicates insulation. Purple and green triangles indicate locations of heating elements.
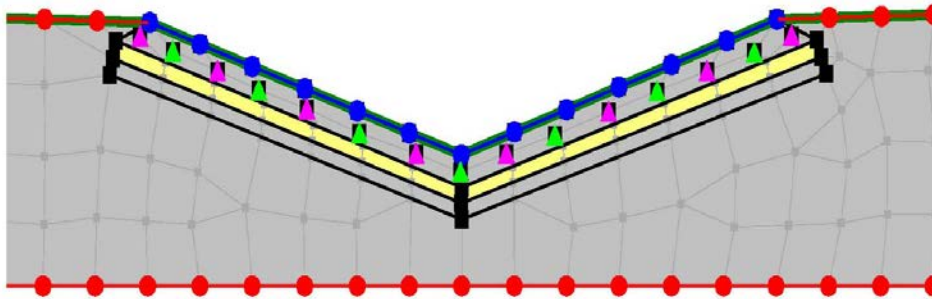
7   Aqueduct Operation in Winter

7.1   Uninsulated and no heat application

During winter operation, the water flow through the proposed aqueduct will lose heat to the frigid atmosphere directly through the air and through the concrete mass of the aqueduct. The heat loss will cause surface ice to form and bed ice to form everywhere that the aqueduct is inundated. The area where ice is formed will be limited by the area inundated by the flow. This means that the flow can have a strong impact on the ice production. The formation of ice in the proposed aqueduct will block the cross section flow area of the aqueduct. This will reduce the available flow area and will raise upstream water levels.

7.2   Application of insulation

Insulating the aqueduct will reduce the heat transfer through the aqueduct structure itself to the frigid air and will reduce the amount of bed ice formed. We assumed that the entire outside of the aqueduct would be covered by insulation as shown in Figure 24. Insulation will not affect the formation of surface ice, which is formed by heat transfer from the top surface of the ice to the frigid air. Note that the calculations provided here are for insulation that has an R-value of about 4 per inch thickness of insulation. This is a conservative lower estimate on the R-value. For example, Dow Extruded Polystyrene Foam Board Insulation (Blueboard Styrofoam insulation) is one type of insulation that may be used in this type of application; it has an R-value of 5 per inch. As this work moves from a concept stage to the design stage, the specific type of insulation suitable for this application needs to be determined. Particularly for this application, with insulation placed on the exterior of the aqueduct, either insulation that is resistant to ultraviolet degradation needs to be used or cladding needs to cover the insulation to shield it from ultraviolet exposure.

7.3   Downstream control

Downstream control seeks to maintain aqueduct flow area by increasing the downstream stage through the use of a hydraulic control structure. This approach seeks to emulate the operation of aqueducts that currently

operate by maintaining a full water depth in the aqueduct throughout the winter. An inflatable dam, such as shown in Figure 28, will raise the downstream water level and will maintain a deep flow through the aqueduct. Surface ice and bed ice will form throughout the aqueduct but flow area will be maintained.

Figure 28. Highgate Falls Power Dam, Swanton, Vermont, fully inflated, 21 January 2000.

Inflatable dams provide the advantage of reduced cost compared to traditional gate structures. Additionally, they have some advantages in winter operation, including the ability to dislodge adhered ice safely when deflated, compared to mechanical structures (Tuthill 2001). The dam can be deflated in place for the open-water season and does not need to be removed. Disadvantages include maintenance costs, relatively short design life, and possible vulnerability to vandalism.

7.4   Application of heat

The installation of heaters in the bed of the aqueduct low-flow channel will prevent the formation bed ice in the low-flow channel and will reduce the thickness of surface ice. Eliminating the formation of bed ice in the low-flow channel will maintain a channel for the flow. Surface ice will form in the low-flow channel even with the bed heaters, but the ice thickness will be reduced compared to the unheated case. A benefit to maintaining the flow area in the low-flow channel is that the flow will be confined to the low-flow channel and will not spread out across the width of the aqueduct. Minimizing the width covered by flow will minimize the ice production.

We developed a preliminary design to provide 60 Btu/hr ft² in the low-flow channel. This design would require 300 W/ft along the low-flow channel. The heat could start 50 ft upstream of the aqueduct entrance if necessary, and insulation would need to be cast into the concrete below the heat panel to reduce the heat loss through the bottom of the aqueduct. Note that the calculations provided here are for insulation that has an R-value of about 4 per inch. As described above, this is a conservative lower estimate on the R-value.

To provide the 300 W/ft, the design calls for 15 heat cables distributed across the width of the low-flow channel, each rated at 20 W/ft. The length of each heat cable is 298 ft (including the channel lead) with at least 60 ft cold lead as required to reach the feed box located on the Maintenance Access Bridge. The total power draw for all 15 heat cables is approximately 90 kW. Raychem 20VPL-CT self-regulating heat cable has provided reliable service in such applications, with individual cables lasting 10 years or more. The heat density of these cables is low enough that they can operate in air without burning out; and the self regulating feature of the cable reduces the wattage in areas where the temperature is warmer, further reducing the chance of burnout, reducing the power consumption, and conserving energy when the temperature in the heat panel gets above 50°F (i.e., due to solar heating or air temperature fluctuations during the winter period).

The main reason for recommending the use of electric heat in this application over a heated fluid (e.g., glycol) pumped through pipes cast into the channel floor is the ease with which electricity can deliver a uniform heat the entire channel length. With a fluid system, if a constant pipe diameter is used the entire length of the heated section and assuming the water temperature is at 32°F the full length of the channel (i.e., an ice cover is maintained over the pilot channel), the heat transfer is highest where the temperature difference between the heat transfer fluid and water is greatest (i.e., at the entrance to the heat panel). The temperature difference then declines rapidly along the heat tubes so that, at the exit, the heat transfer is very low (preliminary calculations show the heat transfer is over a 3000 W/ft at the entrance and less than 30 W/ft at the exit; keep in mind the target heat is 300 W/ft along the entire length). To provide uniform heat transfer the entire length of the heated section requires the heat transfer area to start out small at the entrance and to continually increase

progressing toward the exit. This would greatly increase the complexity of the design (i.e., transitioning from one large pipe at the entrance to branches of smaller and smaller pipes progressing to the exit or the use of fins on the pipes, with no fins at the entrance to more and more fin area at the exit). We note that, due to the constant temperature of the water in the pilot channel (32°F), there is no advantage to using a counter flow heat exchanger design when using a heated fluid.

Using electric heat, we recommend supply power of 480 V. At this voltage, the heat cable manufacturer specifies that each heater will require a 30A breaker. The cables are constructed with watertight connections at the junction between the cable and cold leads, and the cable end is encased in a watertight end cap. These cables are laid in the trays of a 300 ft long heater panel recessed into the low-flow channel. The heat panel covers are ½ in. aluminum plate to promote uniform heat transfer at the water–panel interface. The base of the panels is constructed of steel that is embedded into the concrete face of the low-flow channel Appendix A includes the design drawings.

The design allows for the cables to be placed in channels behind the faceplate of the heat panel. If a cable fails and as long as the entire cable is intact (i.e., the cable has not burned through), it can be readily removed and replaced by removing the end cover plates and pulling the cable out from one end. In the event that a portion of the failed cable cannot be pulled out of the channel, the cable can be replaced by removing the cover plates that extend the full length of the heated section and then laying in the new cable.

Annual inspection of the cables should be conducted to verify that they are all working before the season starts. This is done by checking the current draw for each cable at the breaker box by using a clamp-on amp meter clamped around one leg of the power lead for each cable. Based on the design outlined above, each cable should draw at least 12 amps at start-up (depending on the ambient air temperature, the amperage may start to drop over time as the cable self-regulates the heat). If the amperage is significantly less than this at start up, it is likely the cable is failing or has failed and needs to be replaced.

7.5   Alternative approaches

Alternative approaches to heating the aqueduct include active and passive solar heating and the application of retractable and permanent roofs.

Active solar heating uses solar energy to heat a fluid and then to transfer the heated fluid for immediate heating or storage (US DOE 2012). Active solar heating generally uses electrical or mechanical equipment, such as pumps, to increase usable heat. Flat plate collectors are the most common type of solar heat collector; but evacuated tube and concentrated collectors are also used, more commonly in Europe and China. Fluids are usually water or non-toxic anti-freeze. Though active solar heating is most efficient in cold climates where expenses for fossil fuels are costly, northern areas like Fargo have other issues that reduce solar heating efficiency, such as reduced sunshine in winter; snow cover; and other issues related to system component design, such as piping, pumps, storage tanks, and controls in cold weather. Collectors would be most effective if placed on the top of the aqueduct or on the south- or west-facing side at the appropriate angle to the sun. A system to distribute the heated liquid through the aqueduct would be needed and could be placed in a similar location to the recommended electrical heat conduits. Such a system, however, would provide inconsistent heat along the length of the aqueduct or would require several connections to solar heating collectors. Also, the weight of the solar collectors may be substantial enough to need to be considered in the design of the structure.

Passive solar refers to systems that use solar heat to store or to immediately use solar energy without the needs for pumps or other systems. Passive solar systems use a range of techniques, such as south-facing windows in structures, other techniques that increase thermal mass, and solar chimneys and thermo siphons (US DOE 2013). Though passive solar designs can be low cost, sunless periods can be problematic and high-sun periods in the summer can lead to problems with overheating. Two possible passive solar heating solutions are painting or darkening the aqueduct surface to provide more absorption of sunlight and the use of a retractable or permanent roof.

Applying some kind of paint to darken the concrete would provide solar warming on days when the sun was at the proper angle to warm that part

of the aqueduct (Sipcrete 2014). Moore (1986) discusses a variety of coatings to consider that help with insulation. However, these coatings could also prevent a snow cover from forming (which acts as insulation for the structure). Alternatively, if a snow cover does form, the darkening of the concrete would lose its effectiveness. Also, the darkening would cause the structure to heat to higher than ground temperature in the summer months, which could be detrimental to fish passage and aquatic-life safety. A solution to such a problem could be growing deciduous vegetation on the structure's south and west sides to help to limit unwanted summertime solar heating while encouraging winter solar gain.

A retractable or permanent roof could create an enclosed space and encourage the storage of solar heat. Retractable, transparent roof technology varies from the heavy-duty mechanical roofs used in stadiums, to aquatic center roofs, to folding roofs used for green houses (e.g., OpenAire 2014; UMass 2014). Having the roof placed at an angle would let snow slide off and would still permit solar transmission. Recommended materials would be a twin or a triwall polycarbonate panel, which would provide about 75% light transmission, have a U-factor of 0.50, and be very strong. Polycarbonate costs about $1–$3 per square foot and has a lifespan of about 10 years (Greenhouse 2014).

An option for making solar heating more effective at the site would be thermal energy storage (TES) where heat from the warm season can be stored and then used during the cold season (Hauer 2013). Sensible heat storage, where the heat is stored in liquid or solid form, is the most economical and tested option but requires a large volume for storage. The location of the proposed aqueduct provides some storage areas and advantages. Though space is limited by culturally sensitive areas, the ground surrounding those areas and any areas worked for recreational use provide locations where shallow trench storage could be used. The effective cost of construction for an alternative incorporating heat storage in bore holes could be reduced if boring equipment that is in place for building the structure can be used. The viability of any kind of underground storage must be assessed given the ground conditions at the site. Typical bore hole storage capacity ranges from 10 to 50 kWh/t and storage efficiencies between 75% and 90%. Costs ranges from $0.15 to $15/kWh. Higher technology but more expensive phase change materials for storage are in development and could be considered to reduce needed volume and risks

associated with liquid storage. Heat pumps would be needed to transfer stored heat to distribution systems in the aqueduct.

8   Estimates of Aqueduct Ice Formation

We applied AFISM over the most recent 18 winters, water year 1996 through the present. As previously mentioned, this period begins with the reestablishment of the USGS gage on the Maple River. The USGS data was not available from October 1975 through February 1995. We decided to simulate only the most recent available period given the slight but persistent trends in air temperature and discharge as previously described. Our study simulated five basic scenarios:

1. The aqueduct with no applied heating or downstream control (base case)
2. The aqueduct with downstream control and no applied heating (base case with downstream control); we maintained the downstream elevation to keep a depth of about 11.5 ft in the aqueduct throughout the winter.
3. The aqueduct with applied heating of 5 Btu/hr ft² in the low-flow channel and no downstream control
4. The aqueduct with applied heating of 30 Btu/hr ft² in the low-flow channel and no downstream control
5. The aqueduct with applied heating of 60 Btu/hr ft² in the low-flow channel and no downstream control

We simulated each of these five basic scenarios for three different cases of insulation: no insulation, 3 in. of insulation, and 6 in. of insulation. Table 9 summarizes these 15 simulations. In addition, we simulated the period of record but did not allow ice formation. This allowed a comparison of the open water surface elevations with the scenarios in which ice formed.

Table 9. Summary of simulations.

Insulation	Scenario Title	Description
No insulation on the aqueduct	ICE.0	No heat. No downstream control.
	DSC.0	No heat. Downstream elevation maintained at 892.5 ft.
	H05.0	5 Btu/hr ft² heat in the low-flow channel. No downstream control.
	H30.0	30 Btu/hr ft² heat in the low-flow channel. No downstream control.
	H60.0	60 Btu/hr ft² heat in the low-flow channel. No downstream control.
3 in. of insulation on the aqueduct	ICE.3	No heat. No downstream control.
	DSC.3	No heat. Downstream elevation maintained at 892.5 ft.
	H05.3	5 Btu/hr ft² heat in the low-flow channel. No downstream control.
	H30.3	30 Btu/hr ft² heat in the low-flow channel. No downstream control.
	H60.3	60 Btu/hr ft² heat in the low-flow channel. No downstream control.
6 in. of insulation on the aqueduct	ICE.6	No heat. No downstream control.
	DSC.6	No heat. Downstream elevation maintained at 892.5 ft.
	H05.6	5 Btu/hr ft² heat in the low-flow channel. No downstream control.
	H30.6	30 Btu/hr ft² heat in the low-flow channel. No downstream control.
	H60.6	60 Btu/hr ft² heat in the low-flow channel. No downstream control.
No insulation on the aqueduct	Open	Open water comparison. No ice formation.

8.1 Model boundary conditions and parameters

The model boundary conditions are the upstream flow rate, the air temperature, the upstream water temperature, and the downstream stage. The model operates with a one day time step. We used the daily average discharge recorded at USGS gage 05060100 (USGS 2013) as the simulation flow and the air temperature recorded at the Fargo Hector International Airport (NCDC 2013) as the simulation air temperature. Appendix B displays the daily average discharges and air temperatures for each year of the simulation period. We assumed the upstream water temperature to be 32°F after the AFDD reached a value of 100, and the water temperature remained at that temperature through the remainder of the winter. We de-

veloped the downstream rating curve by using HEC-RAS over a range of flows and ice thicknesses (Figure 29). All elevations are based on the North American Vertical Datum of 1988 (NAVD88). Table 10 lists the parameters used in the model.

Table 10. Parameter values used in the simulations.

	Parameter	Value	Units
k_i	Thermal conductivity of ice	1.27	Btu/(ft hr °F)
k_c	Thermal conductivity of concrete	0.5	Btu/(ft hr °F)
k_w	Thermal conductivity of water	0.552	Btu/(ft hr °F)
k_s	Thermal conductivity of insulation	0.02	Btu/(ft hr °F)
λ	Latent heat of ice	143.3	Btu/lb
ρ_i	Density of ice	57.4	lb/ft³
ρ	Density of water	62.4	lb/ft³
Cp	Specific heat of water	1.007	Btu/(lb °F)
α	Surface ice growth	0.03917	ft per sq root of AFDD
	Datum	881.0	Vertical datum
α_1, α_2	Velocity weighting coefficients	1.0	-
C	Expansion/contraction coefficient	0.3/0.1	-
n	Manning's N roughened concrete	0.04	-
	$AFDD_{min}$	100.0	threshold of AFDD before ice starts
dl	Cross section spacing	5.0	ft
Pr	Water Prandtl number	12.99	-
U	Water kinematic viscosity	1.92E−05	ft²/s
c	Water-to-ice transfer coefficient	0.023	-

8.2   Model simulations

We ran each simulation in the following manner

1. We set the parameters controlling the scenario. These included setting the thickness of insulation (0, 0.25, or 0.50 ft), the heating level of the low-flow channel bed heaters (0, 5.0, 30.0, or 60.0 Btu/hr ft²), and the fixed downstream elevation of 892.5 ft, if required, and selecting the appropriate geometric enhancement factors.
2. We ran the simulation for each winter from the winter 1995–1996 through the present. We started each year on 1 October, and the model progressed in daily time steps. The AFDDs were calculated based on the recorded air temperature as the season progressed. We did not allow ice formation in

the aqueduct until the *AFDD$_{min}$* of 100 AFDD was met. From this point on throughout the winter, ice could form as long as the air temperature was less than 32°F.

3. We ended the simulation each winter after the AFDD was greater than 1000 and the flow equaled or exceeded 300 cfs. We then output the results of the run to the appropriate data files.

Figures 30 and 31 show example results of the model runs. Figure 30 shows the water level at the upstream end of the aqueduct for the cases with no applied heat and no insulation (ICE.0), 3 in. of insulation (ICE.3), and 6 in. of insulation (ICE.6); the case of 6 in. of insulation with varying applied heat fluxes of 60 Btu/hr ft² (H60.6), 30 Btu/hr ft² (H30.6), and 5 Btu/hr ft² (H05.6); and the open water results (Open). The open water results have no ice production. One can see that all the cases are identical prior to 11 November when ice formation commenced. The largest increase in the upstream water level results for the case of no applied heat and no insulation (ICE.0). The buildup of ice throughout the winter decreased the conveyance of the aqueduct and caused the upstream levels to rise. Insulation reduced the volume of ice production, as the next section will show. The cases of 3 in. (ICE.3) and 6 in. (ICE.6) of insulation resulted in smaller upstream water level rises over the course of the winter. The cases of heat application resulted in smaller increases in upstream stage. In fact, most of the increase in the upstream stage for these cases results from the increase of the downstream stage boundary condition due to surface ice formation. As shown in Figure 29, the downstream stage increases with thicker surface ice covers.

Figure 31 displays the estimated ice formation throughout the winter of 2010–2011. In this winter, ice formation did not begin until 23 November 2010.

Figure 29. Downstream rating curves. The water surface elevation above datum (881.0) as a function of discharge and ice thickness.
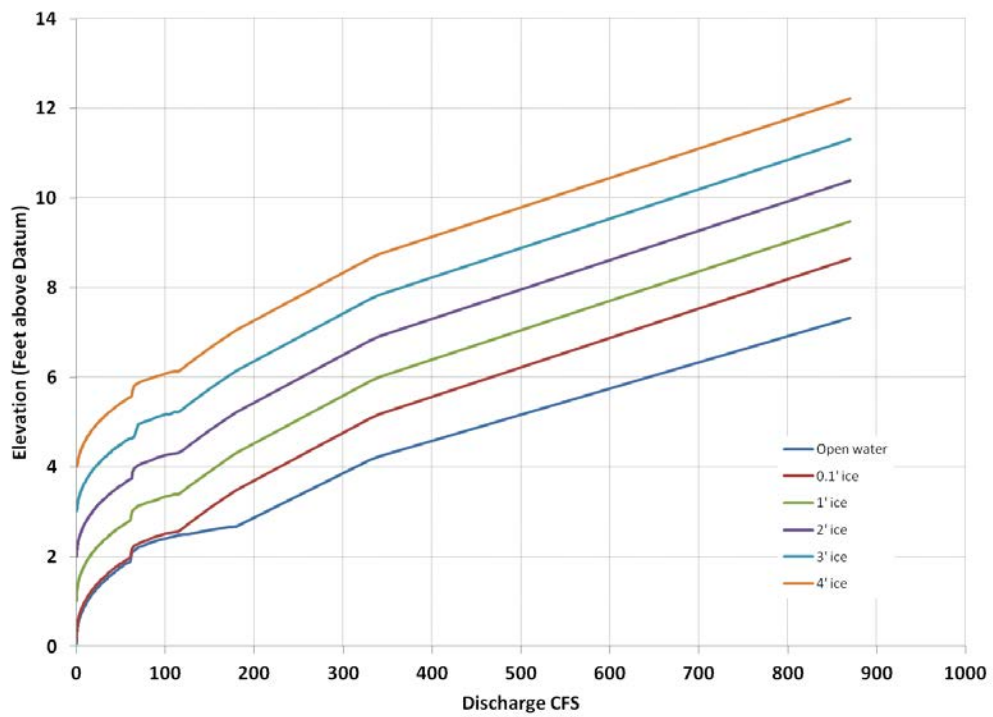

Figure 30. Upstream water levels for water year 1996 for different scenarios and for open water.
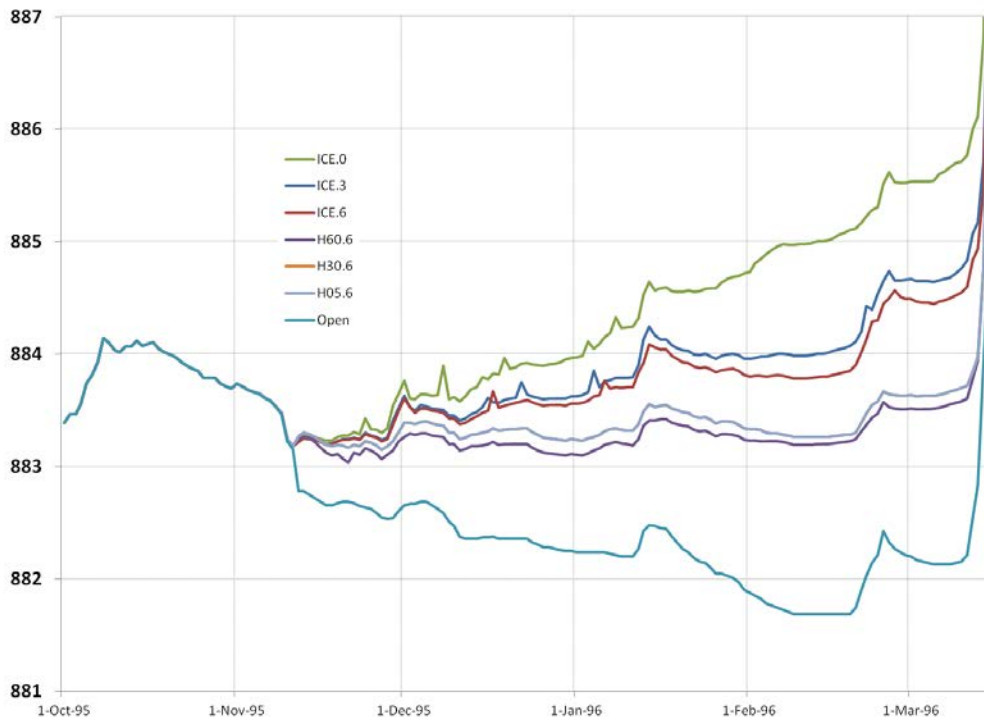
Figure 31. Ice volumes for scenario H60.6 during Water Year 2011.
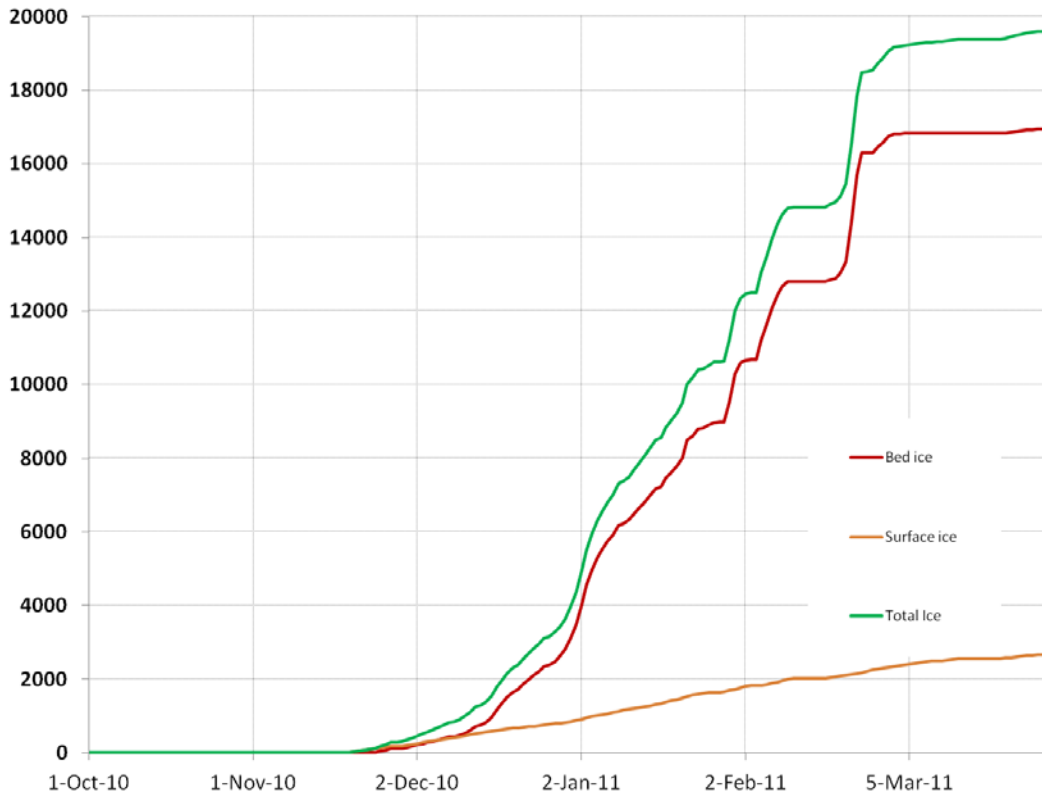
9   Results

9.1   Ice volume

Sections 9.3–9.5 present the results determined by the amount of insula-
tion assumed to be applied to the aqueduct: no insulation, 3 in. of insula-
tion, and 6 in. of insulation. Each section begins with a table summarizing
the results for each winter season. Each table contains the following data:

Column 1: The Water Year. The Water Years cover the period from 1996
through 2013.

Column 2: The end date of the simulation. We started each simulation on
1 October of each Water Year. The end date occurred when the dis-
charge in the aqueduct exceeded 300 cfs.

Column 3: The number of AFDD between 1 October and the end date.

Column 4: The mean discharge during the ice formation period. This was
calculated as the mean discharge between the date when the AFDD
first equaled or exceeded the $AFDD_{min}$ (100) and the end date.

Column 5: The estimated total volume of ice produced under the down-
stream control (DSC) scenario. This is the volume that would be in
place at the end of winter.

Column 6: The estimated total volume of ice produced under the scenar-
io with no applied heat and no downstream control (ICE). This is
the volume that would be in place at the end of winter.

Columns 7, 8, and 9 are the estimated maximum volumes of ice produced
under the scenarios with heat application in the low-flow channel. The
maximum volume generally occurred at the end of the simulation or a few
days before the end. In some years, the ice volume decreased from rising
air temperature just before the large discharge increases that ended the
simulation.

Column 7: The estimated maximum volume of ice produced under the scenario with 60 Btu/hr ft² heat applied in the low-flow channel and no downstream control (H60).

Column 8: The estimated maximum volume of ice produced under the scenario with 30 Btu/hr ft² heat in the low-flow channel and no downstream control (H30).

Column 9: The estimated maximum volume of ice produced under the scenario with 5 Btu/hr ft² heat in the low-flow channel and no downstream control (H05).

In addition, the tables show at the bottom the averages over all the winters for the AFDD, the mean discharges, and each of the five scenarios. The coefficient of variation (COV), the standard deviation divided by the mean, is listed below that.

9.2 Upstream stages

The formation of bed and surface ice will cause water stages upstream of the aqueduct to increase. We estimated the impact of ice formation in the aqueduct on upstream stages by determining the stages that would result in the Maple River channel upstream of the aqueduct. The particular location we chose to examine was the downstream end of at the weir that controls the flow into the spillway that leads to the diversion channel. We calculated the stage at this location for each day of the winter season for every year that we simulated (Water Year 1996–Water Year 2013). We then averaged the stage on each day of the winter season over all the years of the simulation presentation. To estimate the stage in the Maple River channel upstream of the aqueduct, we used the HEC-RAS model to calculate the backwater effect of the aqueduct on the Maple River. In applying the HEC-RAS model for each day of the winter season, we set the downstream boundary condition as the upstream stage of the aqueduct and used the daily observed discharge and the surface ice thickness in the channel. The surface ice thickness was estimated based on the recorded AFDD on that date. We then estimated the water surface elevations in the channel from the upstream limit of the aqueduct to the location of the weir.

9.3   Uninsulated aqueduct

The results of the scenarios for the uninsulated aqueduct are listed in Table 11 and are shown in Figures 32–34 for each winter season. As expected, it is clear that the aqueduct without heating produces the most ice. The unheated cases, one with no downstream control (ICE.0) and one with downstream control (DSC.0), produce roughly the same amount of ice. The COV for each of these cases is closer to the COV of the AFDD (28.1%) than to the COV winter mean discharge (67.2%). This indicates that the ice formation in these unheated cases is substantially controlled by the temperature conditions of the winter and not so much the flow conditions. The scenarios with applied heat produce substantially less ice. This is because, for these cases, bed ice is not produced in the low-flow channel, and the flow area is maintained. Surface ice forms in the low-flow channel, but surface ice may not be present during warm days when the heat from the flowing water would tend to melt the surface ice. The ice forms in these scenarios when the water surface elevation exceeds the low-flow channel and spreads out across the aqueduct. Table 11 shows that the COV is closer to the COV of the winter mean discharge than to the AFDD. This indicates that the ice formation for these heated cases is strongly influenced by the flow conditions.

Figure 32 shows the total volume of ice produced each winter, which can vary, though the heated scenarios produced substantially less ice. Figure 33 plots the total volume of ice formed each winter against the maximum AFDDs for that winter. This further illustrates that there is a strong relationship between the ice volume and the AFDD for the unheated cases while, for the heated case, there appears to be no clear correlation with the AFDD.

Table 11. Ice volumes for the uninsulated aqueduct.

Water Year	End Date	AFDD (°F-days)	Mean Discharge (cfs)	DSC.0 (ft³)	ICE.0 (ft³)	H60.0 (ft³)	H30.0 (ft³)	H05.0 (ft³)
1996	15 Mar. 96	2838	6.1	38938	33814	4632	5445	9593
1997	1 Apr. 97	3059	5.4	40811	35301	4843	5895	9328
1998	24 Feb. 98	1297	20.4	23044	23178	7427	8568	13249
1999	17 Mar. 99	1716	57.3	27871	29202	15981	18516	22444
2000	27 Feb. 00	1381	15.7	23879	24361	7069	9015	13515
2001	26 Mar. 01	2747	24.7	38034	38831	14489	16803	22834
2002	30 Apr. 02	1561	34.0	25939	28485	9513	12104	16068
2003	30 Apr. 03	2286	20.3	33637	28019	4234	5304	7872
2004	23 Mar. 04	2081	16.0	31645	32236	7667	8586	13518
2005	24 Mar. 05	1889	22.5	29546	32669	10763	12521	17393
2006	29 Mar. 06	1576	19.5	26122	29465	11175	12920	18330
2007	19 Mar. 07	1786	11.0	28537	23135	2859	3395	6716
2008	30 Apr. 08	2534	44.7	36021	35004	9092	10621	15678
2009	21 Mar. 09	2655	18.9	37068	38927	12365	14817	19988
2010	12 Mar. 10	1984	20.6	30525	30862	11588	13909	20007
2011	31 Mar. 11	2661	56.5	37180	37276	26871	29328	33084
2012	14 Mar. 12	1085	20.8	20336	20625	6759	8360	11992
2013	22 Apr. 13	2283	15.0	33672	32219	6906	8140	13094
Averages		2079	23.9	31267	30756	9680	11347	15817
Coefficient of Variation		28.1%	63.1%	19.3%	17.7%	57.5%	53.7%	40.6%
Percentage of ICE.0				102.0%	100%	31.6%	37.0%	51.6%

Figure 32. The uninsulated Aqueduct: the total maximum ice volume (ft³) formed over each winter season.
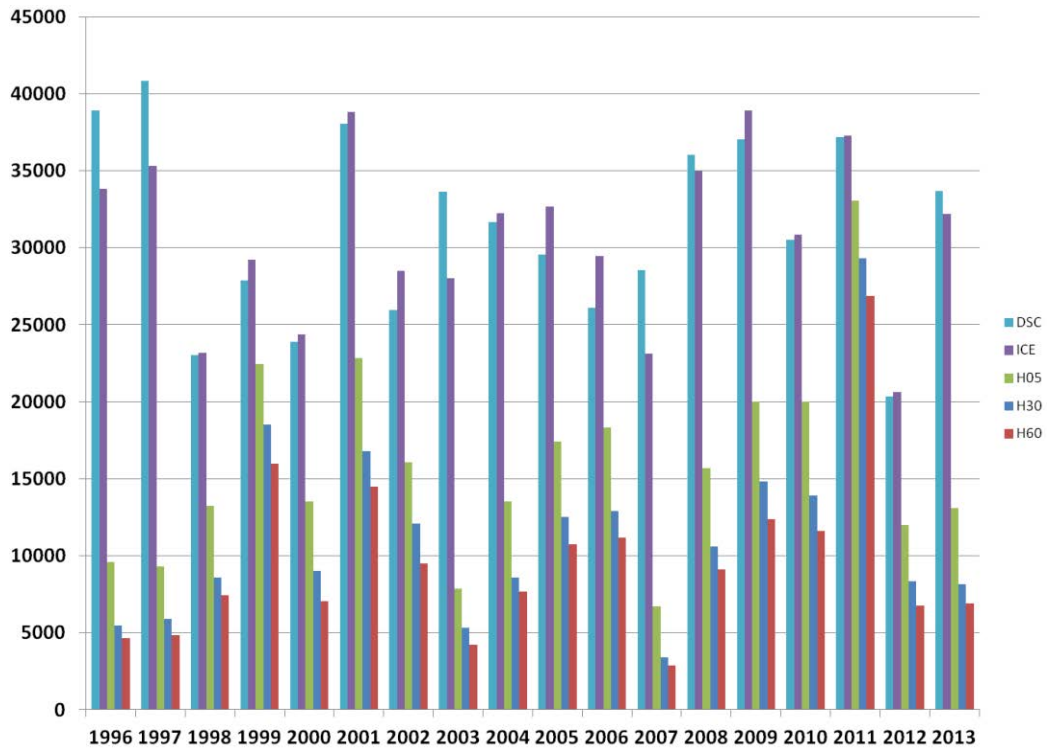

Figure 33. The uninsulated aqueduct: the total maximum ice volume by AFDD (ft³) formed over each winter season.
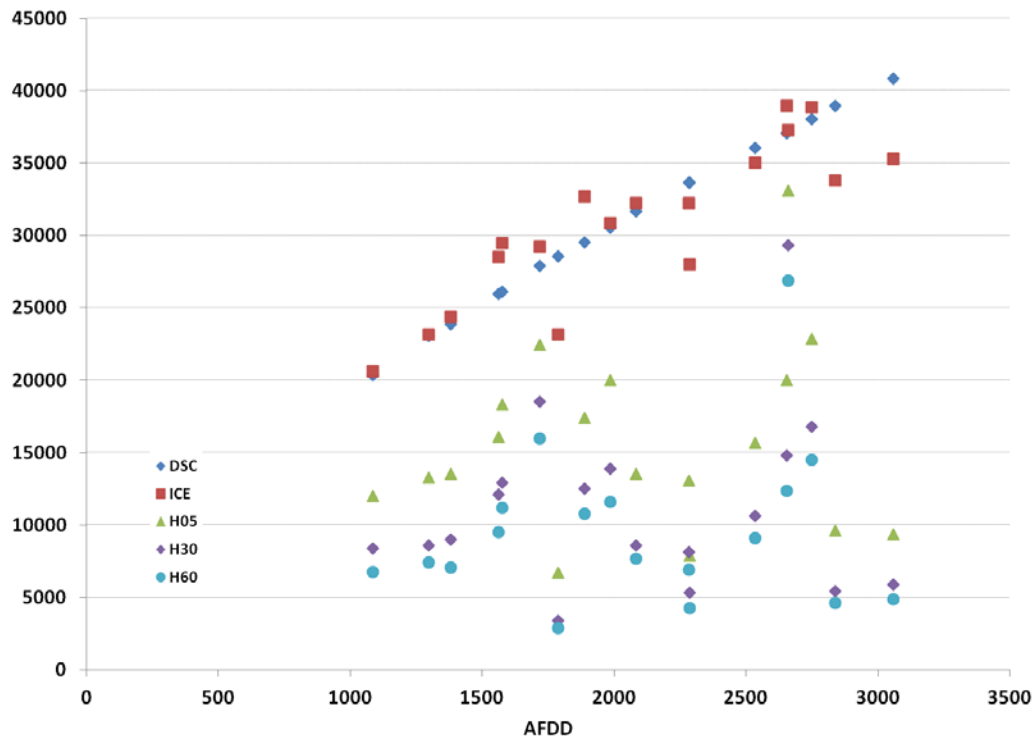
Figure 34. The uninsulated aqueduct: the average stage at the spillway weir location for each day of the winter season.
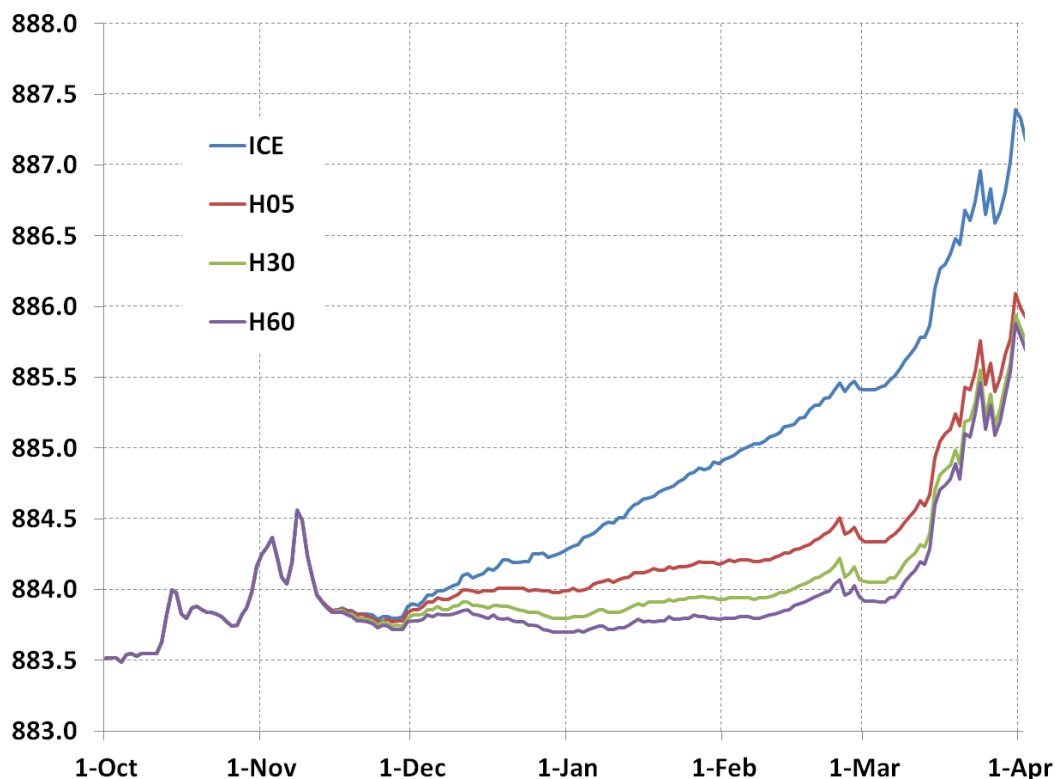

Figure 34 shows the average stage upstream of the aqueduct for each day of the winter season. The average daily stage was calculated by averaging the stage on that day over all the years of simulation. We estimated the stages for the downstream end of at the weir that controls the flow into the spillway that leads to the diversion channel, as described above. One can see that the unheated case results in the largest increase in the stage and that heat reduces the stage increase. In general, the more heat, the lower the increase in stage.

9.4   Aqueduct with 3 in. insulation

The results of the scenarios for the aqueduct with 3 in. of insulation are listed in Table 12 and shown in Figures 35–37 for each winter season. Generally, these results are similar to the uninsulated aqueduct; but for every scenario, less ice is formed over the winter season as is indicated in the table. In the case of downstream control, the volume of ice is reduced 18.3% compared to the uninsulated case. In this scenario, the ice reduction is only in the bed ice; the surface ice volume is not affected. The bed ice is

reduced both by decreasing the heat transfer through the bed of aqueduct, due to the insulation, and by the depth of the water warming the inside of the walls of the aqueduct. The results of the scenarios with heat application indicate that the impact of the insulation is small. The insulation results in a reduction of between only 3.5% and 1.3%.

Table 12. Ice volumes for the aqueduct with 3 in. insulation.

Water Year	End Date	AFDD (°F-days)	Mean Discharge (cfs)	DSC.3 (ft³)	ICE.3 (ft³)	H60.3 (ft³)	H30.3 (ft³)	H05.3 (ft³)
1996	15 Mar. 96	2838	6.1	31155	21275	4589	5426	10013
1997	1 Apr. 97	3059	5.4	32502	20020	4881	5993	9530
1998	24 Feb. 98	1297	20.4	19440	18075	7350	8573	13410
1999	17 Mar. 99	1716	57.3	23068	24830	15427	18007	22240
2000	27 Feb. 00	1381	15.7	20073	17674	7089	9262	13859
2001	26 Mar. 01	2747	24.7	30504	30652	14069	16643	22826
2002	30 Apr. 02	1561	34.0	21625	22422	9367	10471	16285
2003	30 Apr. 03	2286	20.3	27314	15926	4201	5223	7793
2004	23 Mar. 04	2081	16.0	25856	22725	7255	8213	13490
2005	24 Mar. 05	1889	22.5	24310	25654	10282	12333	16900
2006	29 Mar. 06	1576	19.5	21762	23762	10539	12299	18212
2007	19 Mar. 07	1786	11.0	23562	13094	2796	3322	6719
2008	30 Apr. 08	2534	44.7	29048	23638	8823	10585	15644
2009	21 Mar. 09	2655	18.9	29806	28245	12123	14702	20193
2010	12 Mar. 10	1984	20.6	25032	24601	11396	14092	19326
2011	31 Mar. 11	2661	56.5	29887	30679	24778	27121	29664
2012	14 Mar. 12	1085	20.8	17366	16672	6569	8468	12355
2013	22 Apr. 13	2283	15.01	27339	22422	6542	7829	12672
Averages		2079	23.9	25536	22354	9337	11031	15618
Coefficient Of Variation		28.1%	63.1%	17.4%	21.8%	55.3%	51.5%	37.3%
Ice Volume Reduction due to Insulation				18.3%	25.8%	3.5%	2.8%	1.3%
Percentage of ICE.3				112.2%	100%	41.0%	48.5%	68.6%

Figure 35. The aqueduct with 3 in. of outside insulation: the total maximum ice volume (ft³) formed over each winter season.
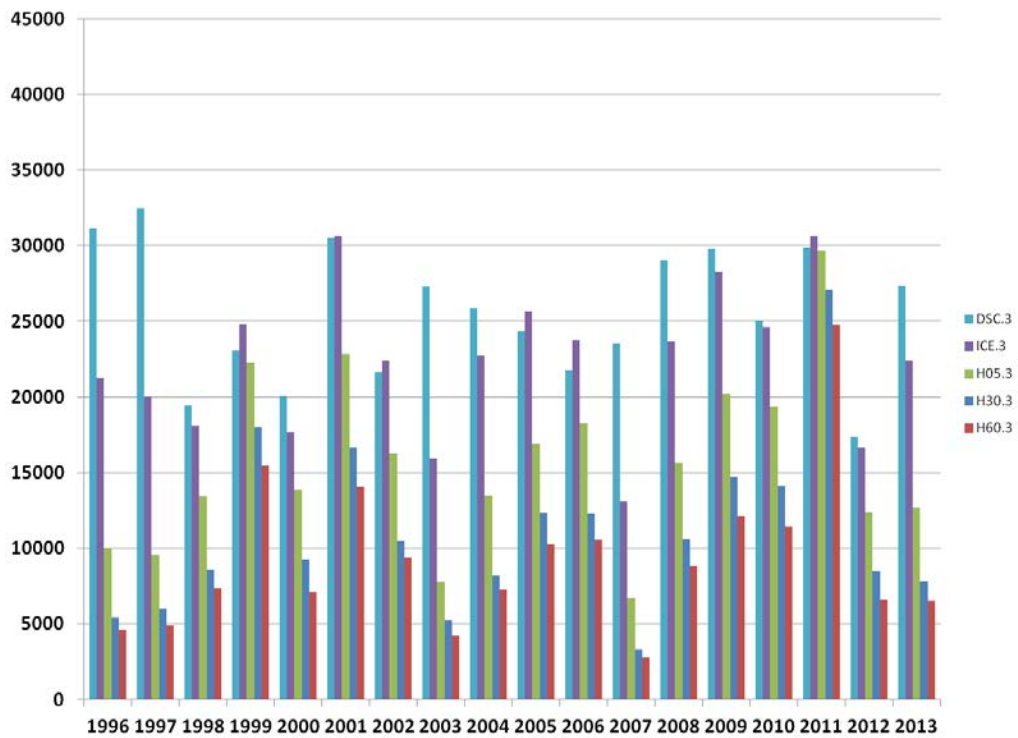

Figure 36. The aqueduct with 3 in. of outside insulation: the total maximum ice volume by AFDD (ft³) formed over each winter season.
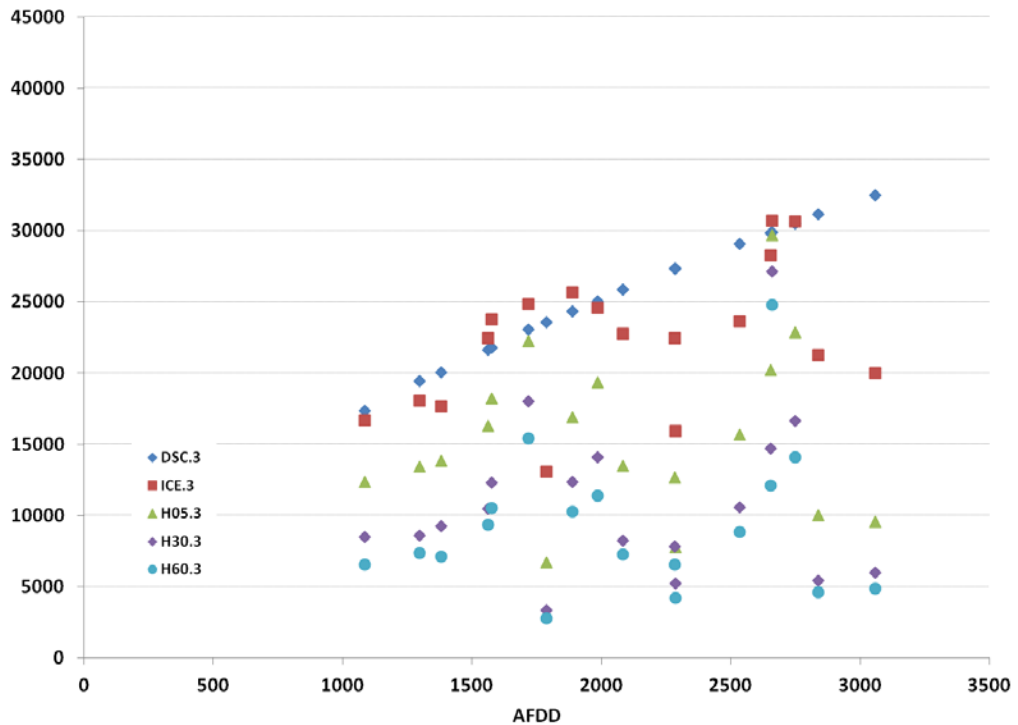
Figure 37 shows the stage upstream of the aqueduct averaged over all winter seasons for each day of the winter season. We estimated the stages for the downstream end of the weir that controls the flow into the spillway that leads to the diversion channel, as described above. One can see that the unheated case results in the largest increase in the stage and that heat reduces the stage increase. In general, the more heat, the lower the increase in stage.

Figure 37. The aqueduct with 3 in. of outside insulation: the average stage at the spillway weir location for each day of the winter season.
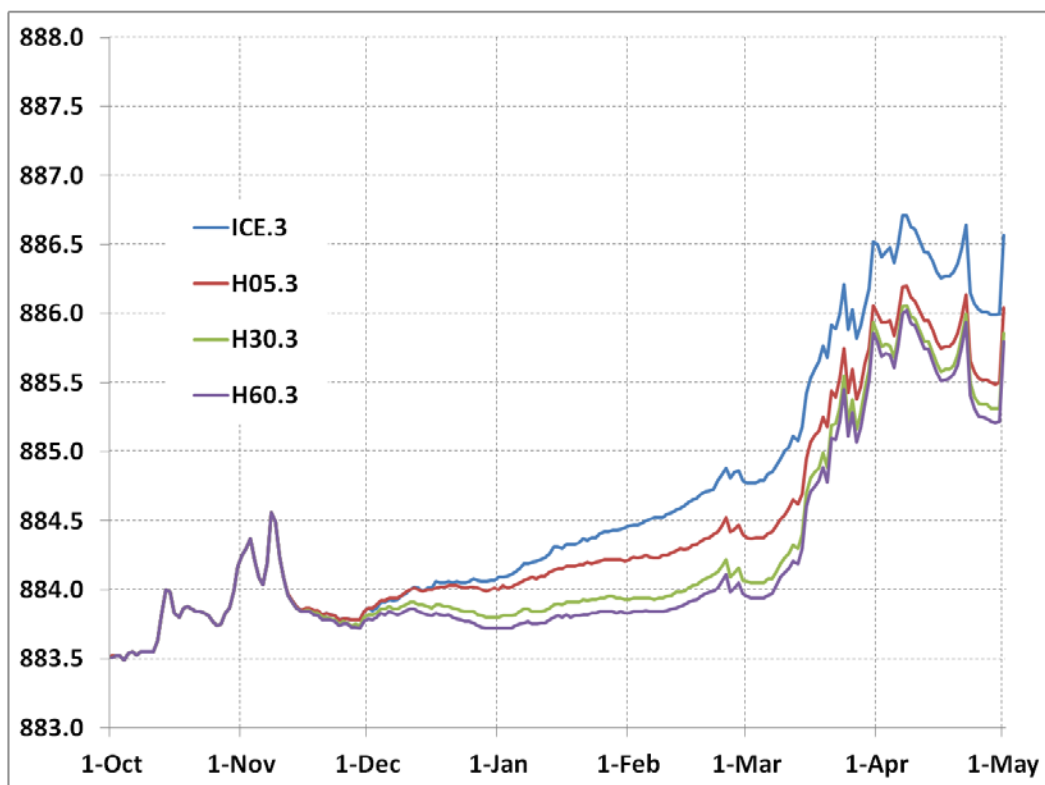
9.5   Aqueduct with 6 in. insulation

The results of the scenarios for the aqueduct with 6 in. of insulation are listed in Table 13 and shown in Figures 38 through 40 for each winter season. Generally, these results are similar to the uninsulated aqueduct; but every scenario resulted in less ice formed over the winter season than in the case of 3 in. of insulation. In the case of downstream control, the volume of ice is reduced 22.9% compared to the uninsulated case. In the case of no downstream control, the ice is reduced 31.8% compared to the uninsulated aqueduct. The results of the scenarios with heat application indi-

cate that the impact of the insulation is small. The insulation results in a reduction of between only 4.1% and 2.2% compared to the uninsulated aqueduct.

Figure 40 shows the stage upstream of the aqueduct averaged over all winter seasons for each day of the winter season. We estimated the stages at the downstream end of the weir that controls the flow into the spillway that leads to the diversion channel, as described above. One can see that, as in the previous cases, the unheated case results in the largest increase in the stage and that heat reduces the stage increase. In general, the more heat, the lower the increase in stage.

Table 13. Ice volumes for the aqueduct with 6 in. of insulation.

Water Year	End Date	AFDD (°F-days)	Mean Discharge (cfs)	DSC.6 (ft³)	ICE.6 (ft³)	H60.6 (ft³)	H30.6 (ft³)	H05.6 (ft³)
1996	15 Mar. 96	2838	6.1	29169	18342	4588	5420	9987
1997	1 Apr. 97	3059	5.4	30370	16118	4872	6003	9263
1998	24 Feb. 98	1297	20.4	18558	17145	7336	8612	13262
1999	17 Mar. 99	1716	57.3	21879	23311	15376	17909	22482
2000	27 Feb. 00	1381	15.7	19141	16704	7096	9266	13868
2001	26 Mar. 01	2747	24.7	28586	28683	14070	16642	22847
2002	30 Apr. 02	1561	34.0	20562	20630	9365	10431	15861
2003	30 Apr. 03	2286	20.3	25723	13185	4195	5204	7761
2004	23 Mar. 04	2081	16.0	24408	20829	7224	8179	13426
2005	24 Mar. 05	1889	22.5	23007	22625	10218	12278	16825
2006	29 Mar. 06	1576	19.5	20688	23418	10533	12361	18036
2007	19 Mar. 07	1786	11.0	22328	11821	2785	3311	6705
2008	30 Apr. 08	2534	44.7	27282	21600	8399	10554	15654
2009	21 Mar. 09	2655	18.9	27962	25959	12092	14706	20186
2010	12 Mar. 10	1984	20.6	23662	22449	11385	14132	19134
2011	31 Mar. 11	2661	56.5	28034	29174	24457	26535	28364
2012	14 Mar. 12	1085	20.8	16645	16044	6605	8463	12151
2013	25 Apr. 13	2283	4.2	25746	21109	6520	7800	12674
Averages		2079	23.2	24097	20508	9284	10989	15472
Coefficient Of Variation		28.1%	67.2%	16.7%	23.6%	55.0%	50.8%	36.7%
Ice Volume Reduction due to Insulation				22.9%	31.8%	4.1%	3.2%	2.2%
Percentage of ICE.6				115.2%	100%	44.4%	52.6%	74.0%

Figure 38. The aqueduct with 6 in. of outside insulation: the total maximum ice volume (ft³) formed over each winter season.
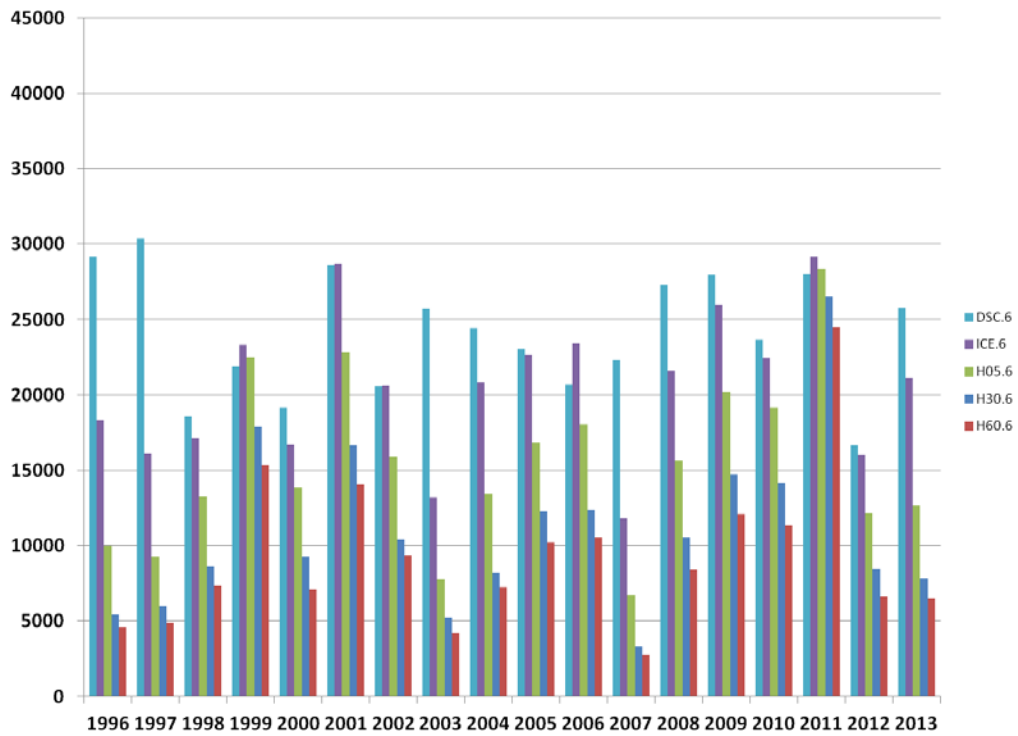

Figure 39. The aqueduct with 6 in. of outside insulation: the total maximum ice volume by AFDD (ft³) formed over each winter season.
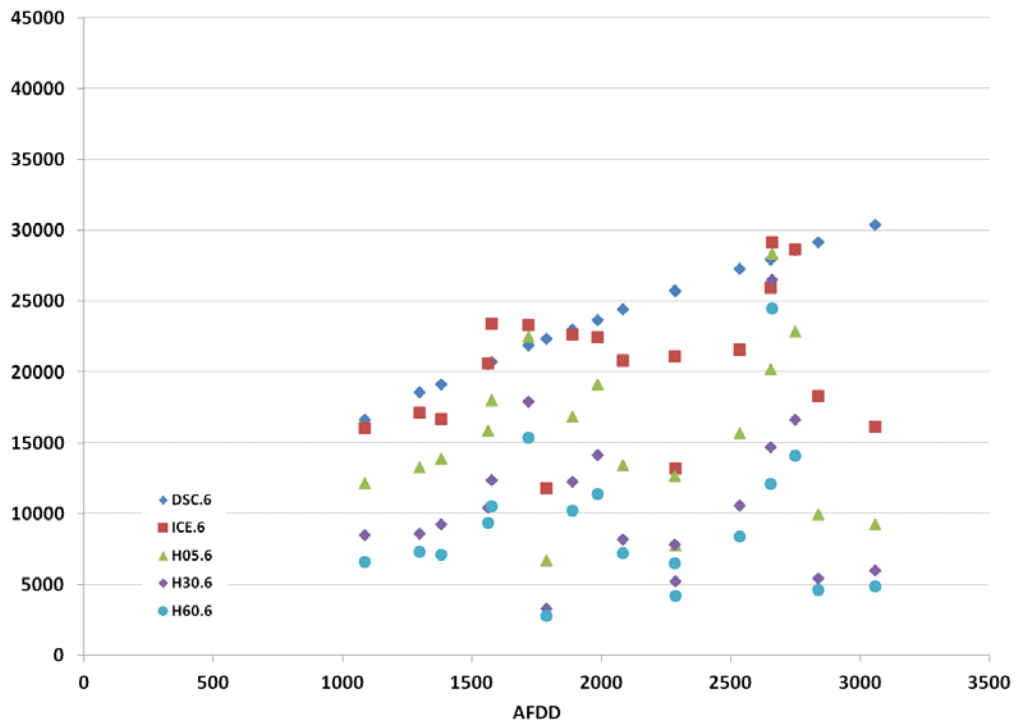
Figure 40. The aqueduct with 6 in. of outside insulation: the average stage at the spillway weir location for each day of the winter season
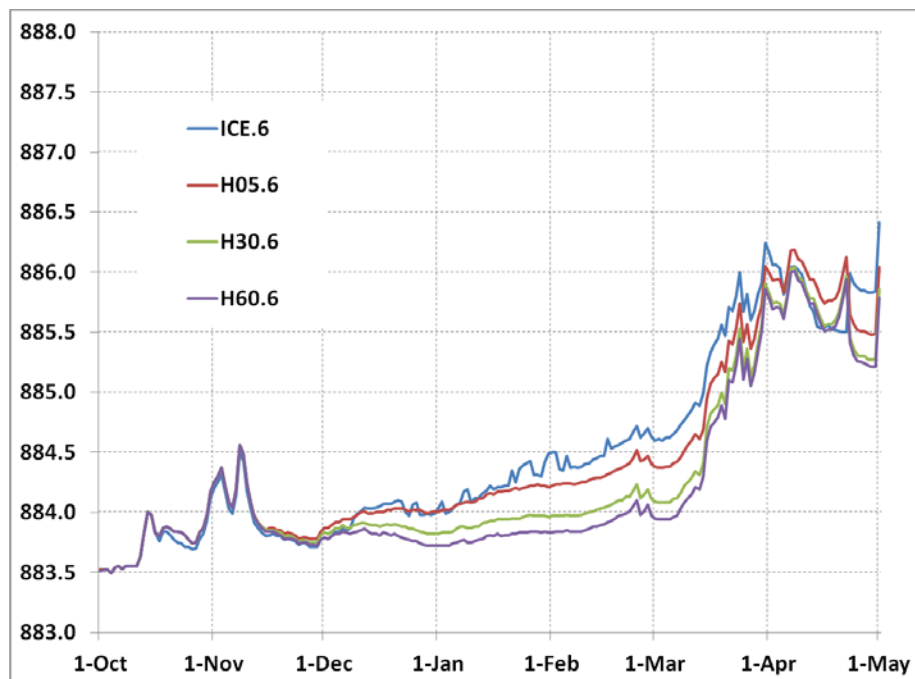
9.6 Results summary

Figure 41 displays the ice volume averaged over the 18 winters of the simulation periods for each scenario and for the three insulation levels. The largest ice volumes were produced by the scenarios without heat: DSC and ICE. The scenario with downstream control (DSC) and the scenario without downstream (ICE) produced about equivalent amount of ice. Under DSC, the downstream stage was set at 892.5 ft, which essentially created a pool about 11.5 ft deep above the center of the low-flow channel throughout the aqueduct. This scenario generated large volumes of ice but could maintain a large flow area, if required. The application of insulation dramatically reduced the ice volume for these two scenarios. Insulation did not reduce the ice volume as dramatically in the scenarios where heat was applied.

The formation of ice in the aqueduct under all the scenarios reduced the conveyance of the aqueduct and caused the upstream stages to rise. Figure 42. displays the stage upstream of the aqueduct for each scenario. The unheated scenarios saw the largest stage rise, but the impact of the insulation in the unheated scenarios was significant. Applying heat to the aqueduct reduced stages compared to the unheated scenarios, but it is interest-

ing to note that when the aqueduct was heated, the impact of the insulation was greatly reduced. In the heated cases, the decrease in the upstream stages is determined almost totally by the amount of heat applied; and the thickness of the insulation has little impact.

Figure 41. The average ice volume (ft³) formed under each scenario.
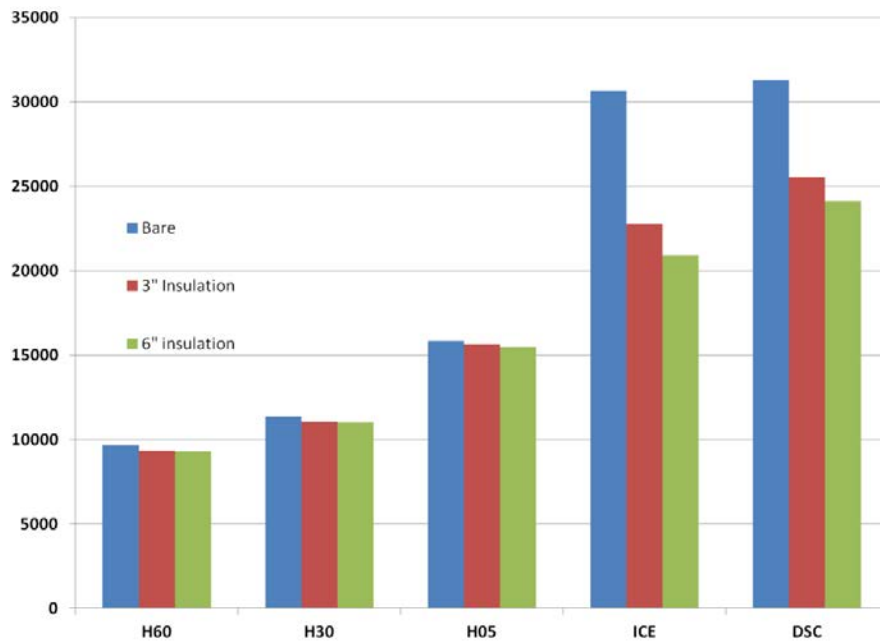
Figure 42. The average stage at the spillway weir location for each day of the winter season under each scenario. The heated scenarios include no insulation, 3 in. of insulation, and 6 in. of insulation.
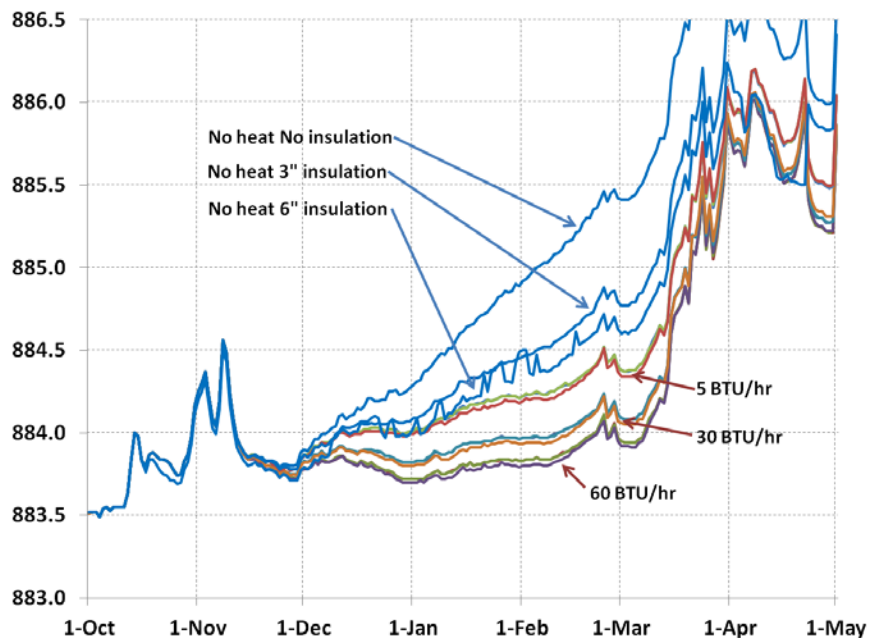
10 Summary

As part of the FM Area Diversion Project, an aqueduct has been proposed to carry the flow of the Maple River over the diversion channel. Aqueducts that operate throughout the winter in cold regions are rare; none are currently operated by the Corps of Engineers.

Winter flows in the Maple River are low. The flows are slowly changing and are often in recession. A review of the meteorological and hydrological conditions indicate that recorded Maple River flows and local air temperatures have increased over the period of record, which extends from about 1948 to the present.

This study quantified the amount of ice that can form under different operating scenarios in the aqueduct during the winter months. We did this by simulating the flow conditions and the ice formation in the aqueduct every day for each operating scenario for the most recent 18 winters for which data is available—the winter of 1995–1996 through the winter of 2012–2013. This allowed us to estimate and compare the ice formation that would result from each operating scenario under the natural variability of the flow and air temperature that occurs at the proposed aqueduct location.

The simulation used an aqueduct flow and ice simulation model developed for this study. The model has five submodules that determine the aqueduct flow conditions and ice conditions. The model operated with a daily time step over each winter starting on 01 October of each year.

We simulated five different scenarios of aqueduct operation:

1. The aqueduct with no applied heating or downstream control (base case)
2. The aqueduct with downstream control and no applied heating (base case with downstream control); we maintained the downstream elevation to keep a depth of about 11.5 ft in the aqueduct throughout the winter
3. The aqueduct with applied heating of 5 Btu/hr ft² in the low-flow channel and no downstream control

4. The aqueduct with applied heating of 30 Btu/hr ft² in the low-flow channel and no downstream control

5. The aqueduct with applied heating of 60 Btu/hr ft² in the low-flow channel and no downstream control

We simulated each of these five basic scenarios for three different cases of insulation applied to the outside of the aqueduct: no insulation, 3 in. of insulation, and 6 in. of insulation. We developed a total of 15 simulations.

Both the basic aqueduct and the basic aqueduct with downstream control produced roughly the same ice volume when they were uninsulated. The AFDD recorded over the winter strongly controlled the volume of ice formed.

Ice volume in the basic aqueduct was reduced 25.8% by 3 in. of insulation and 31.8% by 6 in. of insulation. Ice volume in the basic aqueduct with downstream control was reduced 18.3% by 3 in. of insulation and 22.9% by 6 in. of insulation.

Application of heat significantly reduced the volume of ice formed. In the case of the uninsulated aqueduct, 60 Btu/hr ft² produced only 31.6% of the ice volume of the basic aqueduct without heat, 30 Btu/hr ft² produced only 37.0% of the ice volume of the basic aqueduct without heat, and 5 Btu/hr ft² produced only 51.6% of the ice volume of the basic aqueduct without heat.

The ice formed in the heated aqueduct was influenced by the flow rates and to a lesser degree by the AFDD recorded over the winter. The ice volumes in the heated aqueduct displayed much more year-to-year variability than in the unheated cases.

The use of insulation on the outside of the aqueduct did little to improve the ice reduction performance of the heated aqueduct. Compared to the uninsulated case, the ice volume in the aqueduct heated with 60 Btu/hr ft² in the low-flow channel was reduced 3.5% by 3 in. of insulation and 4.1% by 6 in. of insulation. Compared again to the uninsulated case, the ice volume in the aqueduct heated with 30 Btu/hr ft² in the low-flow channel was reduced 2.8% by 3 in. of insulation and 3.2% by 6 in. of insulation. Finally, when compared to the uninsulated case, the ice volume in the aqueduct

heated with 5 Btu/hr ft² in the low-flow channel was reduced 1.3% by 3 in. of insulation and 2.2% by 6 in. of insulation.

Under all the scenarios, the formation of ice in the aqueduct reduced the conveyance of the aqueduct and caused the upstream stages to rise. Because of ice in the channel downstream of the aqueduct, causing the downstream boundary elevation to increase independent of the ice in the aqueduct, it is difficult to compare the increases in stage. The average upstream stage varied between 3 ft (above datum) for the heat cases and 3.4 to 3.9 ft (above datum) for the unheated scenarios.

References

Ashton, G. D., ed. 1986. *River and lake ice engineering*. Highlands Ranch, CO: Water Resources Publications.

Canal and River Trust. 2013a. Lune Aqueduct. *Canal and River Trust*. http://canalrivertrust.org.uk/directory/41/lune-aqueduct (accessed September 2013).

Canal and River Trust. 2013b. Pontcysyllte Aqueduct. *Canal and River Trust*. http://canalrivertrust.org.uk/directory/37/Pontcysyllte-Aqueduct (accessed September 2013).

Canal Corridor Association. 2009. I and M Canal History. *Canal Corridor Association*. http://www.canalcor.org/CCA_Hist.html (accessed November 2013).

Conro, S. 2011. Hennepin Canal Feeder Aqueduct #9. *Bridgehunter.com*. http://bridgehunter.com/il/bureau/bh50017/ (accessed September 2013).

Crank, J. 1984. *Free and Moving Boundary Problems*. Oxford, UK: Clarendon Press.

Diversion Authority. 2013. About the Project. *F-M Area Diversion*. Fargo, ND: Flood Diversion Board of Authority. http://www.fmdiversion.com/index.php (accessed June 2014).

Clair, M. 2006. Pont Canal de Briare 45250. *Wikipedia.org*. http://commons.wikimedia.org/wiki/File:Pont_Canal_de_Briare_45250.jpg.

Geo-Slope International. 2012. TEMP/W 2012 thermal analysis. *Geo-Slope*. Alberta, Canada: Geo-Slope International. http://www.geo-slope.com/products/tempw.aspx.

Gosink, J. P. 1986. Synopsis of Analytic Solutions for the Temperature Distribution in a River Downstream From a Dam or Reservoir. *Water Resources Research* 22 (6): 979–983.

Greenhouse. 2014. *Greenhouse Megastore*. Danville, IL: International Greenhouse Company. http://www.greenhousemegastore.com/.

Hauer, A. 2013. *Thermal Energy Storage.* IEA-ETSAP and IRENA© Technology Brief E17. https://www.irena.org/DocumentDownloads/Publications/IRENA-ETSAP%20Tech%20Brief%20E17%20Thermal%20Energy%20Storage.pdf.

Henderson, F. M. 1966. *Open Channel Flow*. New York: Macmillan.

Illinois Department of Natural Resources (IDNR). 2013. Hennepin Canal—State Trail. *Illinois Department of Natural Resources*. Sheffield, IL: Illinois Department of Natural Resources. http://dnr.state.il.us/lands/Landmgt/PARKS/R1/HENNPIN.HTM (accessed September 2013).

Ligerien,C. 2013. Briare le pont canal et l écluse des Mantelot (Briare Canal Bridge and Lock of Mantelot). http://ligerien.christian.pagesperso-orange.fr/PONT CANAL DE BRAIRE.htm (accessed September 2013).

Moore, S. W. 1986. *Exposure Testing of Solar Absorber Surfaces*. Los Alamos, NM: Los Alamos National Laboratory. http://www.osti.gov/scitech/servlets/purl/5425469.

National Climate Data Center (NCDC). 2013. Global historical climatology network - daily data. *NOAA National Climate Data Center*. Asheville, NC: National Oceanic and Atmospheric Administration, National Climatic Data Center. http://www.ncdc.noaa.gov/ (accessed May 2013).

Novotny, E. V., and H. G. Stefan. 2007. Stream flow in Minnesota: Indicator of climate change. *Journal of Hydrology* 334 (3): 319–333.

OpenAire. 2014. *OpenAire*. Cedarburg, WI: OpenAire America. http://www.openaire.com/default.aspx.

Rahman, M. M., and Z. Lin. 2013. *Impact of Subsurface Drainage on Streamflows in the Red River of the North Basin*. Technical Report No: ND13-05. Fargo, ND: North Dakota State University, Water Resource Research Institute.

Rochester Public Library. 2013. A Tour around Rochester on the Erie Canal from 1850 to the Present. *Monroe County Library System*. Rochester, NY: Monroe County Library System. http://www.libraryweb.org/rochimag/gallery1a.html.

Sadowski, F. E., Jr. 2012. The Genesee River Aqueduct. *The Erie Canal*. http://eriecanal.org/Rochester-2.html.

Saschen-Anhalt. 2013. Wasserstraßenkreuz Magdeburg. *Saschen-Anhalt*. http://www.sachsen-anhalt.de/index.php?id=772 (accessed September 2013).

Sipcrete. 2014. Sipcrete High Thermal Mass. *Sipcrete*. Turvey Beds, UK: Sipcrete. http://www.sipcrete.com/HTM.htm.

Taylor, I. 2010. SD4863 Diving Under the Ice. *Geograph*. http://www.geograph.org.uk/photo/1662306.

Tuthill, A. 2001. *Performance Survey of Inflatable Dams in Ice-Affected Waters*. Ice Engineering Information Exchange Bulletin. Hanover, NH: U.S. Army Cold Regions Research and Engineering Laboratory.

U. S. Department of Energy (US DOE). 2012. Active Solar Heating. *Energy.gov*. Washington, DC: U.S. Department of Energy. http://energy.gov/energysaver/articles/active-solar-heating.

U. S. Department of Energy (US DOE). 2013. Passive Solar Building Design Basics. *Energy.gov*. Washington, DC: U.S. Department of Energy. http://energy.gov/eere/energybasics/articles/passive-solar-building-design-basics.

U.S. Army Corps of Engineers (USACE). 2002. Engineering and design—ice engineering. U.S. Army Engineer Manual 1110-2-1612. Washington, DC: Department of the Army. http://www.publications.usace.army.mil/USACEPublications/EngineerManuals.

U.S. Army Corps of Engineers (USACE). 2010. *HEC-RAS River Analysis System Hydraulic Reference Manual, Version 4.1.* Davis, CA: Hydrologic Engineering Center.

U.S. Army Corps of Engineers (USACE). 2011. *Final Feasibility Report and Environmental Impact Statement: Fargo-Moorhead Metropolitan Area Flood Risk Management.* http://www.fmdiversion.com/eis.asp (accessed September 2013).

United States Geological Survey (USGS). 1982. *Guidelines for determining Flood Flow Frequency.* Bulletin #17B of the Hydrology Committee. Reston, VA: United States Geological Survey, Interagency Advisory Committee on Water Data.

United States Geological Survey (USGS). 2013. USGS Water Data for the Nation. *National Water Information System.* http://waterdata.usgs.gov/nwis/ (accessed May 2013).

University of Massachusetts (UMass) Amherst .2014. Retractable Roof Greenhouses and Shadehouses. *Greenhouse Crops and Floriculture Program.* Amherst, MA: University of Massachusetts. http://extension.umass.edu/floriculture/fact-sheets/retractable-roof-greenhouses-and-shadehouses.

Wabash and Erie Canal Park. 2009. History of Wabash and Erie Canal in Delphi. *Wabash and Erie Canal Park.* Delphi, IN: Wabash and Erie Canal Park. http://canalcenter.org/park_history.php.

Appendix A: Heater Drawings

DETAIL 2 (SCALE: 1:4)

1-1/2 X 3/4 BAR STOCK

$4\frac{1}{8}$"

1"

2 X 2 L

$1\frac{5}{8}$"

3/8 STEEL PLATE

HEATING ELEMENT

DETAIL 3 (SCALE: 1:4)

71.6°

DETAIL 1 (SCALE: 1:25)

$11\frac{1}{2}$"

DETAIL 2

REMOVABLE COVER 1/2" ALUM

6'

10" TYP

6"

$9\frac{1}{2}$"

HEATING ELEMENT 20W/FT 15 REQ'D

7'-5"
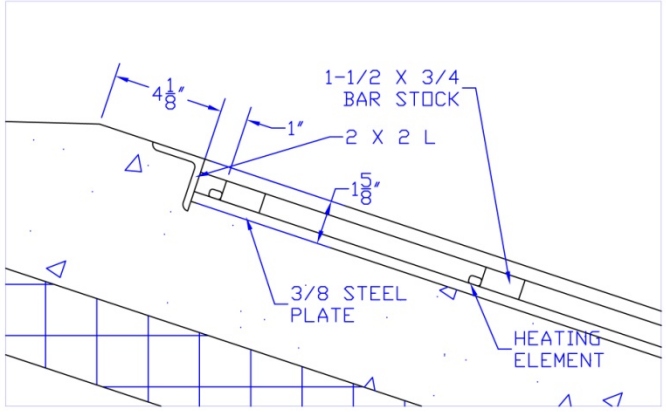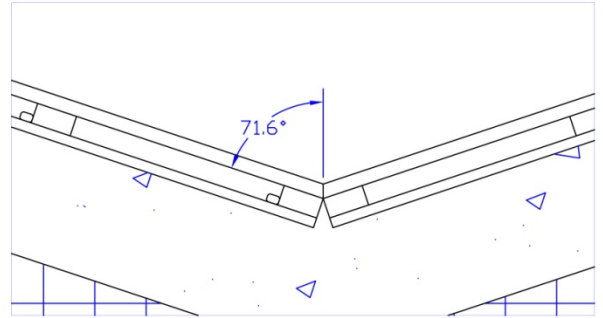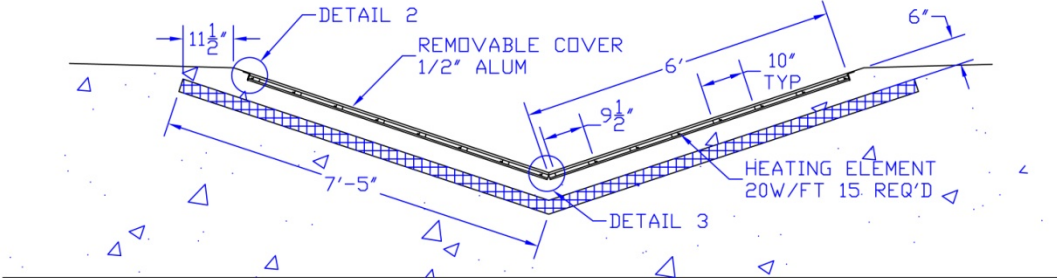
DETAIL 3

1. HEATED LENGTH OF EACH HEATER IS 298 FT. COLD LEAD 60 FT. OR AS REQUIRED TO REACH FEED BOX.

2. LOCATE FEED BOX ON MAINTENANCE ACCESS BRIDGE.

3. WATER TIGHT JUNCTIONS AT COLD LEAD TO HEATER AND AT END CAP.

4. EACH HEATER DRAWS 6kW. TOTAL POWER DRAW 90kW.

5. RECOMMEND 20W/FT. SELF REGULATING HEAT CABLE POWERED AT 480V. 30A BREAKER REQUIRED FOR EACH HEATING ELEMENT.

REVISIONS				
ZONE	REV	DESCRIPTION	DATE	APPROVED

UNLESS OTHERWISE SPECIFIED:
DIMENSIONS ARE IN INCHES
TOLERANCES
DECIMALS   ANGULAR
.XX ± .05   ± 0.5°
.XXX ± .010
DO NOT SCALE DRAWING

HEATER PANEL DETAILS

MAPLE RIVER AQUEDUCT

DRAWN
R. HAEHNEL

CHECKED

DESIGN

SIZE B | FSCM NO. | DWG NO. | REV

SCALE | DATE 28OCT13 | SHEET 2 OF 4

CHANNEL FOR
HEATER FEED

50'

250'

ACCESS BRIDGE

2'

2'

20'
TYP

16'

ACCESS PLATES
(BOTH ENDS) SHEET 4

AQUEDUCT
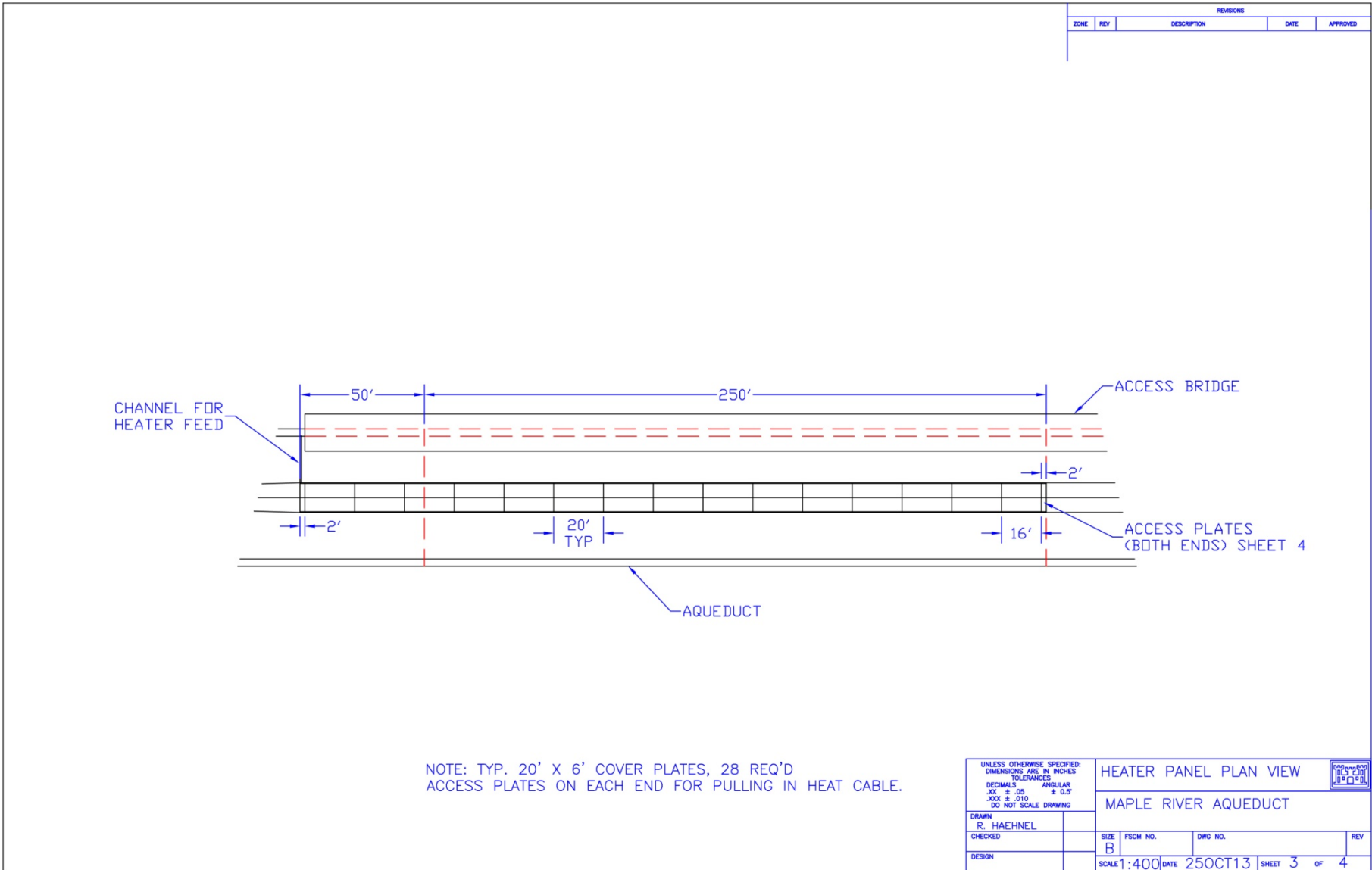
NOTE: TYP. 20' X 6' COVER PLATES, 28 REQ'D
ACCESS PLATES ON EACH END FOR PULLING IN HEAT CABLE.

REVISIONS				
ZONE	REV	DESCRIPTION	DATE	APPROVED

UNLESS OTHERWISE SPECIFIED:
DIMENSIONS ARE IN INCHES
TOLERANCES
DECIMALS   ANGULAR
.XX ± .05   ± 0.5'
.XXX ± .010
DO NOT SCALE DRAWING

DRAWN
R. HAEHNEL

CHECKED

DESIGN

HEATER PANEL PLAN VIEW

MAPLE RIVER AQUEDUCT

SIZE
B

FSCM NO.

DWG NO.

REV

SCALE 1:400   DATE 25OCT13   SHEET 3 OF 4

6" CHANNEL FOR POWER FEED

PATH FOR COLD LEAD

ACCESS PLATE REMOVED

ACCESS PLATE REMOVED

2'

2'

Appendix B: Daily Air Temperature and Flows
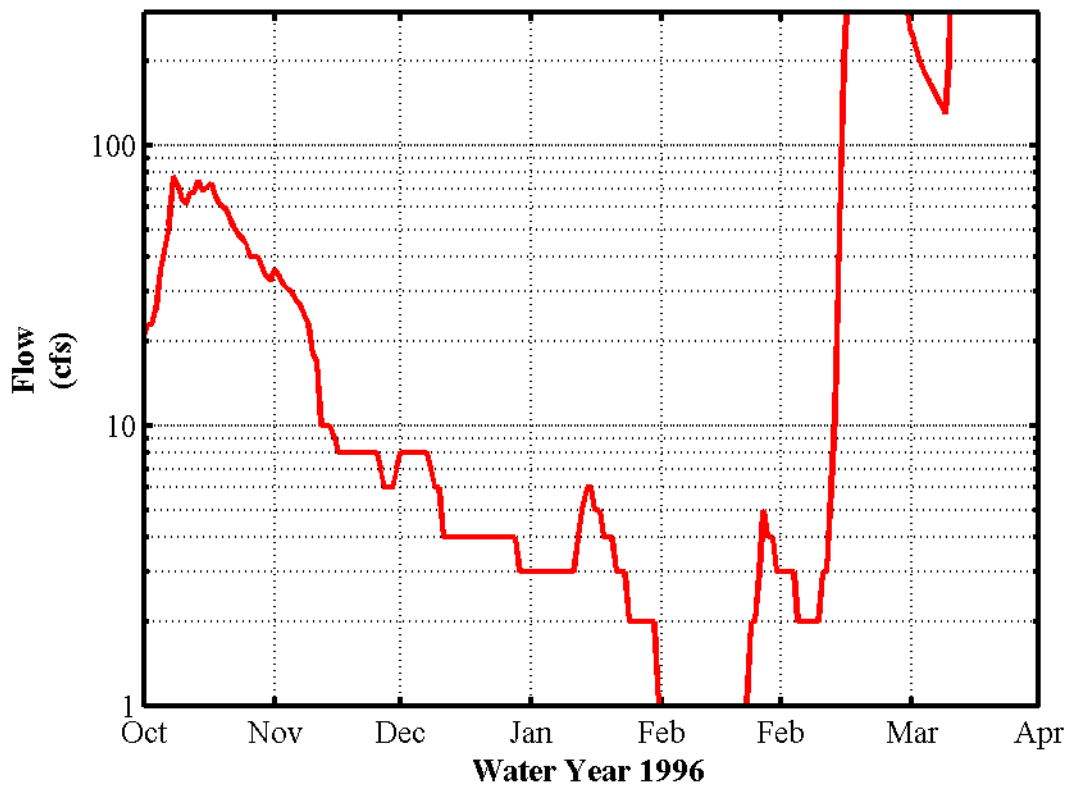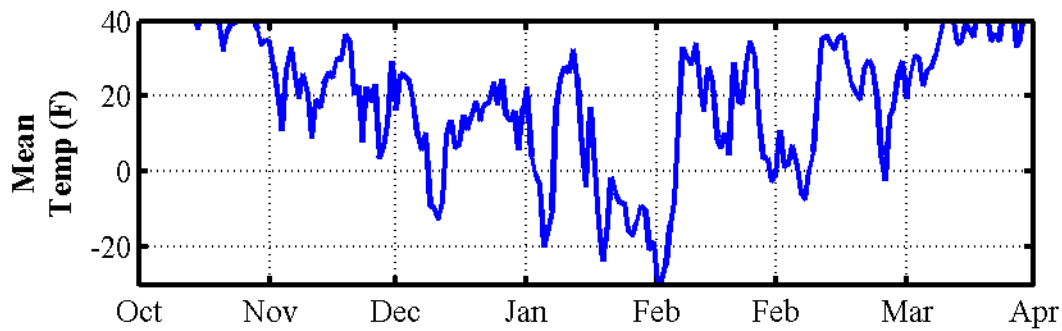
Water Year 1998
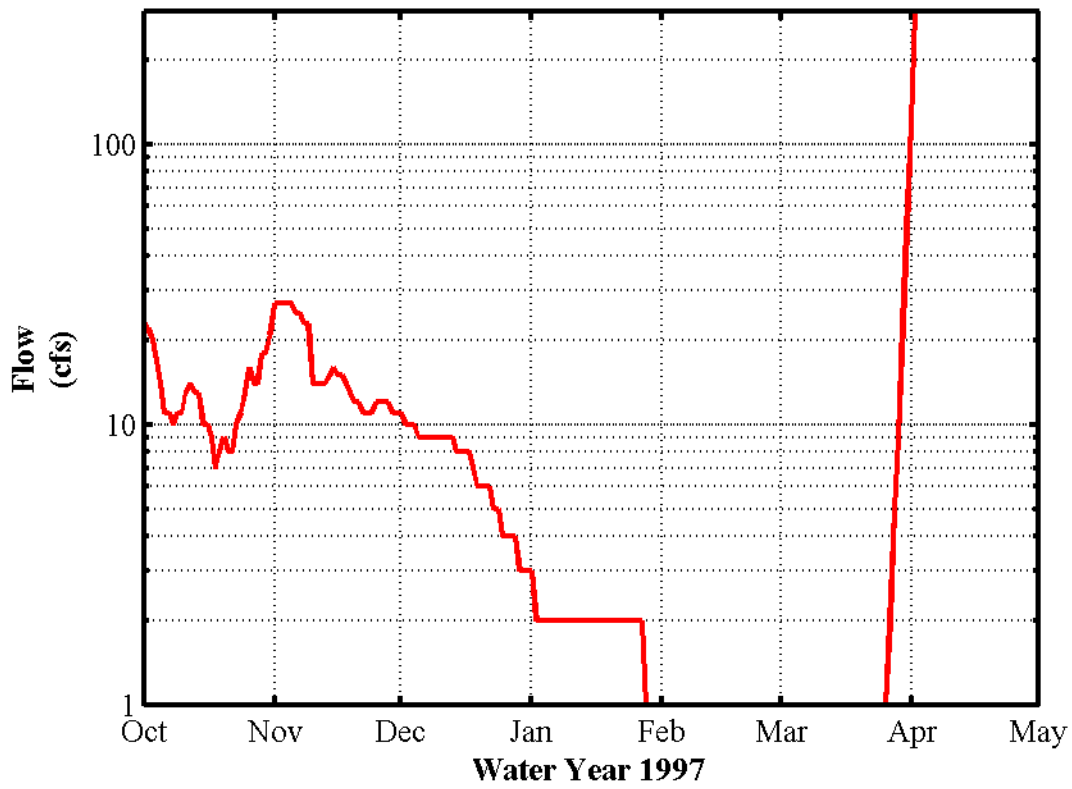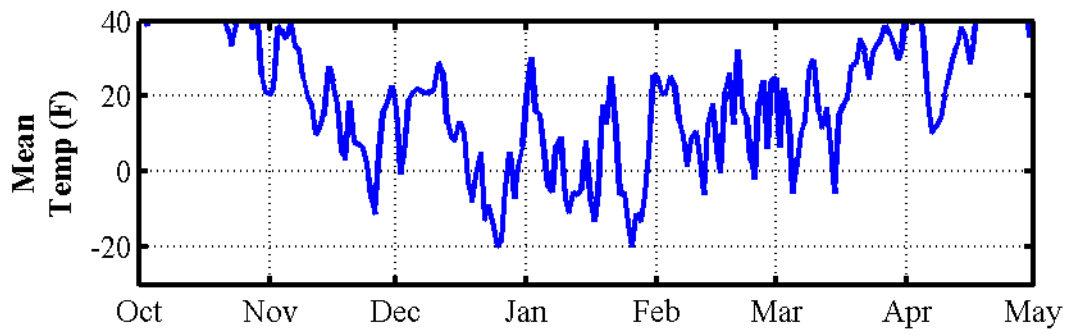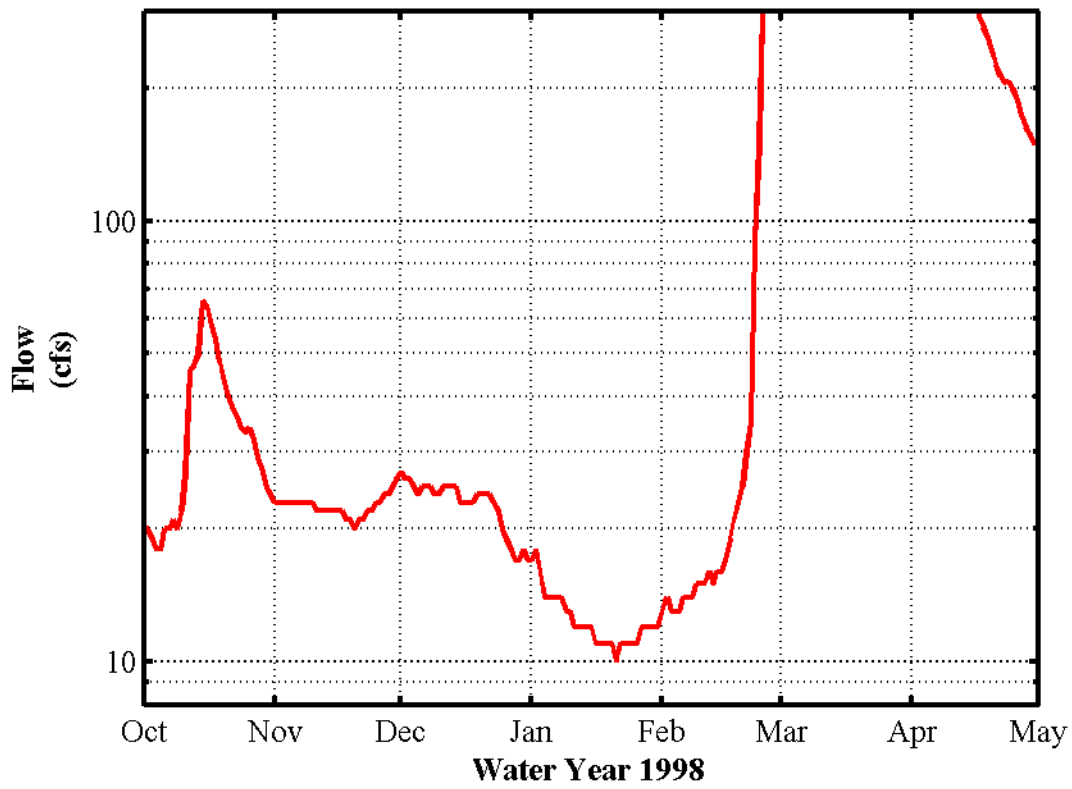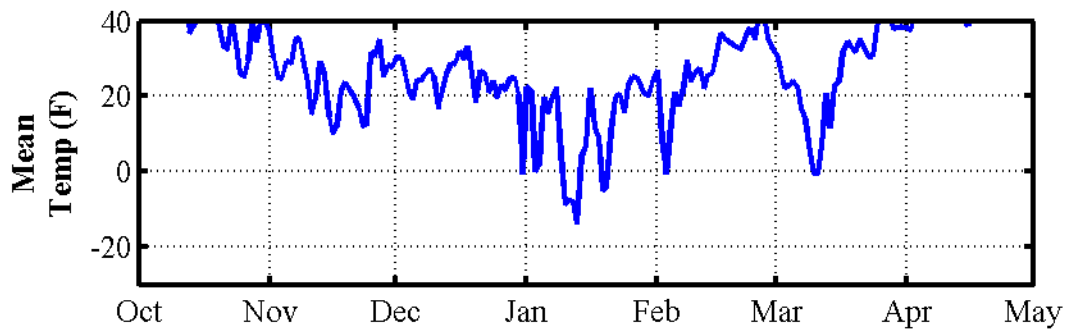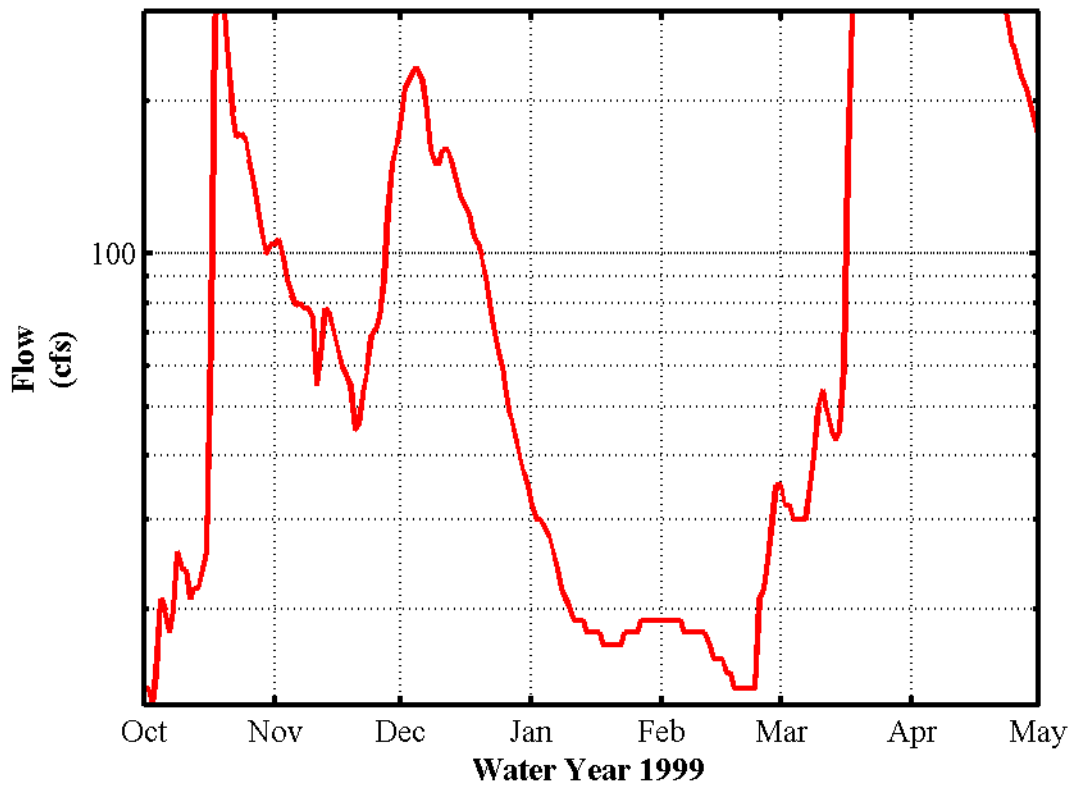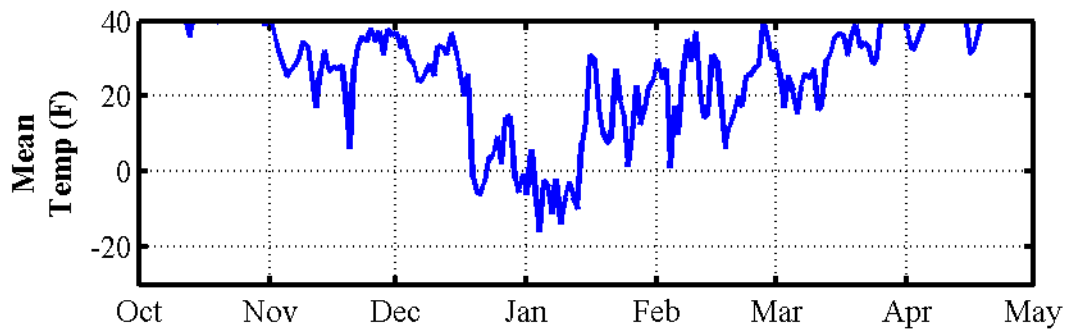
Water Year 1999
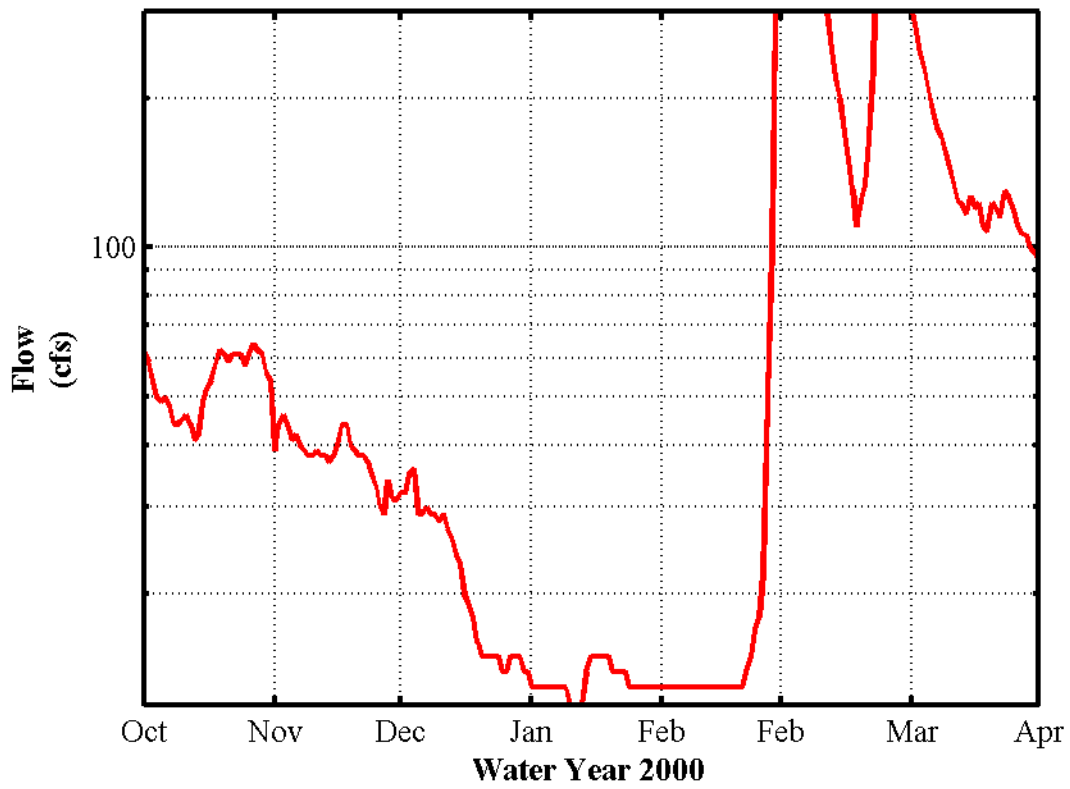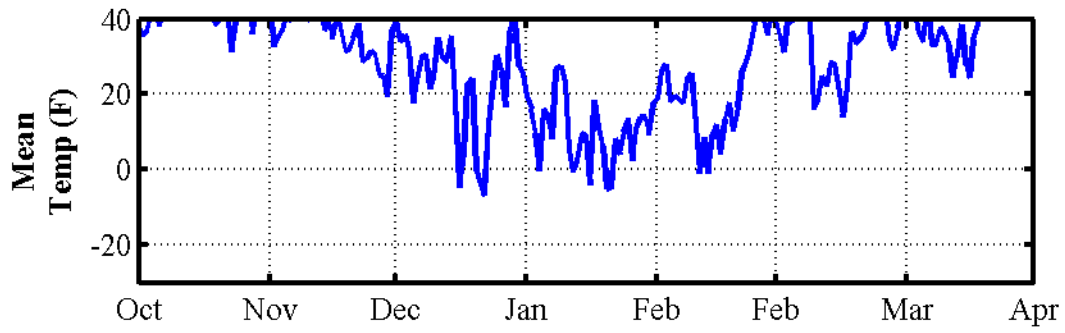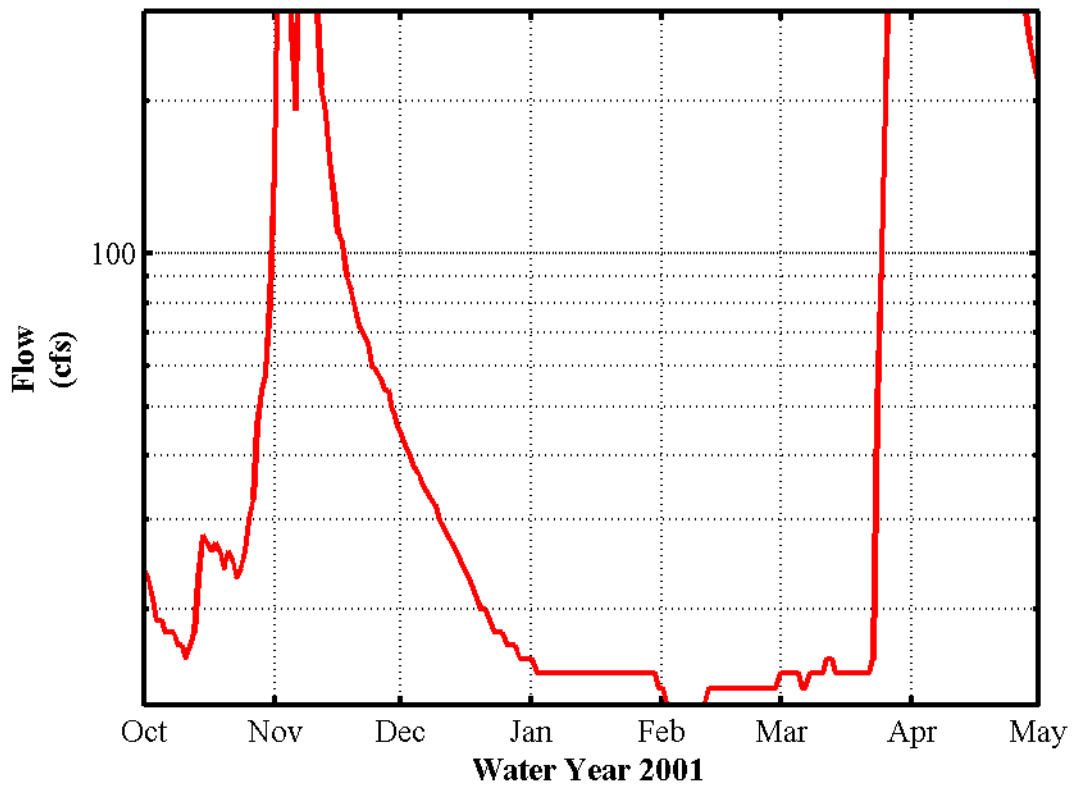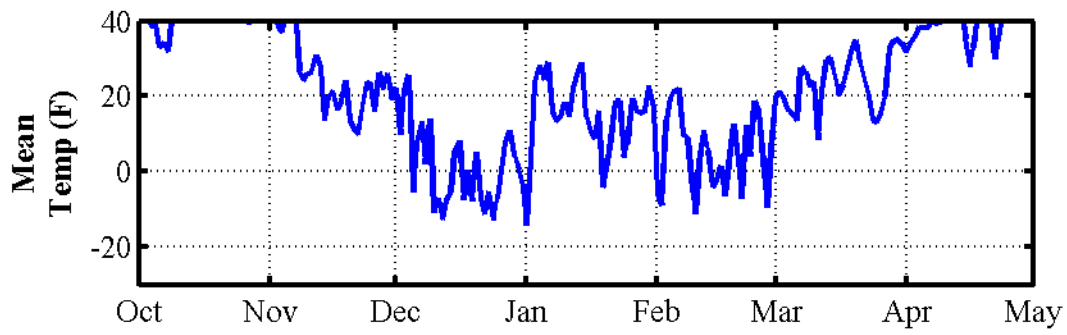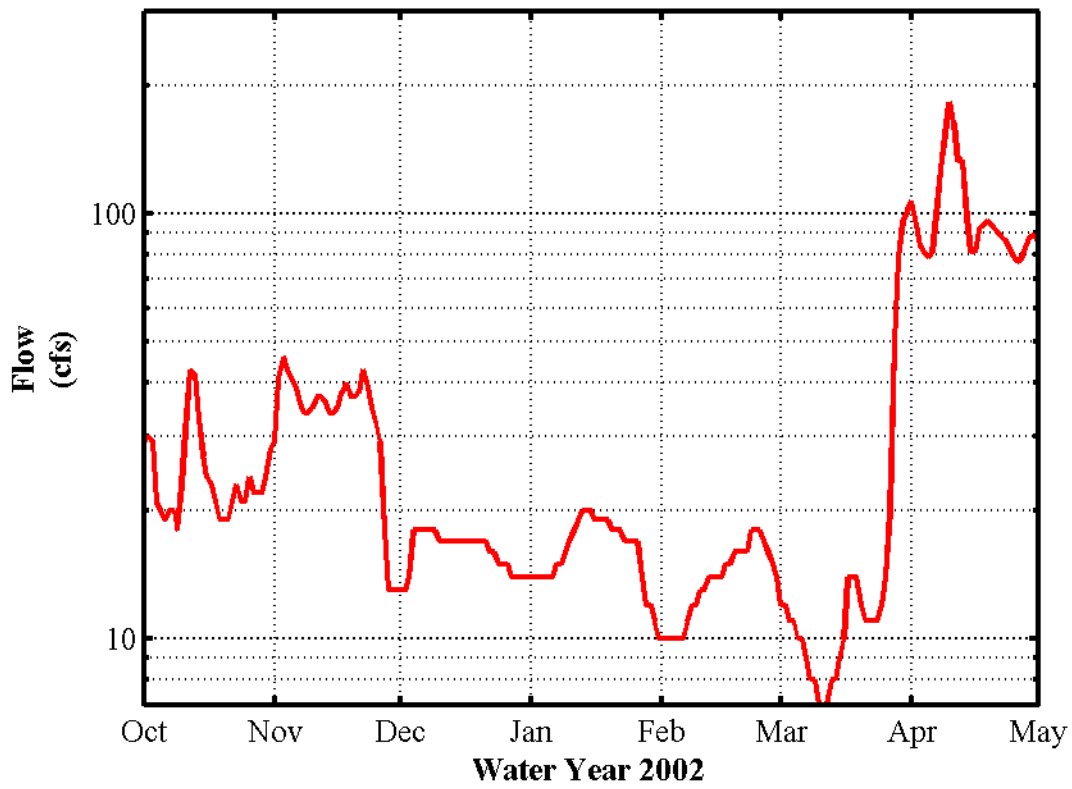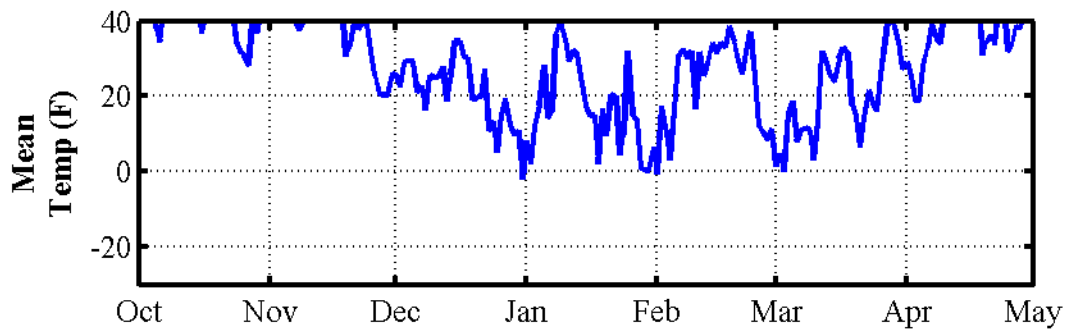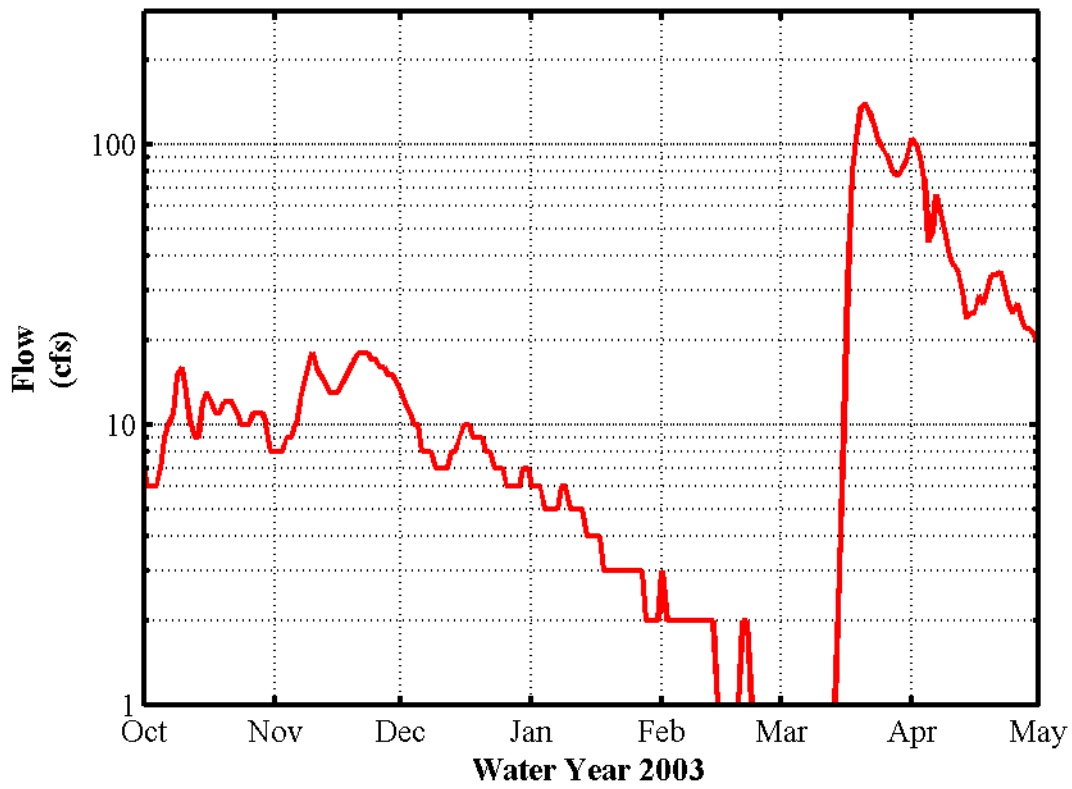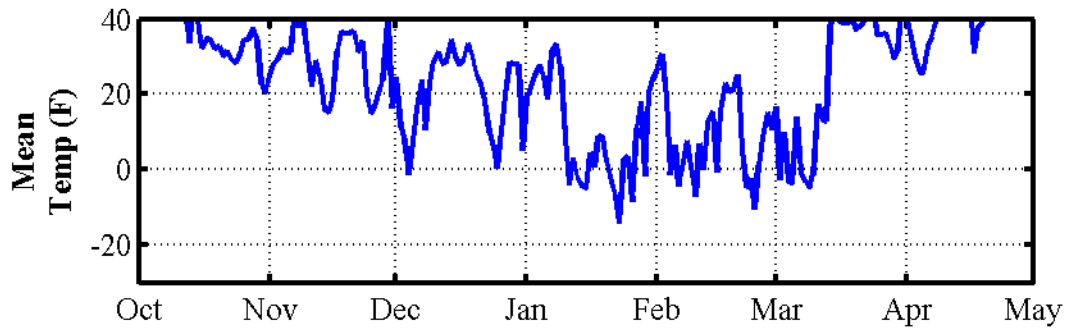
Water Year 2001
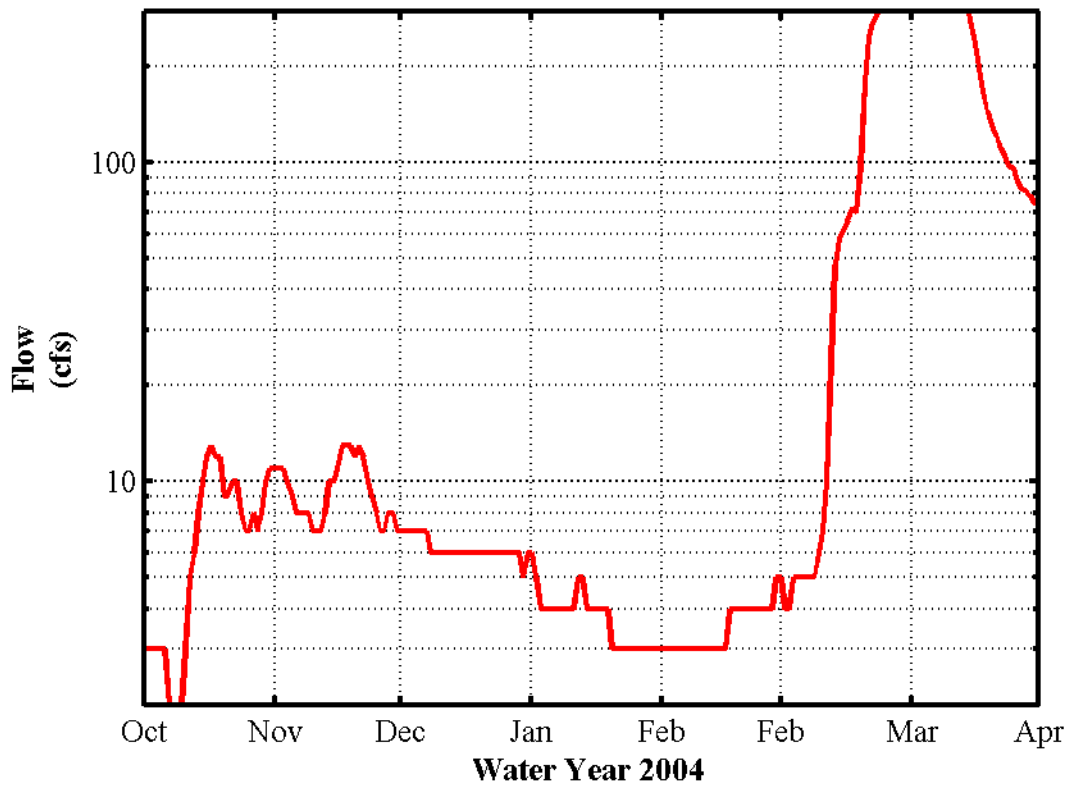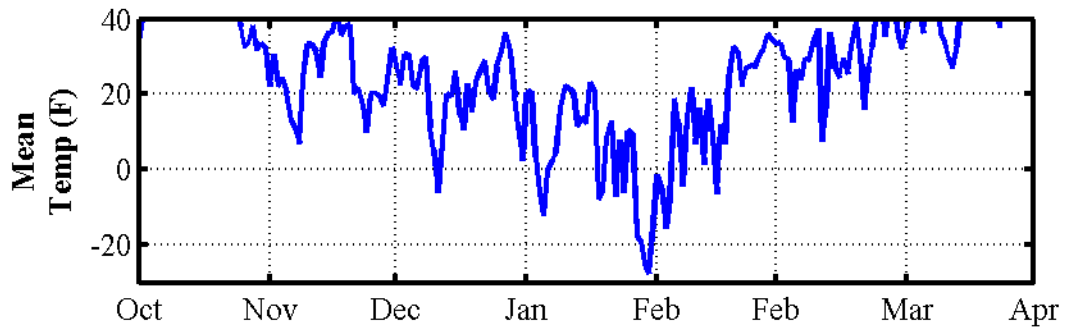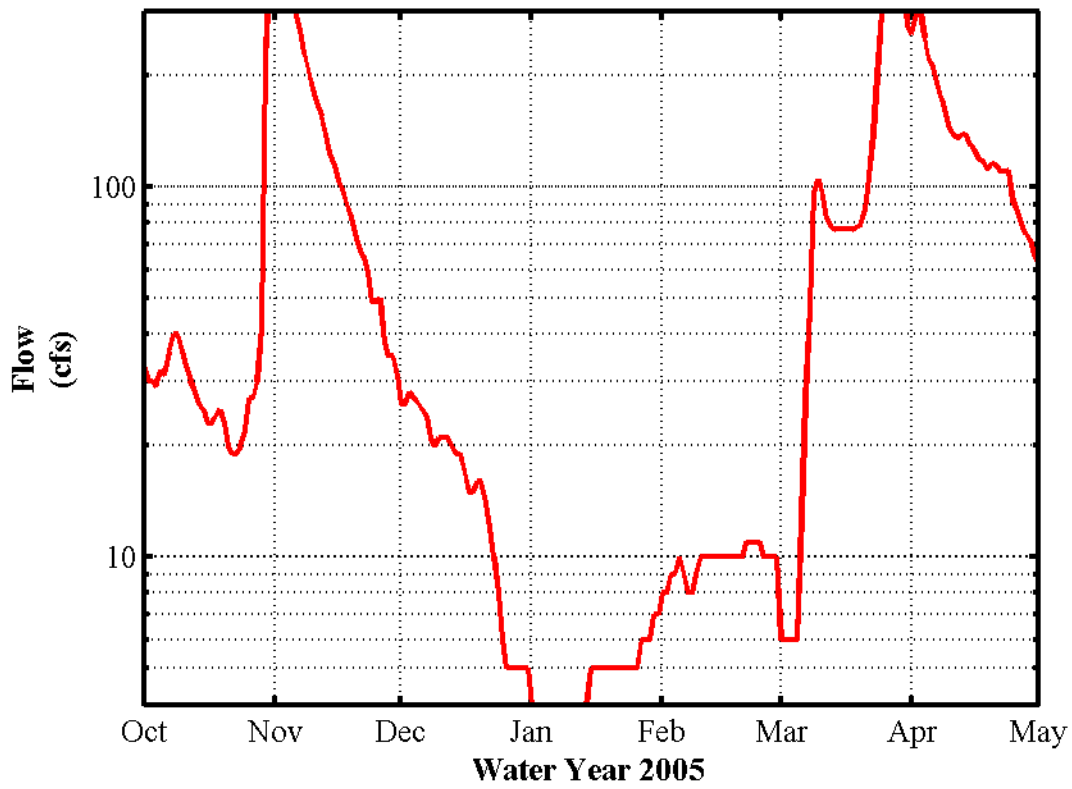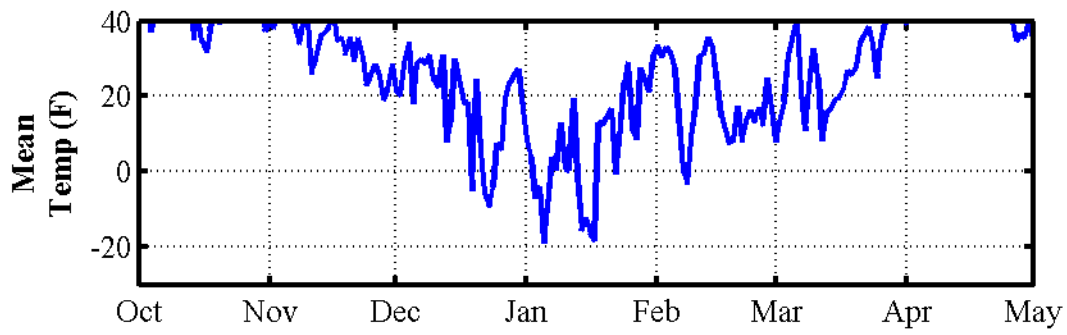
Water Year 2003

Water Year 2004
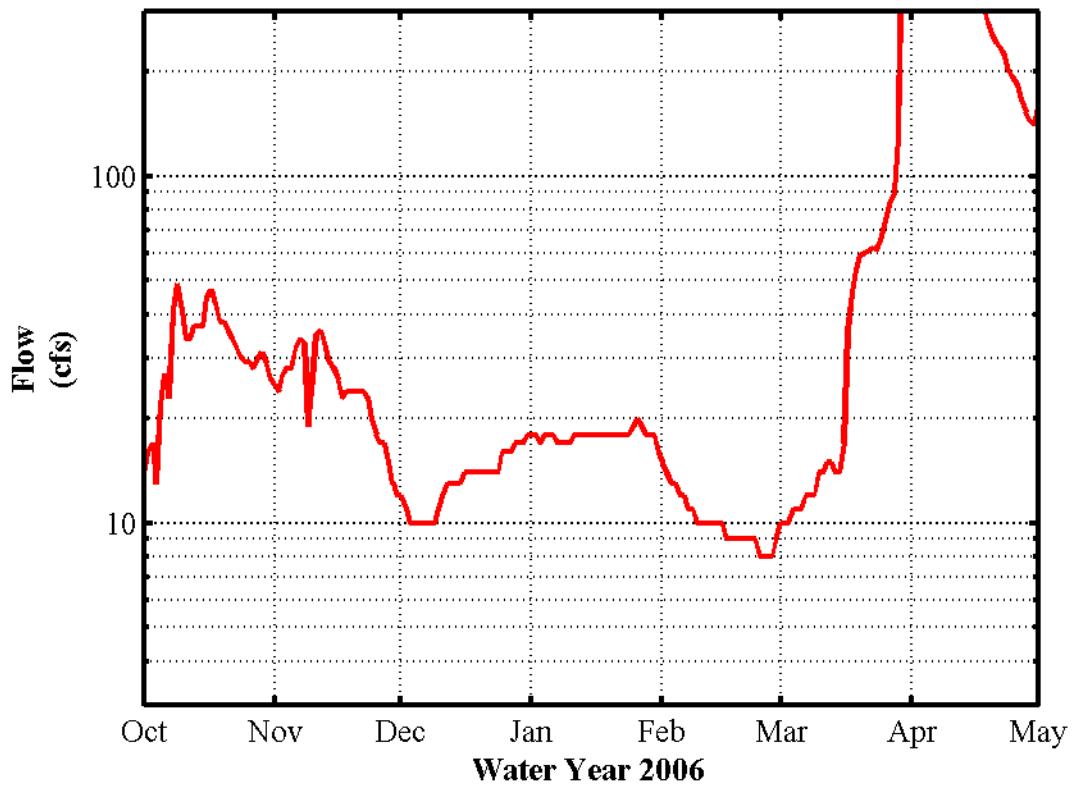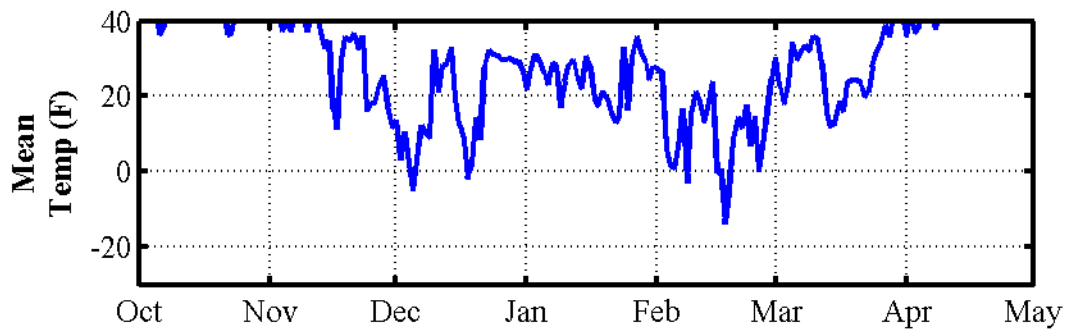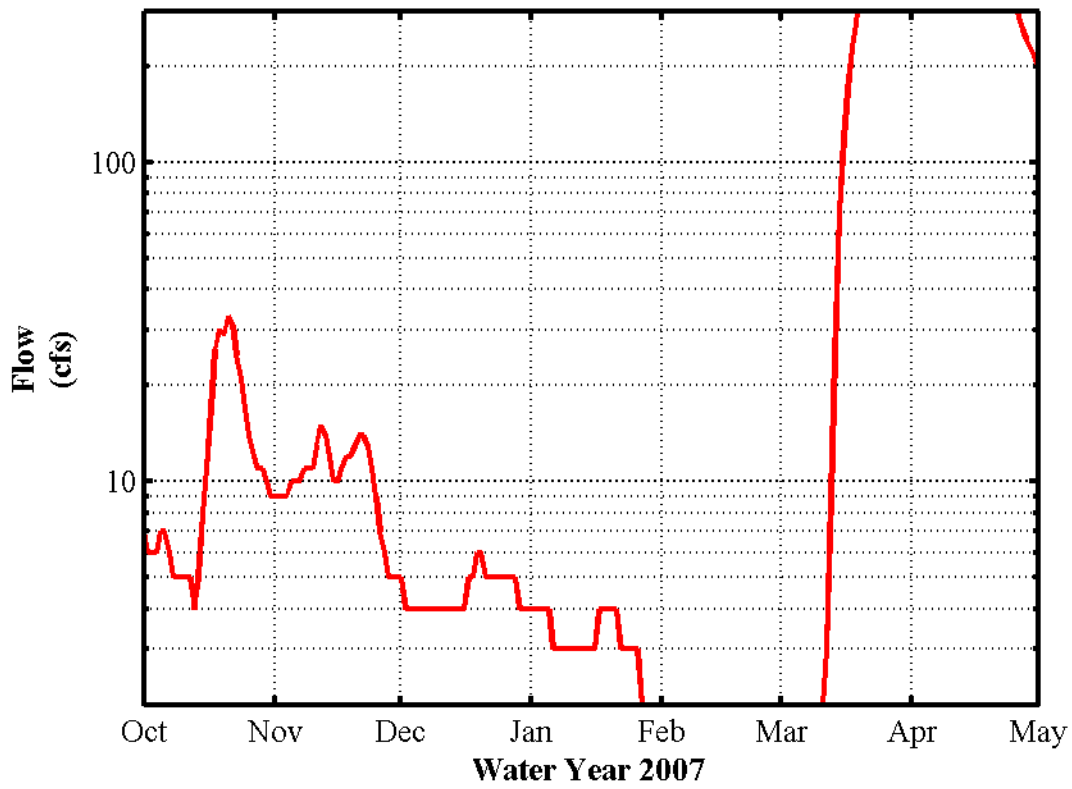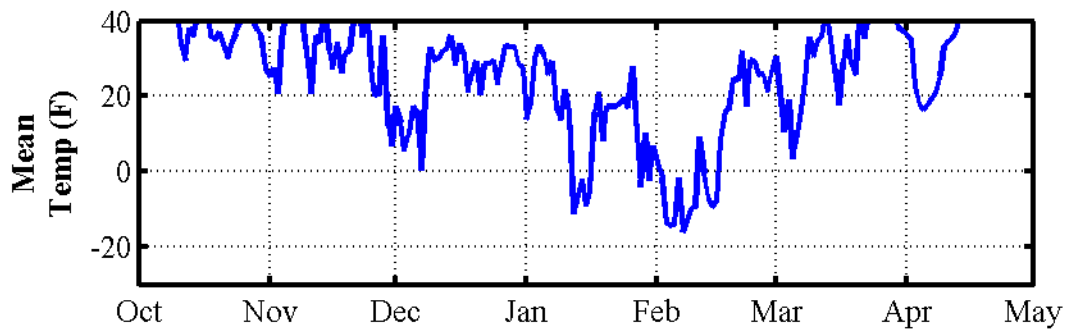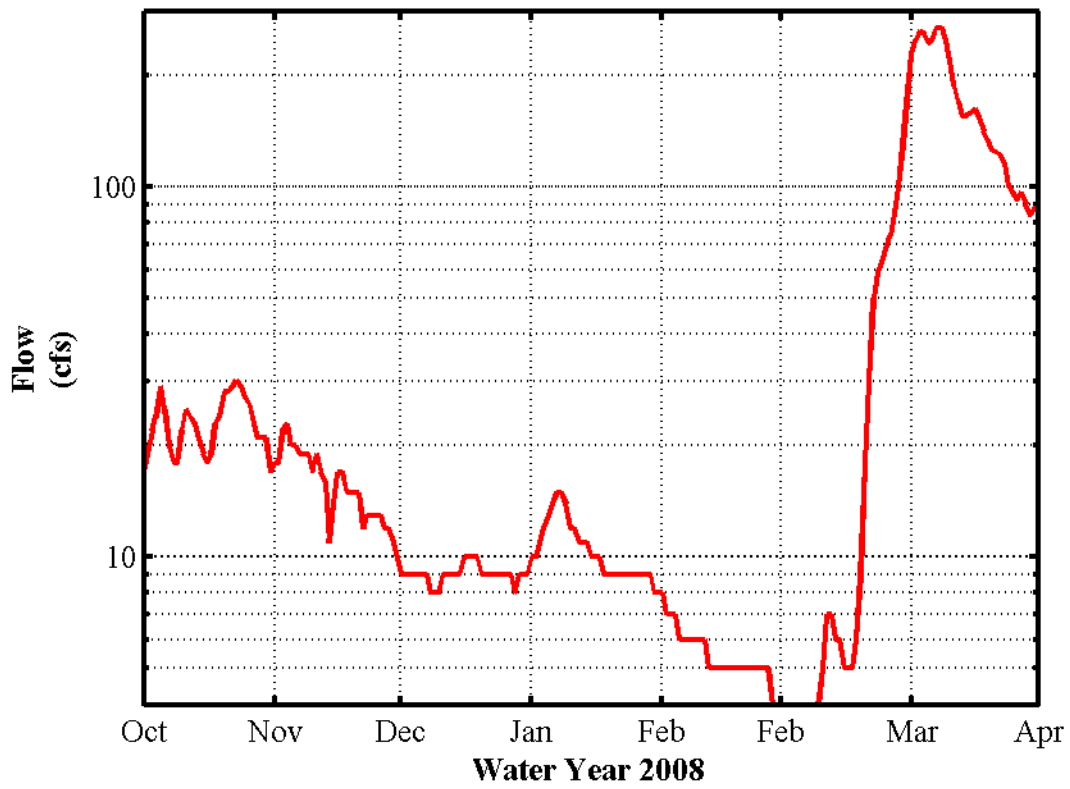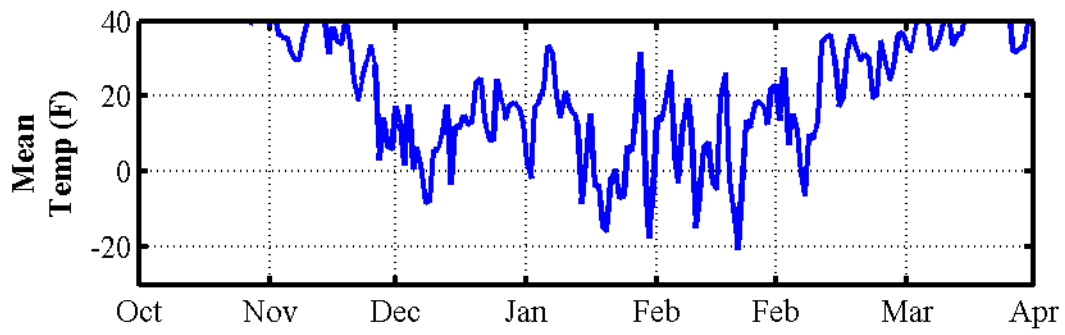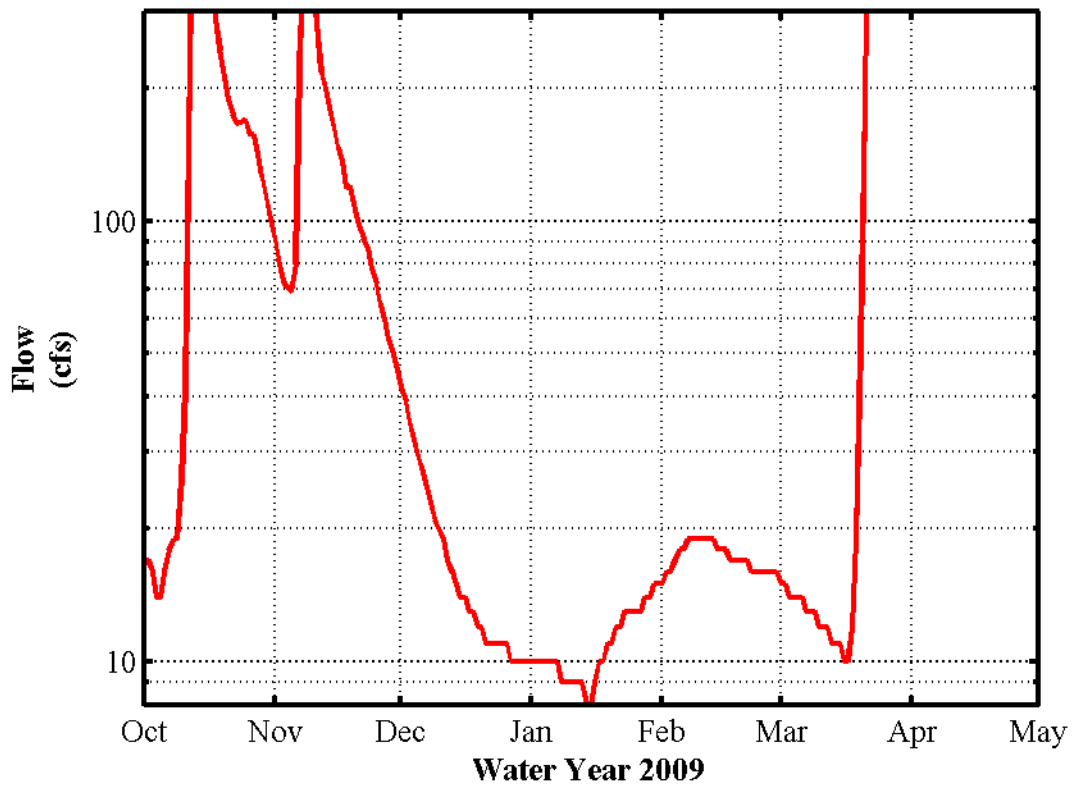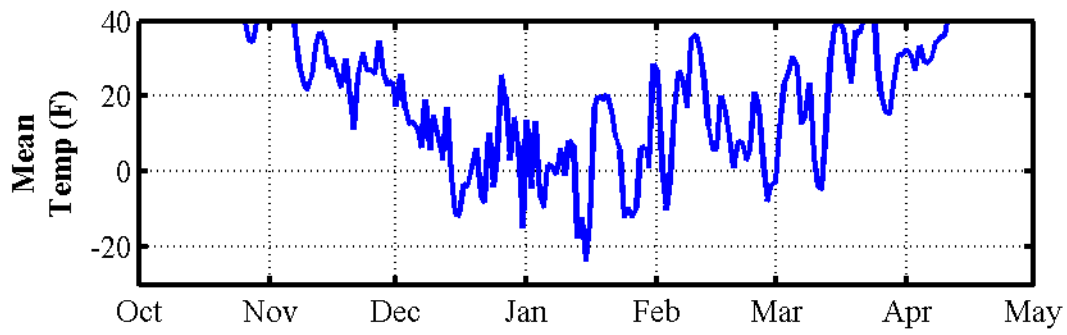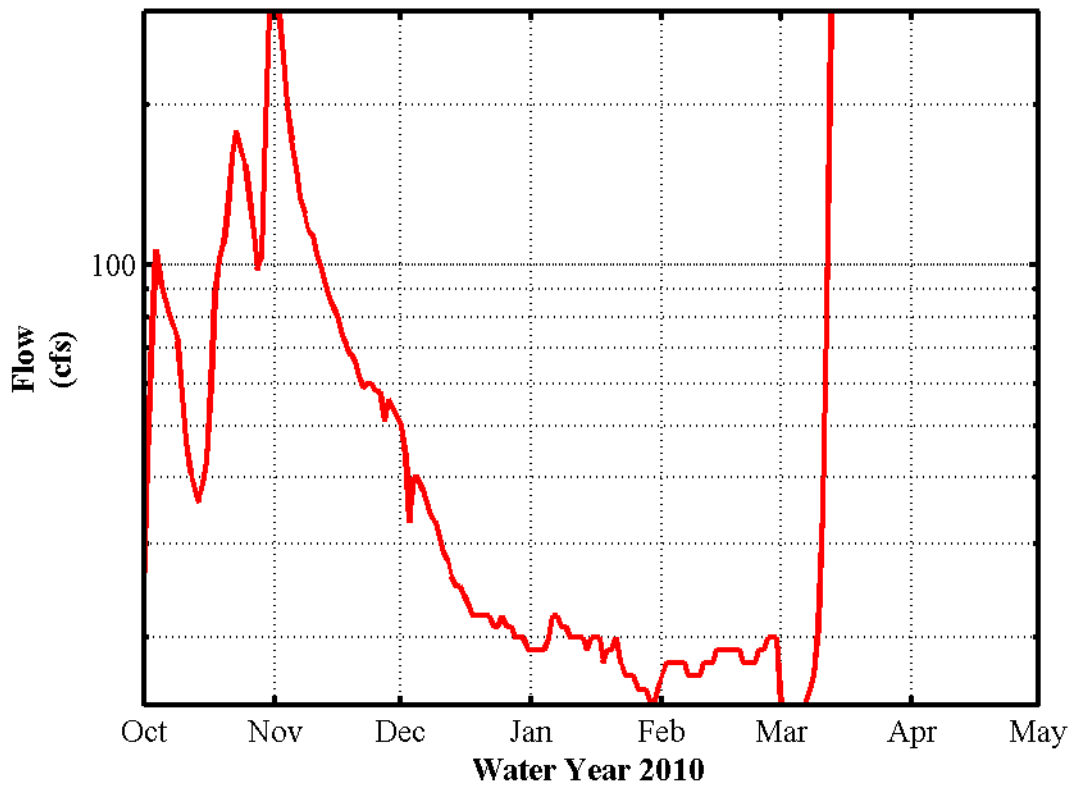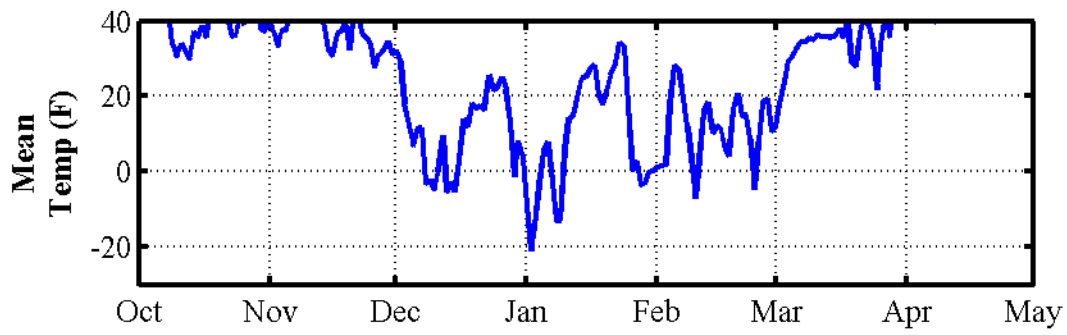
Water Year 2009

Water Year 2010
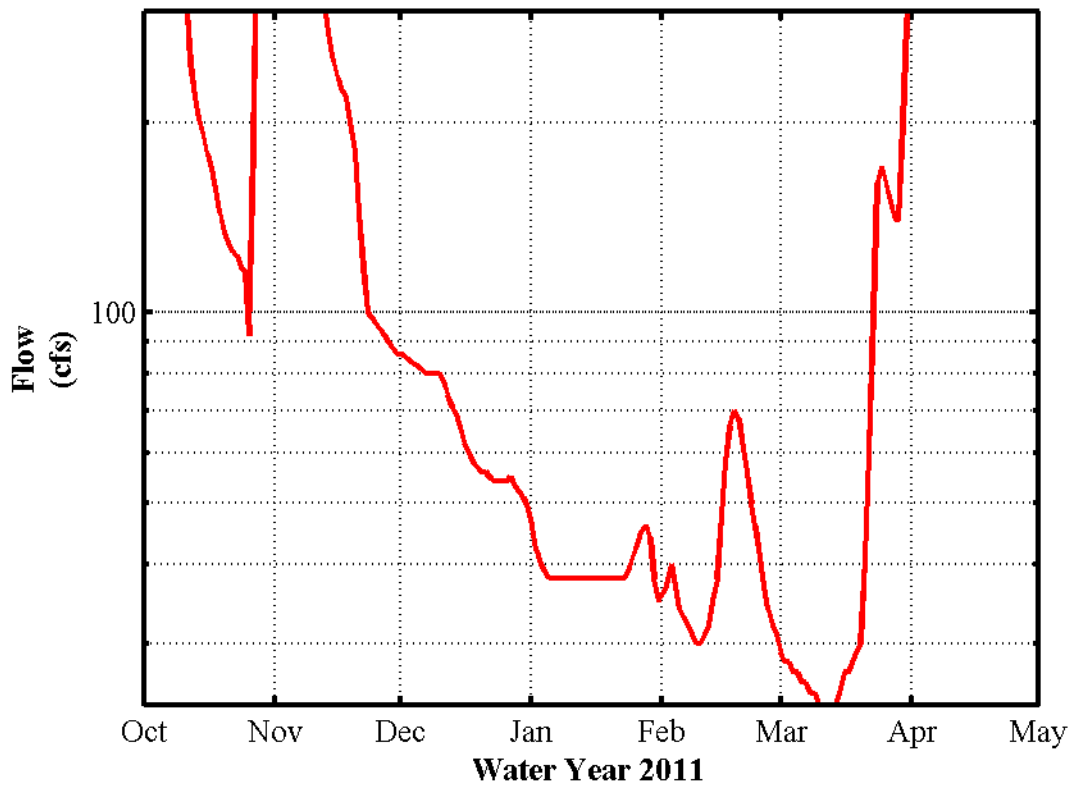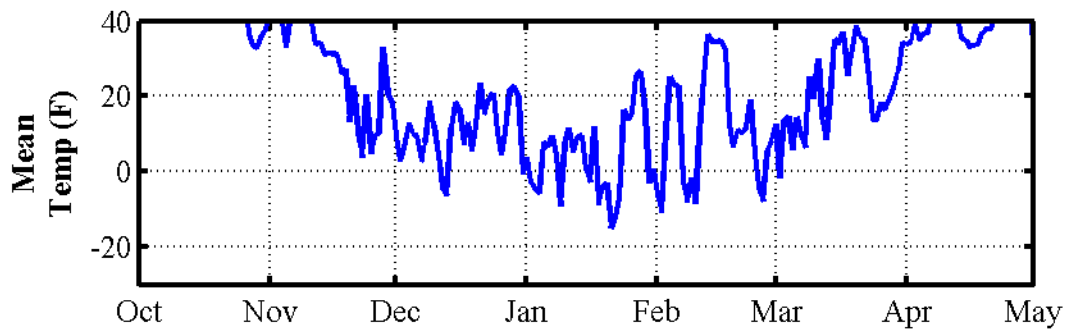
Water Year 2013
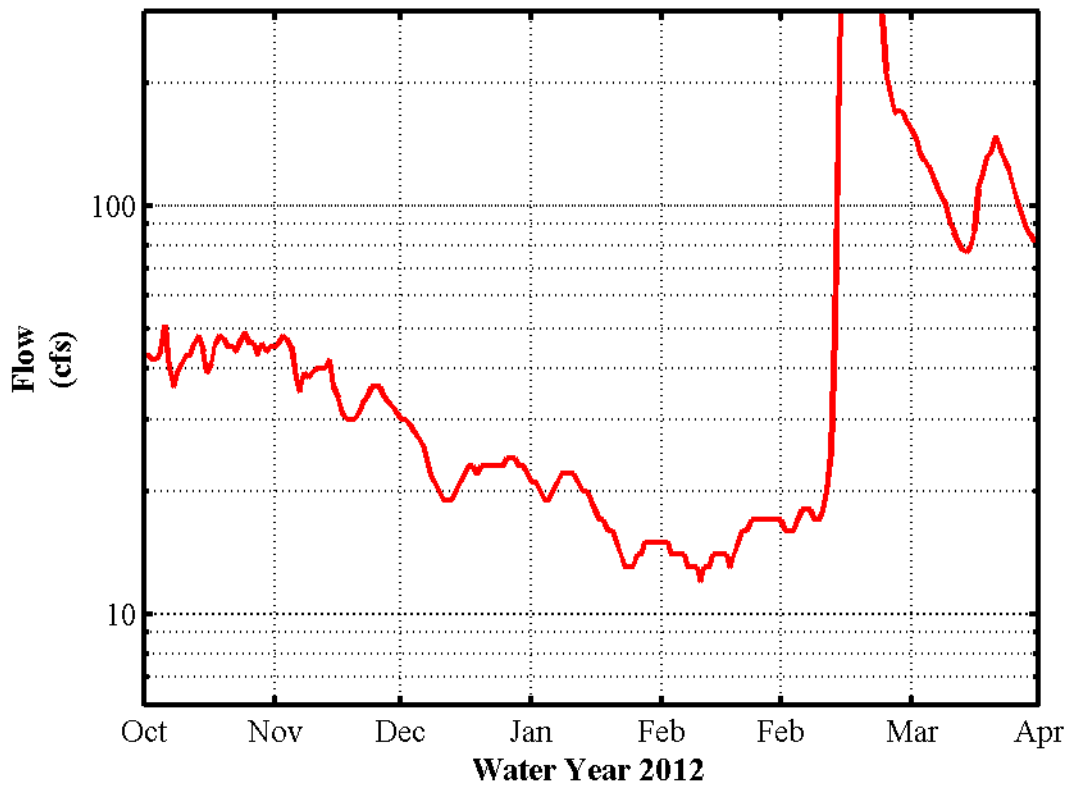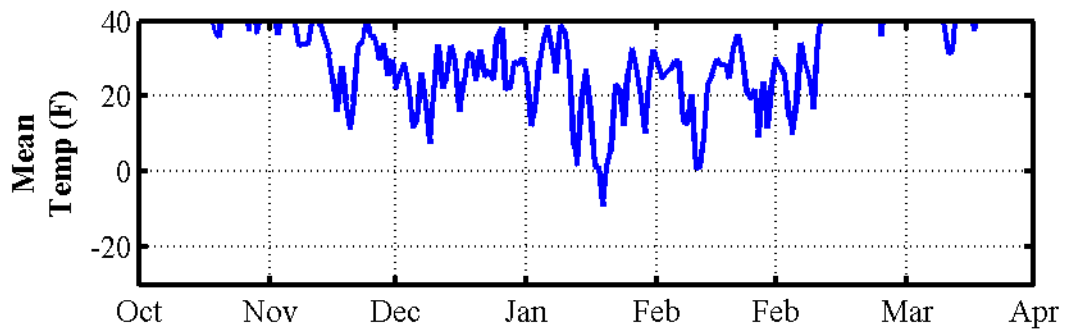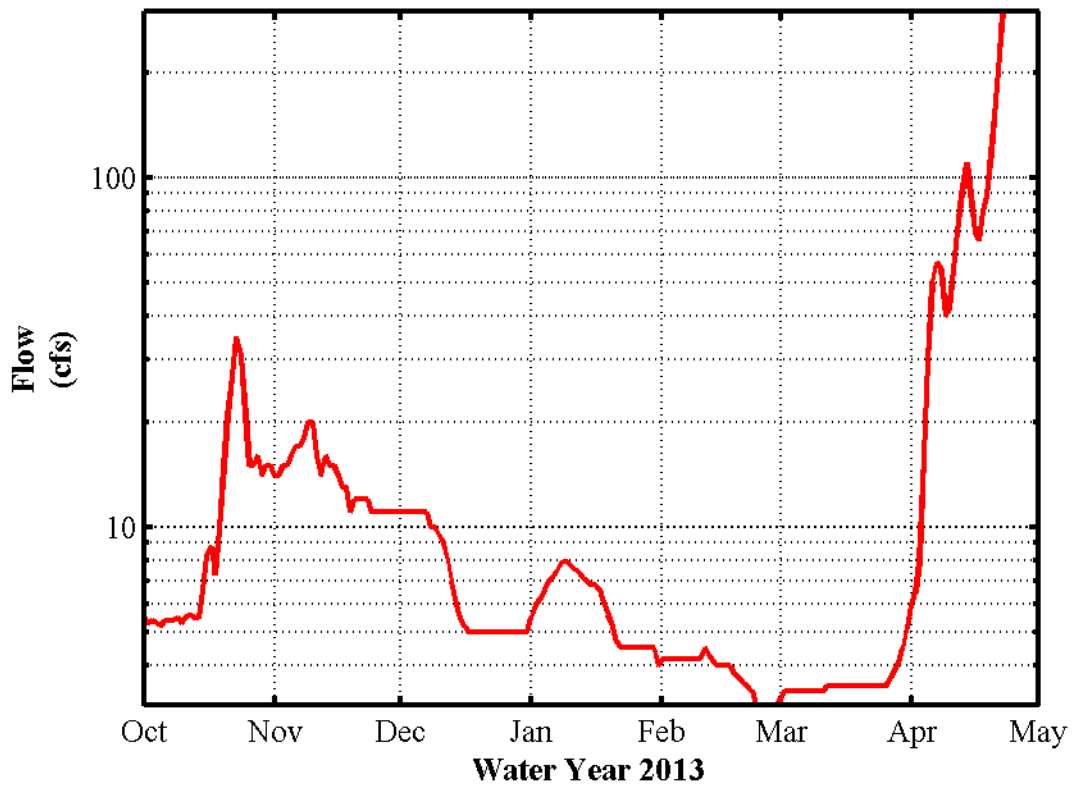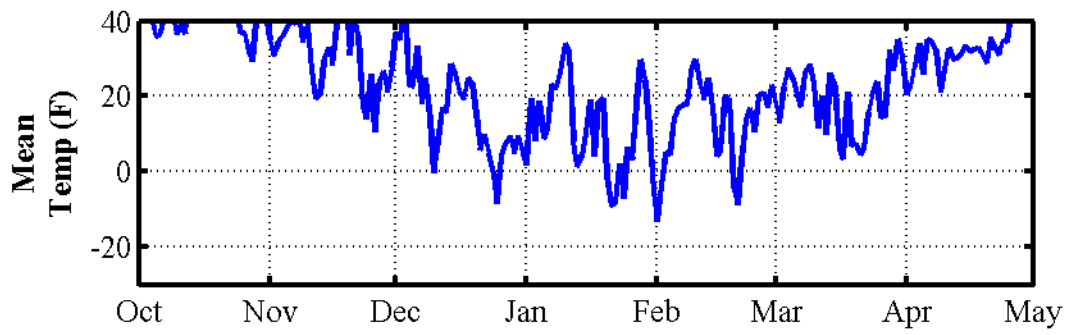
Appendix C: Intense Cold Periods

Table C1. One-day coldest period.

| Water Year	Date	Average Temperature (°F)	Average Flow (cfs)	AFDD
1996	2/1	−29.5	1	1612.3
1994	1/18	−28	-	983.5
1966	1/28	−27.9	3	1085.6
2004	1/30	−27.6	3	868.1
1951	1/29	−27.2	0	1364.2
1977	1/16	−26.2	-	1438.6
1989	2/3	−25.8	-	1079.8
1968	1/6	−25.3	0	475.5
1984	12/23	−25.2	-	357.5
1970	1/18	−25.1	5	868.6
1954	1/21	−24.4	2	453.2
1972	1/15	−24.3	4	562.8
2009	1/15	−23.6	8	847.3
1948	1/23	−23.5	2	651.6
1962	2/28	−23.4	0	1752.7
1965	1/29	−23	1	1411.4
1950	1/26	−22.3	0	1108.2
1952	1/28	−22.3	1	1529.2
1990	12/21	−22.3	-	425
1973	1/8	−22.2	3	908.7
1982	2/3	−21.9	-	1512.1
1974	1/11	−21.2	0	744.6
1985	1/19	−21.1	-	760.3
2010	1/2	−21.1	19	286.9
1961	1/24	−21	0	791.4
2008	2/20	−20.6	5	1414.7
1969	12/31	−20.5	0	232.4
1979	2/16	−20.5	-	2293.2
1956	12/19	−20.4	0	440.3
1997	1/26	−20.1	2	1584.1
1976	1/7	−19.8	-	243.4
1971	1/15	−19.6	0	785
1991	12/30	−19.1	-	161.3
2005	1/5	−19.1	4	76.8

Water Year	Date	Average Temperature (°F)	Average Flow (cfs)	AFDD
1967	1/17	−18.6	0	859.8
1964	12/21	−18.1	0	-350.9
1978	12/10	−18.1	-	39.6
1980	1/9	−17.6	-	407.1
1986	1/7	−17.6	-	1144.8
1949	1/19	−17.1	0	591.5
1955	2/11	−16.4	0	830.3
1963	1/22	−15.9	0	429.4
1999	1/4	−15.9	29	165.5
2007	2/7	−15.9	2	708.6
1957	1/29	−15.6	0	725.7
1993	1/9	−15.6	-	692.1
1992	1/18	−15.4	-	641
2011	1/21	−14.9	38	800.8
2003	1/23	−14.2	3	816.5
2001	1/1	−14.1	16	651.7
1988	1/5	−14	-	100.7
1998	1/13	−13.7	12	331.3
2006	2/17	−13.7	9	503.3
1958	2/15	−13.2	0	849.6
1960	1/5	−13.1	1	385.3
1981	2/11	−13.1	-	1193.7
1959	1/31	−13	0	1124.4
1987	1/23	−12.6	-	498
1975	2/8	−9.1	0	801.8
2012	1/19	−9	16	-246.2
1953	1/16	−8.4	1	403.2
1995	2/11	−7.1	-	582.9
1983	1/26	−7	-	547.3
2000	12/22	−6.8	15	-286.9
2002	12/31	−1.8	14	-264.5
			- Data Not included	

Table C2. Three-day coldest period.

Water Year	Start Date	End Date	Average Temperature (°F)	Average Flow (cfs)	AFDD
1996	2/1	2/3	−27.7	1	1729.9
2004	1/28	1/30	−23.8	3	868.1
1966	1/27	1/29	−23	3	1140.6
1977	1/15	1/17	−22.667	-	1491.8
1970	1/18	1/20	−22.633	3.667	975.4
1994	1/17	1/19	−22.167	-	1036.7
1951	1/28	1/30	−22	0	1413.5
1965	1/28	1/30	−21.1	1	1462.3
1982	2/3	2/5	−20.967	-	1617.1
1989	2/2	2/4	−20.9	-	1129.9
1984	12/22	12/24	−20.7	-	407.5
1973	1/6	1/8	−20.4	3	908.7
1968	1/4	1/6	−19.867	0.667	475.5
1974	12/30	1/1	−19.8	1.667	313.9
1990	12/19	12/21	−19.633	-	425
1972	1/13	1/15	−18.967	4	562.8
2009	1/13	1/15	−17.833	8.333	847.3
1997	12/24	12/26	−17.667	4.333	656.5
1962	2/27	3/1	−17.6	0	1797
1950	1/25	1/27	−16.933	0	1151.9
1979	1/13	1/15	−16.767	-	1195.7
1954	1/20	1/22	−16.6	2	495.2
1991	12/21	12/23	−16.133	-	-103.7
1964	12/19	12/21	−16.067	0	-350.9
1969	12/30	1/1	−16	0	279.3
1952	1/27	1/29	−15.833	1	1581.3
2005	1/15	1/17	−15.667	5	495.8
1949	1/19	1/21	−15.433	0	684.7
1948	1/21	1/23	−14.967	2	651.6
2010	1/1	1/3	−14.933	19	333.6
1955	2/10	2/12	−14.5	0	877.1
2007	2/3	2/5	−14.167	2	627
1961	1/22	1/24	−14.1	0	791.4
1976	1/7	1/9	−13.967	-	329.5
1963	1/21	1/23	−13.933	0	475.4
1985	1/31	2/2	−13.467	-	1167.5
1993	1/8	1/10	−13.433	-	739.3
1967	1/17	1/19	−13.333	0	945.2

Water Year	Start Date	End Date	Average Temperature (°F)	Average Flow (cfs)	AFDD
1978	1/9	1/11	−13.3	-	821.9
1986	11/28	11/30	−13	-	81.6
1956	2/19	2/21	−12.867	0	2002.8
1988	1/4	1/6	−12.433	-	146.1
1980	1/27	1/29	−12.4	-	886.7
2008	2/19	2/21	−11.767	5	1452
1971	2/7	2/9	−11.667	0	1572.2
2011	1/21	1/23	−11.3	38	883.8
2001	12/10	12/12	−10.167	29	-34.5
1998	1/11	1/13	−9.767	12	331.3
1959	1/30	2/1	−9.733	0	1168
1957	1/23	1/25	−9.667	0	583.8
1958	2/15	2/17	−9.433	0	928.7
1960	1/3	1/5	−9.133	1	385.3
1999	1/7	1/9	−9.033	22.333	359
2003	1/21	1/23	−8.167	3	816.5
1981	2/9	2/11	−8	-	1193.7
2006	2/16	2/18	−6.167	9	540.7
1995	2/11	2/13	−5.267	-	655.6
1987	1/22	1/24	−5	-	537.5
1953	1/14	1/16	−4.633	1	403.2
1975	2/8	2/10	−4.167	0	869.2
2000	12/20	12/22	−3.7	15	-286.9
2012	1/17	1/19	−2	16.667	-246.2
1983	1/25	1/27	−1.233	-	574.5
1992	12/3	12/5	−1.133	-	108
2002	1/28	1/30	0.5	11.667	176.6
				- Data Not included	

Table C3. Five-day coldest period.

Water Year	Start Date	End Date	Average Temperature (°F)	Average Flow (cfs)	AFDD
1996	1/30	2/3	−24.48	1.2	1729.9
2004	1/27	1/31	−20.68	3	914.4
1970	1/17	1/21	−20.54	3.8	1027.3
1994	1/15	1/19	−20.48	-	1036.7
1951	1/28	2/1	−19.84	0	1510.7
1973	1/5	1/9	−18.86	3	955.6
1977	1/8	1/12	−18.8	-	1249.6
1968	1/3	1/7	−18.4	0.6	526.6
1984	12/19	12/23	−18.12	-	357.5
1990	12/18	12/22	−17.48	-	472
1966	1/21	1/25	−17.34	2.8	940.3
1989	2/1	2/5	−16.84	-	1171.1
1982	2/2	2/6	−16.42	-	1662.3
1965	1/28	2/1	−16.24	1	1544.2
1974	1/8	1/12	−15.4	0	794.1
1962	1/16	1/20	−15.2	0	786
1954	1/17	1/21	−15.08	2	453.2
1997	12/22	12/26	−14.96	4.8	656.5
1950	1/25	1/29	−14.46	0	1237.4
1979	1/10	1/14	−14.28	-	1149.8
1963	1/19	1/23	−13.38	0	475.4
1985	1/31	2/4	−13.34	-	1257.8
2005	1/13	1/17	−12.7	4.6	495.8
1980	1/26	1/30	−12.48	-	929.5
1969	12/31	1/4	−12.4	0	401.9
1991	12/22	12/26	−12.34	-	22.2
2007	2/3	2/7	−12.02	2	708.6
1961	1/22	1/26	−12	0	873.1
2009	1/12	1/16	−12	8.6	892.6
1972	1/25	1/29	−11.84	3	1015.9
1964	12/18	12/22	−11.72	0	-318.1
1949	1/19	1/23	−10.8	0	756.4
1986	11/27	12/1	−10.64	-	118.5
1952	12/14	12/18	−10.52	6.2	271.5
1988	2/1	2/5	−10.08	-	955
1956	2/17	2/21	−10.06	0	2002.8
1976	1/4	1/8	−10.04	-	288.2
1948	1/22	1/26	−9.8	1.6	754.6

Water Year	Start Date	End Date	Average Temperature (°F)	Average Flow (cfs)	AFDD
1967	2/15	2/19	−9.46	1	1788.1
1978	1/26	1/30	−9.34	-	1460.4
2010	12/31	1/4	−8.88	19	368.9
2001	12/10	12/14	−8.7	28	42.5
1957	1/22	1/26	−8.58	0	622.8
1993	1/6	1/10	−8.56	-	739.3
2011	1/18	1/22	−8.52	38	844.9
1971	1/11	1/15	−8.5	0.2	785
1999	1/9	1/13	−8.12	19.6	513.7
2008	1/17	1/21	−7.94	9.2	598.1
1998	1/10	1/14	−6.76	12.2	359.2
1955	2/9	2/13	−5.62	0	905
1981	2/8	2/12	−4.84	-	1226.7
2003	1/22	1/26	−4.72	3	914.7
1958	2/14	2/18	−4.34	0	958.9
1959	1/16	1/20	−4.24	0	769.4
1975	2/8	2/12	−2.48	0	933.1
2006	2/15	2/19	−2.06	9.2	564.2
1995	2/11	2/15	−1.7	-	712.3
1960	1/4	1/8	−1.2	1	462.8
1992	1/14	1/18	−1.1	-	641
2012	1/17	1/21	0.22	16.2	-189.3
1953	1/13	1/17	0.6	1.2	425
1987	1/22	1/26	0.94	-	581.8
2002	1/28	2/1	1.48	11	234.7
2000	1/19	1/23	1.7	14.2	279.4
1983	2/3	2/7	1.8	-	825.6
				- Data Not included	

Table C4. Ten-day coldest period.

Water Year	Start Date	End Date	Average Temperature (°F)	Average Flow (cfs)	AFDD
1996	1/25	2/3	−18.78	1.6	1729.9
1977	1/8	1/17	−17.62	-	1491.8
1966	1/21	1/30	−16.85	2.9	1182.1
1984	12/16	12/25	−16.06	-	444.1
1968	12/30	1/8	−14.63	0.7	561.5
1994	1/11	1/20	−14.34	-	1081.7
1982	1/7	1/16	−12.83	-	873
1951	1/24	2/2	−12.39	0.2	1544.6
2004	1/26	2/4	−12.34	3	1071.9
1974	12/30	1/8	−12.25	0.8	601
1965	1/26	2/4	−12.14	1	1678.5
1990	12/13	12/22	−12.03	-	472
1979	1/7	1/16	−11.71	-	1242
1963	1/18	1/27	−11.41	0	638.4
1954	1/16	1/25	−10.84	2	595.4
1950	1/25	2/3	−9.98	0	1424.9
1970	1/12	1/21	−9.89	3.9	1027.3
2007	2/1	2/10	−9.14	2	836.7
1991	12/21	12/30	−8.94	-	161.3
1952	12/14	12/23	−8.86	5.3	467.5
1949	1/19	1/28	−8.82	0	950.6
1997	12/18	12/27	−8.54	5.3	692.8
1985	1/30	2/8	−8.32	-	1393.1
1973	12/3	12/12	−7.85	7.4	202.2
1964	12/13	12/22	−7.69	0	-318.1
1948	2/2	2/11	−7.64	0.3	1318.8
1999	1/4	1/13	−7.61	22.7	513.7
1978	1/27	2/5	−7.44	-	1690.8
1962	1/14	1/23	−7.08	0	877.5
1988	2/1	2/10	−6.87	-	1133.3
1986	11/24	12/3	−6.51	-	193.2
1961	1/21	1/30	−6.4	0	999.3
1969	12/29	1/7	−6.07	0	480.4
1972	1/21	1/30	−6.05	3	1055.9
1980	1/23	2/1	−5.96	-	1003
2010	12/31	1/9	−5.96	20.1	544.1
1989	2/1	2/10	−5.76	-	1304.5
1971	1/10	1/19	−5.57	0.1	921.2

Water Year	Start Date	End Date	Average Temperature (°F)	Average Flow (cfs)	AFDD
2001	12/17	12/26	−5.24	19.6	465.3
1956	1/15	1/24	−4.9	0	1308.1
2009	1/7	1/16	−4.61	8.9	892.6
1957	1/22	1/31	−4.28	0	782.7
2008	1/17	1/26	−4.02	9.1	758.6
1967	2/15	2/24	−3.7	0.9	1937.8
1959	1/16	1/25	−3.64	0	944.6
1993	1/1	1/10	−3.38	-	739.3
2011	1/14	1/23	−3.02	38	883.8
2005	1/8	1/17	−2.95	4.3	495.8
1976	1/2	1/11	−2.64	-	370.4
1958	2/8	2/17	−2.58	0	928.7
2003	1/14	1/23	−0.88	3.4	816.5
1955	2/19	2/28	−0.79	0	1270.3
1975	2/5	2/14	0.32	0	993.8
1981	1/2	1/11	0.46	-	582.7
1998	1/10	1/19	1.13	11.7	474.1
1960	2/27	3/7	1.75	0	1756.8
1995	2/28	3/9	3.49	-	1143.1
2000	1/12	1/21	4.23	14.1	227.8
1953	1/11	1/20	4.9	1.3	502.4
2006	2/15	2/24	5.49	9	659
1983	1/30	2/8	5.83	-	848.6
2002	1/26	2/4	6.68	11.6	299.9
1992	1/9	1/18	7.02	-	641
1987	1/15	1/24	7.13	-	537.5
2012	1/12	1/21	7.22	17.9	-189.3
				- Data Not included	

Table C5. Thirty-day coldest period.

Water Year	Start Date	End Date	Average Temperature (°F)	Average Flow (cfs)	AFDD
1982	1/7	2/5	−7.747	-	1617.1
1950	1/3	2/1	−7.25	0	1367.2
1966	1/2	1/31	−6.337	2.967	1212.7
1977	12/20	1/18	−5.213	-	1523
1994	12/22	1/20	−5.037	-	1081.7
1996	1/5	2/3	−4.653	3.033	1729.9
1979	12/30	1/28	−4.51	-	1554.9
1948	1/13	2/11	−4.473	1.333	1318.8
1978	1/8	2/6	−4.19	-	1730.8
1949	1/16	2/14	−4.09	0	1521.8
1972	1/13	2/11	−3.647	2.867	1479.3
1965	1/6	2/4	−3.23	1.133	1678.5
1954	1/2	1/31	−2.08	2.467	802.9
1951	1/17	2/15	−1.867	0.3	1929.8
1963	1/9	2/7	−1.4	0.033	884.1
1970	12/26	1/24	−1.367	3.933	1110.9
1968	12/19	1/17	−1.167	0.9	785.4
1997	12/19	1/17	−1.017	3.133	1312.4
1971	1/11	2/9	−0.99	0.033	1572.2
1974	12/15	1/13	−0.943	1.5	827.7
1959	1/15	2/13	−0.76	0	1538.8
1969	12/29	1/27	−0.62	0	1078.3
2001	12/5	1/3	−0.583	22.8	688.4
1986	11/22	12/21	−0.547	-	739.8
1952	12/12	1/10	−0.53	3.833	965.1
1991	12/16	1/14	−0.233	-	607.9
1984	12/2	12/31	−0.227	-	605.3
1993	12/19	1/17	0.2	-	917.8
2004	1/18	2/16	0.307	3.067	1336.1
1999	12/17	1/15	0.34	47.067	557
2009	12/18	1/16	0.55	10.067	892.6
1985	1/17	2/15	0.73	-	1596.5
1957	1/9	2/7	1.497	0.067	965.3
1989	2/1	3/2	1.67	-	1836.8
2007	1/12	2/10	2.447	2.667	836.7
2005	12/19	1/17	2.663	6.1	495.8
2008	1/17	2/15	2.993	7.5	1268.6
1956	11/23	12/22	3.233	1.133	520.1

Water Year	Start Date	End Date	Average Temperature (°F)	Average Flow (cfs)	AFDD
2011	12/25	1/23	3.39	41.9	883.8
1967	1/26	2/24	3.463	0.967	1937.8
1962	1/4	2/2	3.53	0.167	1085.1
1988	1/18	2/16	3.6	-	1289.9
1990	12/6	1/4	3.833	-	696
1973	11/27	12/26	4.05	7.833	544.5
1955	2/6	3/7	4.527	0	1469.3
1980	1/19	2/17	4.573	-	1381.7
2003	1/12	2/10	4.757	2.833	1241.8
2010	12/11	1/9	5.7	21.9	544.1
1960	2/9	3/9	5.753	0	1787.9
1961	1/8	2/6	6.033	0	1183.9
1975	1/18	2/16	6.483	0	1045.1
1976	1/3	2/1	6.997	-	794.3
1958	1/20	2/18	7.113	0.5	958.9
1981	12/18	1/16	7.93	-	680.3
1964	12/14	1/12	8.083	0	25.8
1995	1/19	2/17	9.387	-	764.9
1953	1/5	2/3	9.773	1.3	772.5
2000	1/2	1/31	9.783	13.367	443.4
1998	12/27	1/25	10.523	13.433	580.3
2006	2/3	3/4	11.15	9.867	773
1983	1/11	2/9	11.397	-	862.9
1992	11/22	12/21	15.183	-	326.1
2002	1/14	2/12	15.63	14.4	340
2012	1/13	2/11	16.88	14.967	41.4
1987	12/30	1/28	18.23	-	598.8
				- Data Not included	

REPORT DOCUMENTATION PAGE

1. REPORT DATE (DD-MM-YYYY)	2. REPORT TYPE	3. DATES COVERED (From - To)
18-09-2014	Final	

4. TITLE AND SUBTITLE

Development of Conceptual Designs for the Prevention of Ice Formation in the Proposed Maple River Aqueduct

5a. CONTRACT NUMBER

5b. GRANT NUMBER

5c. PROGRAM ELEMENT

6. AUTHOR(S)

Steven F. Daly , Meredith Carr , Kevin Bjella , and Robert Haehnel

5d. PROJECT NUMBER

5e. TASK NUMBER

5f. WORK UNIT NUMBER

7. PERFORMING ORGANIZATION NAME(S) AND ADDRESS(ES)

U.S. Army Engineer Research and Development Center (ERDC)
Cold Regions Research and Engineering Laboratory (CRREL)
72 Lyme Road,
Hanover, NH 03755-1290

8. PERFORMING ORGANIZATION REPORT NUMBER

ERDC/CRREL TR-14-18

9. SPONSORING / MONITORING AGENCY NAME(S) AND ADDRESS(ES)

U.S. Army Corps of Engineers, St. Paul District
St. Paul, MN 55101

10. SPONSOR/MONITOR'S ACRONYM(S)

11. SPONSOR/MONITOR'S REPORT NUMBER(S)

12. DISTRIBUTION / AVAILABILITY STATEMENT

Approved for public release; distribution is unlimited.

13. SUPPLEMENTARY NOTES

14. ABSTRACT

The Fargo-Moorhead Metropolitan Area Flood Risk Management Project is to include an aqueduct to carry the flow of the Maple River over a proposed diversion channel. This study quantified the amount of ice that forms in the aqueduct under different winter operating scenarios. To achieve this, this study developed an aqueduct flow and ice simulation that simulated five different operation scenarios: the proposed aqueduct alone, a case with downstream stage control, and three different cases of applied heating. Each scenario was run with 6 in., 3 in., and no insulation on the outside of the aqueduct. The flow conditions and the ice formation in the aqueduct were simulated every day for the winters of 1995 to 2013, allowing estimates to account for the natural variability of the flow and air temperature. The simulation found that, though ice formation in all scenarios caused the stages to rise, the unheated scenarios saw the largest stage rise; and the impact of the insulation in the unheated scenarios was significant. Applying heat reduced stages compared to the unheated cases, the amount of heat applied determined the decrease in the upstream stages, and insulation had less impact when heat was applied.

15. SUBJECT TERMS

Aqueduct, bed ice, flow modeling, heating, ice formation, ice modeling, insulation, winter flow

16. SECURITY CLASSIFICATION OF:			17. LIMITATION OF ABSTRACT	18. NUMBER OF PAGES	19a. NAME OF RESPONSIBLE PERSON
a. REPORT	**b. ABSTRACT**	**c. THIS PAGE**	SAR	122	**19b. TELEPHONE NUMBER (include area code)**
Unclassified	Unclassified	Unclassified			